UNIVERSITÉ DU QUÉBEC À TROIS-RIVIÈRES

COMPREHENSIVE STUDY AND DEVELOPMENT OF OPEN-SOURCE PRESSURE PUMP FOR MICROFLUIDIC APPLICATIONS

MÉMOIRE PRÉSENTÉ

COMME EXIGENCE PARTIELLE DE LA

MAÎTRISE EN INGÉNIERIE CONCENTRATION GÉNIE MÉCANIQUE

PAR

ZEIN MOHAMMAD

FÉVRIER 2026

UNIVERSITÉ DU QUÉBEC À TROIS-RIVIÈRES

MAÎTRISE EN INGÉNIERIE CONCENTRATION GÉNIE MÉCANIQUE (M. Sc. A.)

Direction de recherche :

Marie Hébert	Directrice de recherche
Sousso Kelouwani	Codirecteur de recherche

Jury d'évaluation

Nadjet Zioui	Évaluatrice interne
Amine Miled	Évaluateur externe
Marie Hébert	Directrice de recherche

Résumé

La microfluidique est une technologie qui manipule et analyse de très petits volumes de fluide à l'intérieur de microcanaux. En raison de ses caractéristiques, telles que la miniaturisation, l'efficacité et la régulation précise, cette technologie a introduit de nouvelles capacités dans diverses applications et est devenue un outil clé dans divers domaines. L'efficacité et la précision des systèmes microfluidiques dépendent de la méthode d'actionnement utilisée pour manipuler l'écoulement des fluides à l'intérieur des dispositifs. Récemment, les systèmes microfluidiques évoluent de plus en plus vers des plateformes microfluidiques actives, parallèlement à l'émergence des concepts de jumeaux numériques en microfluidique. Ces évolutions ont suscité un intérêt accru pour des méthodes d'actionnement capables d'offrir une régulation rapide, stable et en boucle fermée. Dans ce mémoire, une revue mettant en évidence les avantages et les inconvénients des principales méthodes d'actionnement est présentée. Les options commerciales ainsi que les projets open-source sont inclus dans ce mémoire. Les pompes à pression se distinguent par leur performance élevée et leur capacité à satisfaire les exigences d'un plus large éventail d'applications, là où les autres méthodes de pompage sont limitées. Toutefois, les pompes à pression commerciales restent coûteuses et requièrent une source de pression externe, alors que les solutions open-source se caractérisent par un temps de stabilisation plus long, ce qui limite leur utilisation aux applications passives. De plus, la majorité des pompes à pression open-source disponibles reposent fortement sur des régulateurs commerciaux fonctionnant comme des systèmes fermés, ce qui limite leur intégration dans des systèmes microfluidiques actifs. Afin de surmonter ces limitations, une pompe à pression open-source est proposée. La pompe intègre un système de compression et un régulateur économique constitué de deux électrovannes proportionnelles et d'un capteur de pression. Un système de

régulation proportionnelle–intégrale–dérivée (PID) est conçu pour réguler le mécanisme du régulateur. Après les tests, le régulateur peut maintenir une régulation précise de la pression même à des niveaux inférieurs à 5 psi (0,344 bar), avec une précision de ±0,01 psi (±0,7 mbar), comparable à celle du régulateur commercial Marsh Bellofram. Cependant, le régulateur proposé atteint un temps de stabilisation plus rapide d'environ ≈100 ms, comparé à $\approx$ 200 ms pour le régulateur commercial, tout en étant proposé à un prix bien plus bas ($\sim$ 250\$ vs. $\sim 1,000$\$). Ainsi, la pompe proposée améliore l'accessibilité des pompes à pression dans les environnements à infrastructure limitée et constitue une alternative économique aux options commerciales. Elle assure également une régulation précise et rapide du flux, adaptée à un plus large éventail d'applications que les solutions open-source actuelles, en particulier dans les systèmes microfluidiques actifs.

Abstract

Microfluidics is a technology that controls and analyzes tiny volumes of fluid within networks of microchannels. Owing to its features, such as miniaturization, efficiency, and precise control, this technology has introduced new capabilities across various applications and has become a key tool in diverse fields. The efficiency and precision of microfluidic systems are affected by the actuation method employed to manipulate fluid flow within the devices. Recently, microfluidic systems are increasingly shifting toward active microfluidic platforms, along with the emergence of digital twin concepts in microfluidics. These developments have increased interest in actuation methods that provide fast, stable, and closed-loop control. In this master's thesis, a review of the main actuation methods is presented. Both commercial options and open-source projects are considered. Pressure pumps are distinguished by their high performance and ability to meet the requirements of a wider range of applications than other pumping methods. However, commercial pressure pumps are expensive and require an external pressure source, whereas open-source solutions exhibit slower settling times, limiting their use to passive applications. In addition, most available open-source pressure pumps rely heavily on commercial regulators that are closed systems, limiting customization and integration into active microfluidic systems. To address these limitations, an open-source pressure pump is proposed. The pump features an onboard compression system and an affordable regulator composed of dual proportional solenoid valves and a pressure sensor. A proportional-integral-derivative PID control system is implemented to regulate the dual-valve regulator system. After testing, the regulator can maintain precise pressure control even at levels below 5 psi (0.344 bar), with accuracy ±0.01 psi (±0.7 mbar) comparable to that of the commercial Marsh Bellofram regulator. However, the proposed regulator achieves a faster settling time of $\approx$ 100 ms, compared to $\approx$ 200 ms for the

commercial regulator, at a much lower price ($\sim$ 250\$ vs. $\sim 1,000$\$). Therefore, the proposed pump improves the accessibility of pressure pumps in environments with limited infrastructure and offers a cost-effective alternative to commercial options. It also delivers precise and fast flow control suitable for a broader range of applications than current open-source solutions, particularly for active microfluidic systems.

Remerciements

I wish to express my deep appreciation to my supervisor, Professor Marie Hebert, for her guidance, valuable support, and kind recommendations throughout this academic journey. I am sincerely thankful to Professor Sousso Kelouwani and Professor Lotfi Toubal for their support.

I would like to thank the funding organization Conseil de Recherches en Sciences Naturelles et en Génie du Canada (CRSNG) for their financial support, as well as le Programme de Bourses Créneaux d'Expertise de l'UQTR for the scholarship that made this opportunity possible.

A Special thought goes to my family and friends, who have always been my source of strength, motivation, and inspiration.

Table of contents

List of tables

List of figures

Liste des symboles

PID	Proportional–Integral–Derivative controller
LQR	Linear Quadratic Regulator
K_p	Proportional gain
K_i	Integral gain
K_d	Derivative gain
ρ	Fluid density (kg/m^3)
u	Velocity vector field (m/s)
t	Time (s)
p	Pressure (Pa)
μ	Dynamic viscosity (Pa $\cdot$ s)
f	Body force per unit volume (N/m^3)
Δp	Pressure drop across the channel (Pa)
R_{chip}	Hydraulic resistance (Pa·s/m^3)
Q	Volumetric flow rate (m^3/s)
U_0	Reference velocity (m·s^{-1})
L_0	Reference length (m)
η	Dynamic viscosity (Pa·s)
D	Diffusion coefficient (m^2·s^{-1})
γ	Surface or interfacial tension (N·m^{-1})
τ_p	Polymer relaxation time (s)

$\dot{\gamma}$	Shear rate (s^{-1})
τ_{flow}	Characteristic flow time (s)
h_l	Channel height (m)
U_b	Buoyant velocity scale ($m \cdot s^{-1}$)
β	Slip length (m)
f_{mech}	Mechanical frequency of the syringe pump (Hz)
$\overline{Q}_i$	Average inlet flow rate (m^3/s)
D_i	Syringe inner diameter (m)
s	Pitch of the lead screw (m)
T_i	Period of the main peaks of the peristaltic pump.
n	Number of rollers per rotation
ω	Rotation speed of the motor shaft (rad/s)
V	Volume of the gas (m^3)
m	Mass of the gas (kg)
T	Air temperature within the control volume (K)
$\dot{m}_{\text{in}}$	Mass flow input to the system (kg/s)
$\dot{m}_{\text{out}}$	Mass flow output from the system (kg/s)
i_{in}	Electric current supplied to input valve (A)
i_{out}	Electric current supplied to output valve (A)
u_{1in}	Control signal applied to input valve
u_{2out}	Control Signal applied to output valve

u_{pid}	PID controller output
U_{max}	Maximum DAC output value (Valve fully open)
$\dot{E}_{\text{in}}$	Power entering the system (W)
$\dot{E}_{\text{out}}$	Power leaving the system (W)
$\dot{m}_{\text{a}}$	Air mass flow rate (kg/s)
h	Enthalpy (J/kg)
c_p	Specific heat capacity at constant pressure (J/(kg·K))
A	Cross-sectional area of the liquid reservoir (m)
U	Total internal energy (J)
c_v	Specific heat at constant volume (J/(kg·K))
X	Fluid displacement (m)
$\dot{X}$	Fluid displacement rate (m/s)
V_0	Air Initial volume in the reservoir (m^3)
h_0	Initial volume of the fluid (m)
R_x	Specific gas constant for air (J/(kg·K))

Chapter 1 - Introduction

1.1 Background and Motivation

Microfluidic technology creates new opportunities for research and development across diverse fields that conventional bulky laboratory methods cannot achieve [1]. Its key advantages include precise fluid control, compact design, high throughput, and reduced reagent consumption. Biotechnology [2], chemical synthesis [3], soft microrobotics [4], environmental science [5], and many other fields benefit from this technology. Improving the accessibility of microfluidic platforms and their components can further advance the field by enabling broader participation and research [6, 7].

The growth of open-source (OS) hardware has expanded access to scientific instruments, particularly in resource-limited laboratories that lack access to commercial technologies. Open-source approaches enable researchers from diverse backgrounds to create, adapt, and share laboratory tools tailored to their needs. These approaches complement traditional commercial systems by promoting openness and participation while providing broader access to technologies designed to deliver performance comparable to the commercial devices [8–10]. In microfluidics, the development of easy-to-use and publicly shared tools has gained increasing attention, with ongoing efforts to improve the adaptability and affordability of components required for microfluidic research [6, 11].

The actuation devices used to control flows within microchannels are critical components in microfluidics, as they greatly influence the performance, stability, and usability of microfluidic systems [12]. The selection of an appropriate actuation method is determined based on the specific requirements of the application. Most microfluidic systems are classified into two categories: passive and active systems [13]. For example,

in applications involving pneumatic actuation, fast response and precise control over low pressure ranges are essential for active microfluidic devices [14, 15]. In contrast, passive devices typically rely only on stable and higher pressure [16].

Compared to other actuation methods, pressure pumps are notable for their high performance, which meets the requirements of a wide range of microfluidic applications. These pumps offer smooth, pulse-free flow, precise control and fast response to pressure changes, and a low risk of contamination in microfluidic chips [17]. Pressure pumps operate by regulating the supplied compressed air to a user-defined pressure. The regulated air then pushes fluids from a container to a microfluidic chip. Expanding access to this precise and vital tool for the microfluidic field remains an active area of development. Thus, improving the accessibility of pressure pumps has the potential to benefit research in the microfluidic field, particularly in light of the rapid growth of active microfluidic systems and the emerging use of digital twins in microfluidics [18].

1.2 Problem Statement

Active microfluidic systems impose strict requirements on flow control, including fast response, high stability, and precise pressure regulation. Although various actuation approaches exist, the rise of active microfluidic systems has increased the demand for pressure pumps, which meet the performance specifications required by these applications [19]. However, commercial pressure pumps are often expensive and restricted to well-equipped laboratories, excluding many researchers who could benefit from these technologies. Moreover, active microfluidic systems that rely on a feedback loop require actuators that can be customized and integrated into their setup. This is challenging with commercial systems, which are typically provided as "black box" systems. Several studies have introduced open-source pressure pumps at a fraction of the cost of commercial

devices. Nevertheless, most of these designs are primarily tailored for passive microfluidic applications, as they focus on achieving stable pressure control while overlooking the response time required to reach the desired pressure [20–22]. Fast response time is essential for active microfluidic applications. Thus, a low-cost pressure pump capable of fast pressure changes is still lacking.

In addition, although dual-valve control designs have been discussed in the literature [23–25], their application in pressure regulation for microfluidic platforms has not yet been thoroughly explored or documented. Microfluidic systems operate under pressure conditions different from those of industrial applications. Microfluidic devices typically require relatively low pressures (below 2 bar) and demand much higher precision, on the order of a few millibars ($\approx$ 2 mbar). Commercial dual-valve regulators that exhibit characteristics suitable for microfluidic applications do not disclose their design or operating principles. Therefore, users cannot improve, tune, or modify these systems to meet the specific pressure requirements of their applications, which limits their integration in customized closed-loop systems. Such customization is essential for active microfluidic systems that use feedback loops.

Furthermore, the fundamental principle of microfluidics is miniaturization, yet most pressure pumps require a bulky external pressure source, which contradicts this objective. Therefore, there is still a need for an integrated, portable pressure pump that can be easily carried and used anywhere to generate and regulate pressure without the need for laboratories with specialized infrastructure.

1.3 Research Question

How can an open-source, all-in-one pressure generation and regulation unit be performance-tuned to interface efficiently with active microfluidic devices while maintaining low cost, portability, and short pressure-settling times ?

1.4 Objectives

1. Review and compare various actuation devices commonly used in microfluidics by evaluating key performance indicators (KPIs), including power, response time, stability, efficiency, density, and cost.
2. Build a compression unit that is compact and cost-efficient, capable of supplying the required pressure to the regulator.
3. Develop a pressure regulator optimized for microfluidic systems and openly share its design and working principle, instead of relying on the commercial pressure regulators that are primarily tailored for industrial applications.
4. Develop a control strategy for the regulator to achieve accurate pressure control with fast settling times suitable for active microfluidic platforms. Implement the controller on an accessible microcontroller and design it to be easily replicated and adapted by users without unnecessary complexity.
5. Experimentally evaluate the performance of the integrated pressure pump and conduct a comparative evaluation of its pressure regulation characteristics against a commercial regulator.

1.5 Contribution

The pressure pump proposed in this work offers a low-cost solution ($\sim$ \$650) compared to both commercial ($>$ \$6000) and open-source solutions ($>$ \$2000) reported in the

literature, while uniquely integrating a compact compression unit with a dual-valve pressure regulator suitable for active microfluidic applications. The regulator developed here can operate using a small compression unit that supplies approximately 10 psi and 1 L/min, whereas many commercial pressure regulators require a higher capacity external pressure source. Experimental comparison with the commercial Marsh Bellofram T2000 regulator demonstrated that the developed regulator provides comparable pressure regulation accuracy of about ±0.01 psi (±0.7 mbar) from the set pressure, while achieving faster settling times($\sim$ 100 ms vs. $\sim$ 200 ms), a more compact design ($\sim$ 120 cm^3/0.3 kg vs. $\sim$ 400 cm^3/1.35 kg), and a lower price ($\sim$ \$250 vs. $\sim$ \$1000).

This work is publicly shared and designed to be easily replicable, improving the adoption of the pressure pump that is compatible with active microfluidic applications in laboratories with limited infrastructure. This could support education and research, and also contribute to the advancement of active microfluidic systems by enabling wider participation in the field.

1.6 Dissertation Structure

Chapter 2 presents a literature review of microfluidics, including its fundamental principles, physical basis, and representative applications. It also reviews the various actuation systems employed in microfluidic systems and compares them using key performance indicators (KPIs). This chapter also includes an overview of how dual proportional solenoid valve control has been used in the literature and the control approaches applied to these systems.

Chapter 3 provides the methodology followed in developing the pressure pump. It begins by presenting the Simulink model used to analyze and represent the system.

Subsequently, the hardware assembly is presented, including the compression unit, the regulator system and the electronic circuit. This chapter also outlines the software implementation and provides a straightforward tuning procedure for the PID controller. Finally, it describes the procedure followed to compare the performance of the developed pressure regulator with the commercial Marsh Bellofram regulator.

Chapter 4 presents the results and performance evaluation of the developed pressure pump. It also includes the characteristics of the developed regulator compared to the commercial one, as well as a comparison between the integrated pressure pump and existing commercial and open-source pressure pumps.

Chapter 5 provides the conclusion by summarizing the major outcomes of the conducted research. It further discusses the limitations of the developed system and offers suggestions for future enhancements.

Chapter 2 - Literature Review

The literature is structured into four main sections. Owing to the multidisciplinary nature of microfluidics, Section 2.1 introduces the fundamental principles of microfluidics. This section offers an overview of the field and its potential across various application domains, and it provides a common foundation for readers from different backgrounds to follow the microfluidic concepts addressed in this thesis. Section 2.2 reviews representative actuation systems used in microfluidics and compares their advantages and limitations. Section 2.3 focuses on pneumatic systems, discussing their distinctive characteristics and highlighting their advantages for active microfluidic systems. Section 2.4 presents a critical analysis of the actuation methods and the available pressure pumps, through which the research gap addressed in this thesis is identified and discussed.

2.1 Principles and Applications of Microfluidic Technologies

Microfluidic systems manipulate fluids in minuscule volumes within fabricated microscopic channels, typically tens to hundreds of micrometres in size. The development of microfluidic systems originated from several major domains: molecular analysis, molecular biology, and microelectronics. Firstly, the chemists' successes in analyzing molecular samples in small tubes inspired them to advance the field by further miniaturizing the systems and expanding their applications to more areas. In addition, the revolution in genomics and DNA sequencing shifted the focus towards microfluidics. This revealed distinct new potentials in these areas. Finally, the fabrication techniques for microelectronics, such as photolithography applied to Micro-Electro-mechanical Systems (MEMS) technologies, initially inspired the same manufacturing process for microfluidics on silicon or glass substrates. This approach functioned at first, but later scientists switched to polydimethylsiloxane (PDMS) as it is more efficient for biological use [26]. Since then,

the field has expanded, where some scientists concentrate on evolving microfluidic devices and tools, while others study the fundamentals behind this technology.

This section provides an overview of the fabrication methods used for microfluidic devices and the fundamental physics principles applied in microfluidics. It also illustrates the two main types of microfluidic chips: active and passive approaches. Droplet-based microfluidic techniques are then introduced. Finally, examples of real-world applications of microfluidic technology are presented.

2.1.1 Microfluidic Devices Fabrication

Photolithography was the first method employed to manufacture microfluidic devices [27–29]. However, this traditional technique has several constraints, such as high cost, long processing time, and limited control over channel geometry. It is also restricted to certain types of materials (silicon, quartz, or glass) that may be undesirable for certain applications due to their material properties and contamination risks [29].

Following this method, soft lithography was developed and gained widespread adoption due to its significant contributions to this field. Soft lithography relies on elastomeric materials, most commonly polydimethylsiloxane (PDMS), for fabricating microfluidic devices. Soft lithography transfers patterns from master devices using several techniques, including microcontact printing (μCP), replica moulding (REM), microtransfer moulding (μTM), micromoulding in capillaries (MIMIC), and solvent-assisted micromoulding (SAMIN). These techniques are discussed in detail in the study done by Xia and Whitesides [30].

PDMS possesses several unique and advantageous characteristics. It is affordable, and it has a shear modulus of 0.25 MPa and an approximate Young's modulus of 0.5 MPa.

Its modulus can be easily adjusted with the curing temperature. This elastomeric property allows PDMS to conform to a surface and establish atomic-level contact that is beneficial in creating and sealing microfluidic devices. It is also non-toxic and widely available at reasonable prices from commercial sources. It has an optical transparency of around 300 nm, which enables observing droplets. Although it is intrinsically hydrophobic (with a water contact angle of 110°), the surface of this material can be changed to become hydrophilic (with a water contact angle of about 10°) by brief exposure to an oxygen plasma. Once oxidized, it can effectively attach and seal to a wide range of substrates, either reversibly or irreversibly [31].

Owing to the importance of polymeric microfluidic devices, several works have been introduced to develop their fabrication methods. Scott and Ali [32] provide a review that summarizes the recent approaches used in manufacturing polymer microfluidic devices. The review lists two main categories: mould manufacturing methods (such as micro-cutting, ultrasonic machining, and others) and replication methods. Replication methods are further divided into two main approaches: low-volume production techniques (including soft lithography, lamination, laser ablation, and 3D printing) and high-volume production techniques (including hot embossing, injection moulding, and film or sheet operations).

2.1.2 Nanoliter-scale Fluid Dynamics

In contrast to microelectronics, the fundamental physics behind the microfluidics systems is dramatically influenced by the change in the size scale of the channels. Fluid motions are generally governed by the Navier–Stokes equation, which is derived from Newton's second law equation for motion applied to fluid dynamics:

$$\rho\left(\frac{\partial \mathbf{u}}{\partial t}+\mathbf{u}\cdot\nabla\mathbf{u}\right)=-\nabla p+\mu\nabla^2\mathbf{u}+\mathbf{f} \tag{2.1}$$

where ρ is the fluid density, $\mathbf{u}$ is the velocity, p is the pressure, μ is the dynamic viscosity, and $\mathbf{f}$ represents body forces. However, in microfluidics, inertia is often neglected compared to viscous forces, as flow tends to be laminar. Eliminating the nonlinear part from equation 2.1 will result in the Stokes equation (Equation 2.2):

$$0=-\nabla p+\mu\nabla^2\mathbf{u}+\mathbf{f} \tag{2.2}$$

Additionally, under certain conditions, including steady, laminar flow in microchannels [33], the Stokes equations can be simplified to the Hagen-Poisseuille law (Equation 2.3) [34], where the pressure drop is directly proportional to the flow rate based on the hydraulic resistance of the channels. The hydraulic resistance depends on the properties of the system (e.g., channel dimensions, fluid viscosity).

$$\Delta p = R_{chip}Q \tag{2.3}$$

where Δp $[Pa]$ is the pressure differential, R_{hyd} $[Pa\cdot s/m^3]$ is the hydraulic resistance and Q $[m^3/s]$ is the volumetric flow rate.

Microfluidic systems are affected by a diverse set of physical phenomena. Thus, dimensionless numbers are significant and widely adopted in microfluidics as they reveal the dominant forces and transport phenomena by expressing the ratio between these effects. Table 2-1 provides an overview of these numbers adopted from research done

by Squires [35].

Table 2-1 Essential dimensionless numbers in microfluidics

Symbol	Dimensionless Number	Ratio	Significance
Re	Reynolds	$\frac{\rho U_0 L_0}{\eta}$	inertial / viscous
Pe	Péclet	$\frac{U_0 L_0}{D}$	convection / diffusion
Ca	Capillary	$\frac{\eta U_0}{\gamma}$	viscous / interfacial
Wi	Weissenberg	$\tau_p \dot{\gamma}$	polymer relaxation time / shear time
De	Deborah	$\frac{\tau_p}{\tau_{\text{flow}}}$	polymer relaxation / flow time
El	Elasticity	$\frac{\tau_p \eta}{\rho h_l^2}$	elastic effects / inertial effects
Gr	Grashof	$\frac{\rho U_b L_0}{\eta}$	Re for buoyant flow
Ra	Rayleigh	$\frac{U_b L_0}{D}$	Pe for buoyant flow
Kn	Knudsen	$\frac{\beta}{L_0}$	slip length / macroscopic length

The Reynolds number (Re) describes how inertial forces compare to viscous forces. The Péclet number (Pe) implies the importance of convective and diffusive transport. The capillary number (Ca) expresses the significance of interfacial tension. The Deborah, Weissenberg, and elasticity numbers (De, Wi, and El) describe elastic effects caused by deformable micro-structural elements such as polymers. The Grashof and Rayleigh numbers (Gr and Ra) represent density-driven flows. Finally, the Knudsen number illustrates the importance of non-continuum molecular effects.

For instance, the low value of the Reynolds number indicates that viscous forces

dominate over inertial forces in the system. This dominance results in laminar flow, which is usually observed at the microscale. The capillary number (Ca) is a significant dimensionless number for microfluidic devices. It is particularly essential in systems with a mean continuous phase velocity because it compares the relative importance of viscous stresses to surface tension forces. In droplet-based microfluidic applications, the value of interfacial tension is influenced by the amount of surfactant molecules on a surface. If the concentration of surfactants changes, it can cause the value of interfacial tension to vary, which can impact the formation, movement, and fusion of droplets [36].

2.1.3 Flow Control Approaches

After discussing the fundamental equations of microfluidic systems, the approaches used to control the fluid in the microchannel are discussed. These methods can be classified into two main approaches: passive and active. These approaches are widely implemented to provide various microfluidic operations such as sorting [37], separation [38], mixing [39, 40], isolation [41], droplet manipulation [13, 42, 43], and several other processes.

Passive

Passive devices depend on natural forces and the geometry of the microchannels in manipulating the fluid, without the need for external energy sources. These forces include capillary forces, viscous forces, gravity, surface tension, and other forces. Passive devices are commonly employed in numerous microfluidic applications because of their affordability, simplicity of fabrication, and ease of use. However, they require a larger channel geometry, which results in a larger footprint compared to active platforms. In addition, they function as an open-loop system, offering limited control over the flow, and are sensitive to external disturbances [44].

Active

On the other hand, active devices rely on external forces such as controlled pressure [14], electric [45], and magnetic fields [46]. These systems incorporate sensors and controllers that operate in a closed-loop system, as shown in Figure 2.1, and sometimes rely on the dynamic system model [47–49]. As a result, active systems provide more flexibility, enabling more precise and faster flow control, as well as providing better resilience against external disturbances.

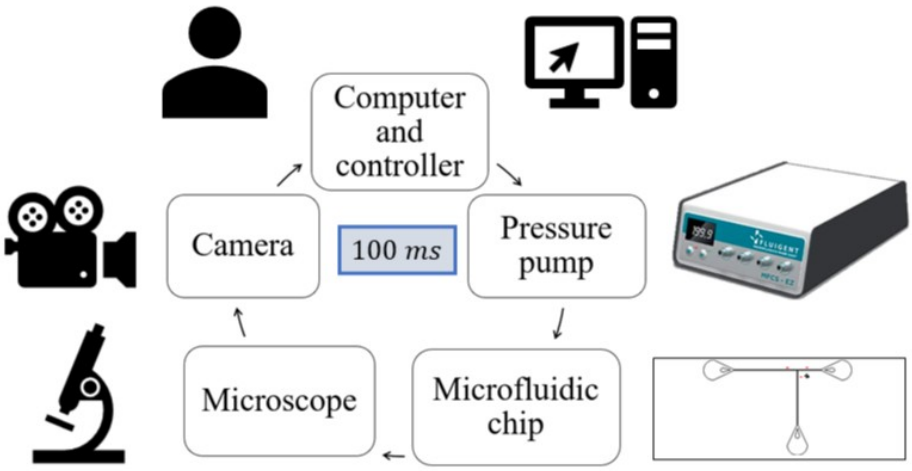

Figure 2.1 Diagram illustrating the loop for an active microfluidic system, integrating camera and microscope to provide feedback input to the control system [15].

2.1.4 Microfluidic Droplets

One of the major domains that involves passive and active approaches in microfluidic applications is the generation and manipulation of droplets in microchannels. The manipulation of droplets within microchannels has gained attention because of the need to generate droplets of precise sizes for material science purposes and the desire to perform chemical or biochemical reactions in small volumes [50, 51]. Droplet microfluidics offers

several unique benefits, including less usage of reagents, shorter reaction times, and, most importantly, reducing the risk of contamination. This is because in droplet microfluidics, the reagents are encapsulated within the droplets, which eliminates direct contact with the channel's surface. This reduces contamination risks and mitigates reagent absorption by PDMS materials [52].

Manipulating droplets in microchannels introduces more complex physics compared to single-phase flows due to the presence of interfacial tension. This phenomenon and its variation should be taken into account in the modeling because they lead to nonlinearity in the system [53]. Interfacial tension can be represented as a force per unit length present at the boundary between two fluids with a magnitude of γ (N m^{-1}). Alternatively, it can be described as an energy per unit area (J m^{-2}) that leads the system to minimize the total surface area and reduce the free energy of the interface.

Passive Droplets Manipulation

Droplet formation is the initial stage in droplet-based microfluidic systems. Achieving precise control over the size, volume, and generation frequency is essential to produce uniform and monodisperse droplets and particles. Monodisperse droplets are critical for many microfluidic applications [44]. Generating droplets can be accomplished using passive or active methods, and both present distinct advantages and drawbacks.

In the passive approach, the parameters mainly impacting the formation of droplets include the geometry of channels, viscous forces resulting from flow dynamics, and interfacial tension [54]. Three main passive approaches for generating droplets have been developed based on these physical mechanisms: cross-flow (T-junction), flow-focusing, and co-flow, shown in Figure 2.2 [2, 55].

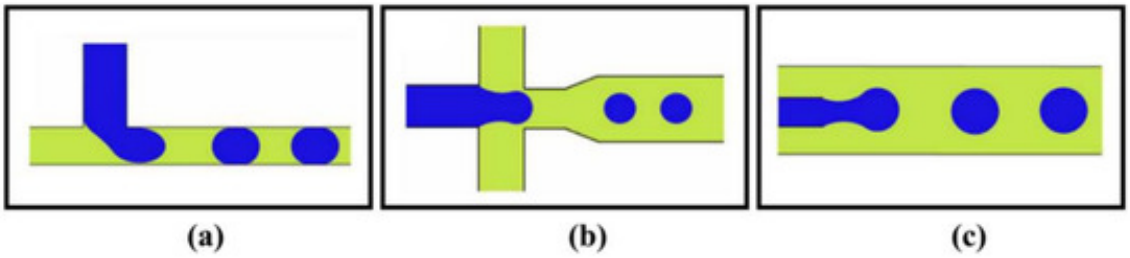

Figure 2.2 Schematic presenting three passive approaches to generate droplets in microfluidic devices (a) cross-flow, (b) Flow-focusing, (c) Co-flow [2].

Thorsen et al [56] were the first to report droplet formation in a T-shaped device. Pressure-controlled flows in microchannels are used to create droplets of water in oil streams. As shown in Figure 2.2 (a), two phases flow through two orthogonal channels, and droplets form upon their intersection. Garsteck et al [57] identified two regimes that occur when adjusting the parameter: squeezing and dripping regimes. The dripping behaviour takes place when the capillary number is high and the geometric ratio, the ratio of channel width, is minimal. While the squeezing regime happens when the capillary number is very small, and the geometry ratio is around 1. In addition, the jetting regime was later discovered at very high capillary numbers. Shen et al. [58] conducted a comprehensive study of these regimes, explaining their physical principles.

The flow-focusing device was introduced by Anna et al. [59], and Dreyfus et al. [60]. This method is shown in Figure 2.2(b), where the dispersed flow is injected in a central channel between two counter-continuous flows. The continuous flow squeezes the dispersed flow, leading to the production of droplets. The size of the droplets can be controlled by adjusting the flow of the fluids and by changing the geometry of the channels. By altering the parameters, four regimes were additionally studied in the flow-focusing device, including squeezing, dripping, jetting, and thread formation. Compared to the cross-flow configuration, the droplets produced by the flow focusing design are smaller

in size and exhibit a more spherical shape, resulting in less contact with the channel walls, which makes it more efficient for high-volume production [61].

The co-flow device was early adopted in microfluidics by Cramer et al. [62]. As illustrated in Figure 2.2(c), two immiscible streams flow in parallel. The dispersed stream flows through an inner channel that is surrounded by continuous flow. This causes the formation of the droplet due to the shear force at the interface. Two main regimes are identified: dripping and jetting. In dripping, droplets directly split off near the inner channel, whereas in jetting, a flow thread forms before the droplet detaches.

Once droplets are formed, they are carried through microfluidic channels by the carrier fluid. Two-phase flows have garnered significant interest and attention. These flows can be classified into two types: bubbly flows and slug flows. In bubbly flows, the droplets are smaller than the channel size. Drops usually flow at the same speed as the carrier fluid, and they follow the streamlines of the external phase. This means that drops closer to the channel centerline will have faster velocity than those closer to the edges, and drops arriving at a bifurcation will take the path that the carrier fluid dictates. In slug flows, droplets occupy most of the channel's cross-section. From a hydrodynamics perspective, the slug flow scenario is more intriguing because the flow is influenced by capillary effects and the deformability of the drop interfaces.

In passive systems, inconsistencies in droplet formation can occur due to factors such as device-to-device variations, ambient conditions, and fluctuations in surface chemistry. However, active mechanisms can be applied to the same passive geometries to overcome these limitations. Active systems rely on programmable systems or integrate closed-loop control based on feedback from sensors. This offers flexible and precise control over droplet size [63]. Figure 2.3 presents a system developed by Naz et al. [64] that

significantly improved the consistency against disturbances and the stability of droplet length. The system employs a passive method using a T-junction to generate droplets while integrating a real-time pressure sensor and a PI controller to regulate the proportional valve in a closed-loop system.

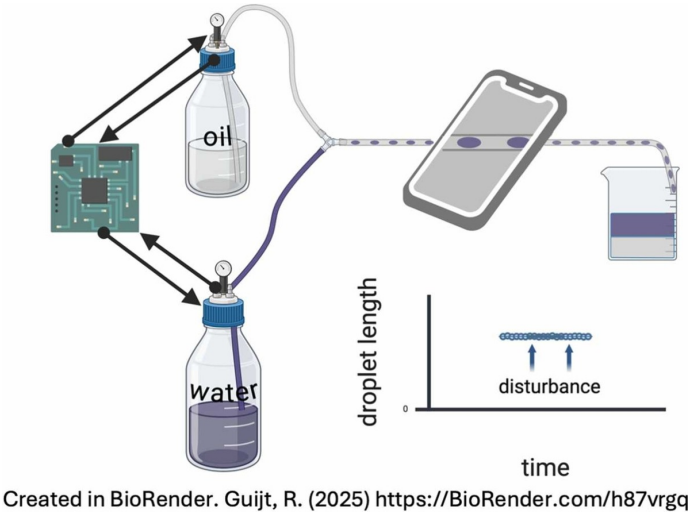

Figure 2.3 A closed-loop control system for droplet generation using the passive T-junction method [64].

Active Droplets Manipulation

Hebert et al. [7] conducted a comprehensive review of active approaches to manipulate droplets. The study emphasized that to enhance the adoption of microfluidics, it is necessary to facilitate its implementation, especially for people outside the microfluidic field. The importance of modularity and automation in microfluidics is highlighted, which can be achieved by adopting active systems to help reduce the knowledge barrier for users. Figure 2.4 outlines the types of active microfluidics presented in the review. The study classifies the active control into three types: single manipulation, single application, and platform studies.

Droplet manipulations, such as generation [65, 66], merging [67], mixing [68–70],

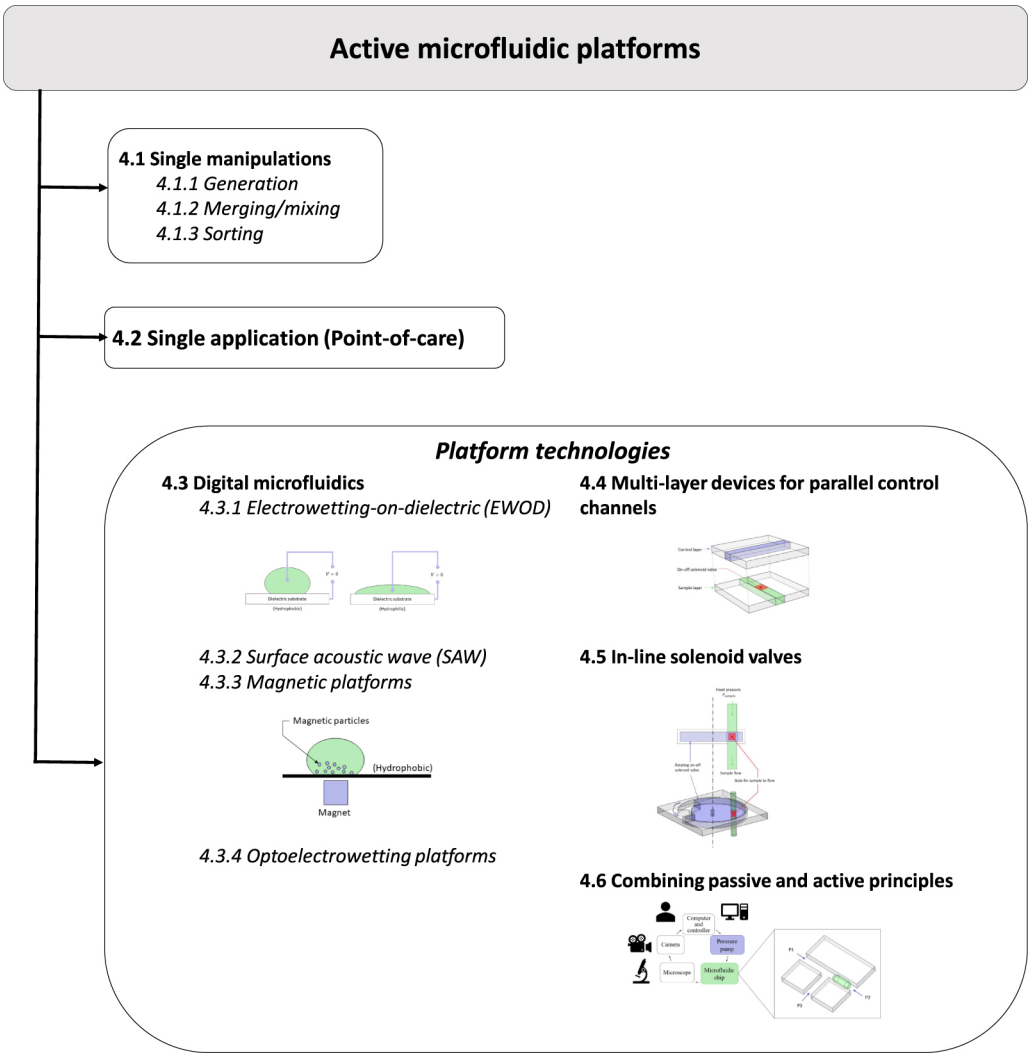

Figure 2.4 Summary of key active microfluidic platforms [7].

and sorting [71–73], are often automated using a variety of approaches that involve the application of an external force. Single-manipulation studies focus on a single task. For example, a chip dedicated only to generating droplets.

Single applications, such as Point-of-care (POC) platforms, are primarily adopted in diagnosis technologies. These devices have a significant advantage, as the users simply provide the sample as input, and the device delivers the result as output [74–76]. However, these technologies are still limited to a single application, lacking the flexibility for diverse microfluidic tasks.

In contrast to droplet microfluidics, which manipulates droplets in a microchannel, digital microfluidics handles larger droplets on an electrode array. Several strategies have been developed that offer strong potential for manipulating droplets. These techniques include Electrowetting-on-dielectric (EWOD) [77], Surface-Acoustic-Waves (SAWs) [78], magnetic forces [79], and optoelectrowetting [80].For more details, the references associated with the techniques provide comprehensive reviews.

In addition, multi-layer platforms consist of at least two layers. A microchannel network contains samples within a single layer. Another layer is used for control functions. The flow of samples within the micro-channel network is actively regulated by digitally actuated on/off valves. Examples of such valves: Quake's valves [81], Wax valves [82], In-line solenoid valves [83] .

Last but not least, combining passive and active principles offers numerous advantages and results in higher efficiency compared to traditional methods. In these systems, flow is manipulated in a passive way but regulated through a closed-loop system based on visual feedback [84]. For instance, Wong et al. [85] developed an approach to handle individual

droplets by driving electropneumatic transducers using computer vision and feedback. Their method offers enormous potential for allowing droplet microfluidics as a technology for a wide range of applications. The developed software, RoboDrop, allows users to interact with individual droplets using the computer mouse. RoboDrop can manufacture, combine, divide, trap, and sort drops in real time. This provides a single microfluidic droplet device that might be employed to execute multiple functions.

These articles provide more detailed information on several passive and active methods for mixing and merging droplets in microfluidic systems. [39, 86–89].

2.1.5 Real-World Microfluidic applications

Microfluidics has unlocked new potential and possibilities across a wide range of real-world applications. In biology, microfluidics is employed for cell analysis [90], drug discovery [91, 92], lab-on-chip [93], and many biotechnological technologies [94]. In chemistry, microfluidics is increasingly applied in material synthesis [95–97] due to its precise control over reaction processes. Microfluidics is additionally used in environmental monitoring, such as for water analysis [98–100]. In this section, selected examples from the literature that adopt microfluidic technology in their applications are presented.

Cell Analysis

Single-cell isolation is a critical first step before time-course analysis of individual cells. According to Ota et al. [101], traditional methods to isolate cells exist and are widely used. However, the utilization of microfluidic technology has dramatically improved this field. A method for single-cell isolation is performed using a glass microfluidic device with semiclosed microchannels, shown in Figure 2.5. The study demonstrates a way to

isolate single cells of the highly motile microalgae Euglena gracilis using semiclosed microchannels with only liquid flow. Using Raman microscopy, the separated single cells were then identified in isolating channels and continually cultured to monitor the production of subcellular granules consisting of paramylon, a polysaccharide metabolite produced via photosynthesis.

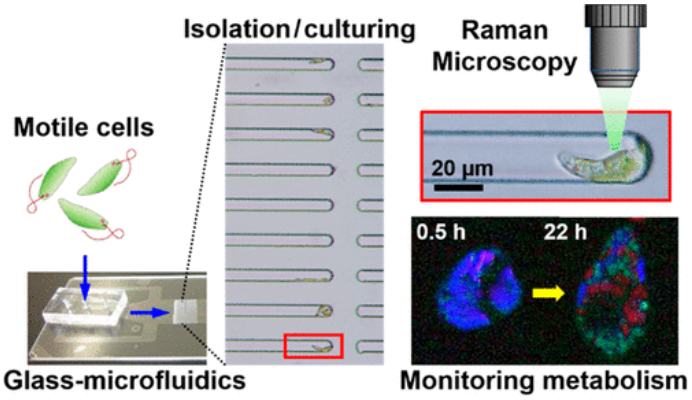

Figure 2.5 Isolating single cell E.gracilis using a microfluidic chip [101].

Moreover, Ma et al. [102] developed a method capable of analyzing over 1,000 single cells in a single experiment. As shown in Figure 2.6, in a microfluidic device, single cells were encapsulated with RT-PCR reagents and lysis buffer in nanoliter (nL) droplets. The cell suspension and reagents were delivered by two separate channels and combined just before the oil emulsion. The cells lysed quickly within their separate droplets. The droplets were collected in a PCR tube and subjected to thermal cycling. The cells then contained fluorescent amplification products and were loaded into microchambers designed to trap droplets in monolayers for analysis using an automated imaging platform. In addition, a systematic review of current developments and prospects in bacterial single-cell research using microfluidics has been presented by Guo et al. [103].

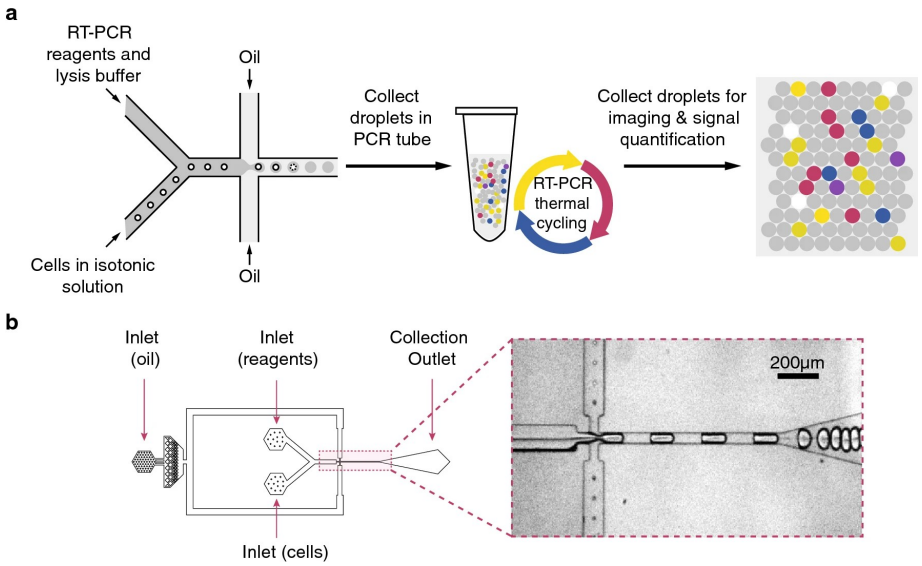

Figure 2.6 Overview of the droplet microfluidic process for single-cell RT-PCR [102].

Drug screening and Discovery

Vedula et al. [104] engineered a microfluidic platform that replicates the kidney-specific active function of reabsorption. The device architecture comprises a porous membrane with submicron surface topography, which enables the screening of new drugs for potential kidney toxicity without the need for animal models. Kwak et al. [105] developed an in vitro tumor model to recapitulate the tumor microenvironment. The device is named tumor-microenvironment-on-chip (T-MOC), and it consists of 3-dimensional microfluidic channels. Tumor cells and endothelial cells are cultured within an extracellular matrix under perfusion of interstitial fluid. The study demonstrated that T-MOC is capable of mimicking the complex transport process within the tumors.

Moreover, Shourabi et al. [106] designed a microfluidic chip presented in Figure 2.7. The device is capable of subjecting cells to controlled shear stress, osmotic pressure gradients, and drug concentrations. This chip is developed to be adopted as a general

platform for several cell analysis tests.

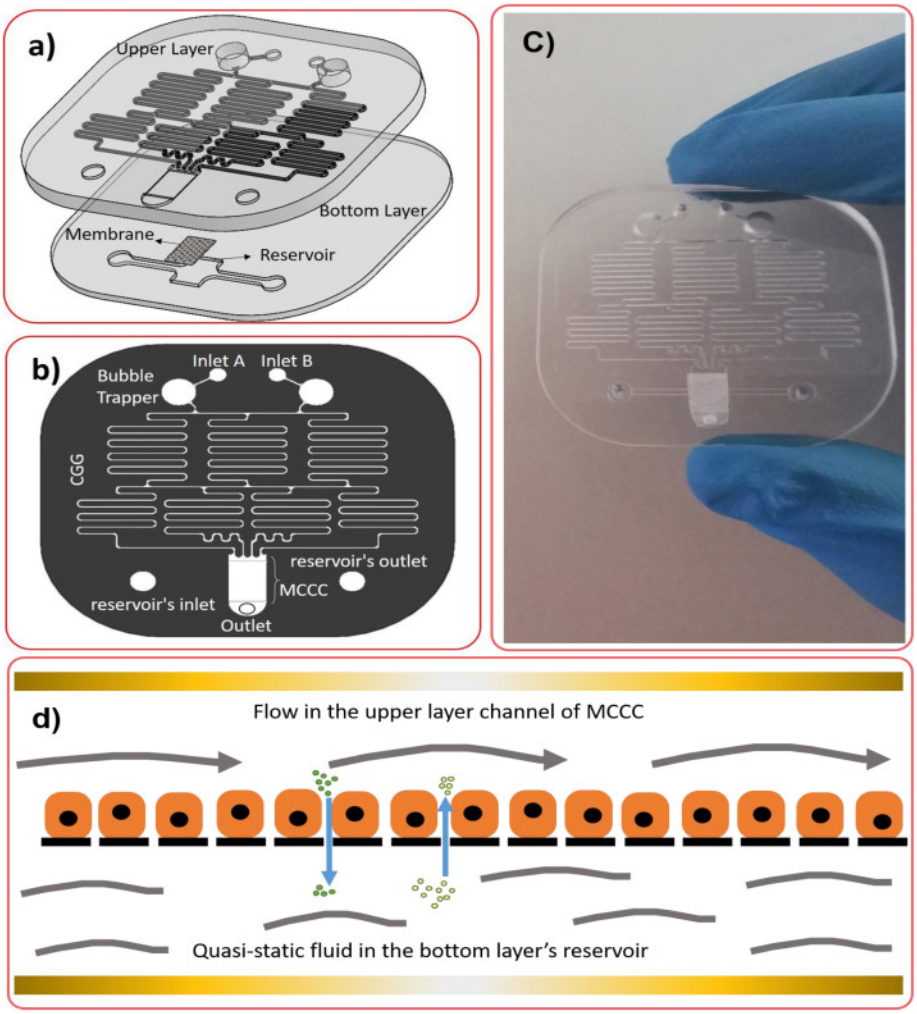

Figure 2.7 Functional overview of Microfluidic chip that mimics shear stress and osmotic gradients on cell monolayers [106].

Material Synthesis

Kwon et al. [107] developed a microfluidic system for the continuous production of ZnSe/ZnS quantum dots (QDs). The device provides control over the size and the quality of the dots by adjusting the flow rate of the solutions. These quantum dots were then successively used in light-emitting diodes (LEDs). Furthermore, Liang et al. [108] demonstrated that microfluidic technology has enabled the synthesis of the single-crystal

NCM811 cathode from highly reactive Ni0.8Co0.1Mn0.1(OH)2.

2.2 Actuation Methods for Microfluidic Systems

The work presented in this chapter corresponds to a review article submitted to the journal Heliyon: Zein, M.; Kelouwani, S.; Hébert, M. A Comparative Review of Actuation Methods for Microfluidic Systems. Heliyon 2025, currently under minor revision.

A microfluidic system typically consists of various components, including the microfluidic chip where operations take place, modules for adding reagents and samples, mechanisms for fluid movement throughout the chip (such as pumps and valves), and other necessary devices depending on the application. Although substantial research has focused on the functionality and performance of microfluidic chips, actuation systems are often treated as external components, with comparatively fewer studies focusing on actuation devices. Nevertheless, the performance of microfluidic chips significantly depends on the actuation system and the mechanism employed to control the fluid within the channels.

The complex nature of microfluidic devices makes it necessary to implement actuation systems that perform reliably and are easy to use, as these factors improve the devices' efficiency and their adoption by end users. In many applications, the actuation system must meet specific performance requirements.

Microfluidic actuation systems can be categorized as either passive or active types. Several review articles have summarized academic research studies based on these categories, either passive [16, 109] or active [63, 110]. In contrast, this section reviews actuation solutions that are accessible to users, including commercial systems and components as well as open-source projects, and compares their characteristics based on a set of key performance indicators (KPIs) relevant to microfluidic applications. This

comparison aims to facilitate the selection of appropriate actuation solutions based on specific application requirements.

This section begins by introducing the set of key performance indicators (KPIs) used to evaluate microfluidic actuation systems. Next, representative actuation approaches are reviewed, starting with methods that utilize external forces, such as gravity and human-powered actuation. Then, microactuators are presented, highlighting their compact form. Subsequently, positive displacement methods are covered, including syringe pumps and peristaltic pumps, which are widely adopted in microfluidics. Since the focus of this thesis is on pneumatic actuation systems and their role in active microfluidic applications, these approaches are examined more thoroughly in the following section 2.3.

2.2.1 Key performance Indicator Framework

Table 2-2 outlines the main characteristics necessary for understanding and improving the performance of various actuation methods. KPIs offer a structured approach to analyze multiple systems, considering that each application prioritizes certain KPIs differently. An example can be found in microfluidic applications involving pressure control. Passive applications require a high and stable pressure source, while active applications depend on fast and precise pressure control. Moreover, point-of-care microfluidic systems require the system to be lightweight and compact while maintaining high efficiency. Density and cost ratios are used to contextualize the first four indicators (power, response time, stability, and efficiency). For instance, the power divided by the mass gives specific power, division by the volume gives power density, indicating power output per size, and division by the cost to assess power per dollar. Density is an essential factor in portable systems. The costs presented in this study are approximate to facilitate the comparison analyses, but they are subject to change.

Table 2-2 Key Performance Indicators (KPIs) for comparing microfluidic actuation platforms

KPI		**Description**
Hydraulic Power	Power	The primary function of the actuator is to provide hydraulic power to the system. The power output of the pump is the multiplication of flow rate with pressure ($\dot{W}_{hyd} = Q \cdot \Delta p$).
	Pressure	Higher pressure is important for systems with greater hydraulic resistance (e.g., passive microfluidics).
	Flow rate	Higher flow rates are required for high throughput or larger-scale applications (e.g., cell sorting).
Response time		Characterizes how fast the actuation adapts to a change in setpoint. Faster response time is essential for active systems requiring fast and frequent modifications (e.g., active microfluidics).
Stability		Minimizing the variations with time about the setpoint is essential for passive systems requiring a smooth and continuous operation.
Efficiency		Quantifies the conversion between the input power and output hydraulic power. The actuation efficiency affects the overall system efficiency, especially for autonomous systems using onboard energy sources (e.g., battery for portable systems).
Ratios	Density (mass and volume)	Affects the system's integration and portability. Specific weight and volume can be used to compare different solutions.
	Cost	Acquisition and maintenance costs (including expected lifespan). Affects the accessibility of the system to encourage its adoption for various applications.

2.2.2 External Force Actuation

Actuation methods that depend on external forces are discussed. The focus here is limited to systems actuated by human input or gravity. Human and gravity actuation methods often operate without electricity as their main source of energy. Thus, these methods are generally suitable for low-demand applications and often lack the level of performance and controllability required for active microfluidic applications. Other external-force actuation methods, such as centrifugal pumps, are not included in this section. Pertinent review articles provide more information on centrifugal actuation methods: [111–115].

Human-Powered Actuation

Human-actuated pumps are typically developed in research articles as prototypes or open-source projects. Commercial pumps are rarely available because human-actuated pumps generally have limited performance that does not meet the requirements of many applications. Review articles providing thorough details of hand-operated microfluidic devices for point-of-care testing are presented by Park et al. [116] and Du et al. [117].

The advantages of using human force in actuating systems are their simplicity of construction, low cost, and independence from an external power source. These strengths are desirable for portable microfluidic applications. On the other hand, their drawbacks include limited hydraulic power, challenges in achieving stability, and difficulty in providing specific flow conditions. Although their response time is relatively fast, their drawbacks restrict their adoption in many applications.

Microfluidic pumps and valves actuated by fingers are presented by Park et al. [118]. The system is actuated by pressing and releasing a single button. The button is positioned between the pump and the switching valve, controlling the systems through a pneumatic-driven deformable PDMS membrane. Pressing the button compresses the PDMS, increasing the pressure in one chamber. The deformation will close one chamber and open the other, allowing the fluid to flow through the designated path in the switching valve. Releasing the button will allow the other chamber to open, directing the fluid through a different path in the switching valve. About 2-4 μL of volume is dispensed by a single finger push. The system performance is validated by performing nucleic acid purification.

Finger-actuated systems are enabled by advances in complex microfabrication techniques, which integrate different membranes and chambers in microfluidic chips. For example, these systems rely on the development of fluidic diodes that enable flow in one path and prevent backflow when the PDMS membrane is pressed. This technology also allows for generating pressure up to 75 mbar from a finger force [119].

For more finger-actuated projects suitable for analyzing blood, generating concentration gradients, and many more, refer to these studies: [120–124].

A simple syringe was used to inject the fluid by hand into the microfluidic device [125]. The design concept is similar to that of a syringe pump but much simpler, as the system operates manually without relying on a motor, a control system, or electric power. However, this comes at the expense of reduced flow rate accuracy. Nonetheless, the pump can be effective for certain applications, as it has demonstrated satisfactory sorting of particle size and platelets.

Moreover, Thurgood et al. [126] offer a new concept by using commercially available latex balloons to generate pressure for driving fluid from a vial to the microfluidic chip, as illustrated in Figure 2.8. The generated pressure and resulting flow rate are directly influenced by the balloon's wall thickness, material, and size. This proposed pressure pump is low-cost, easy to set up, and self-sufficient (it does not require a compressor, regulators, or electric power). The study presents results demonstrating the pump's performance across different operating scenarios. The pump was tested under various channel configurations, fluid viscosities, temperatures (which affect balloon wall elasticity), balloon fatigue over repeated inflations, chip outlet height, long-term pumping, and balloon wall thickness. The pump successfully enables fluid mixing and droplet generation. The droplet size can be controlled by manually squeezing the balloon, which rapidly changes the flow rate in the system. However, the accuracy provided by the pump is low, the maximum achievable pressure is limited, and the pressure drops with time as the balloon deflates.

Thus, the balloon membrane stores energy, which eliminates the need for electric power. This approach is similar to certain other pumps actuated by springs [127, 128].

Gravity-Driven Actuation

Gravity-actuated pumps rely on the weight of the liquid to create the pressure that drives flow. Water is the liquid typically used in such systems. Like human-powered pumps, these systems' key advantage is avoiding reliance on an electric power source.

One method of gravity actuation is the use of a water column to generate hydrostatic pressure. However, one of the major restrictions of these systems is their low pressure,

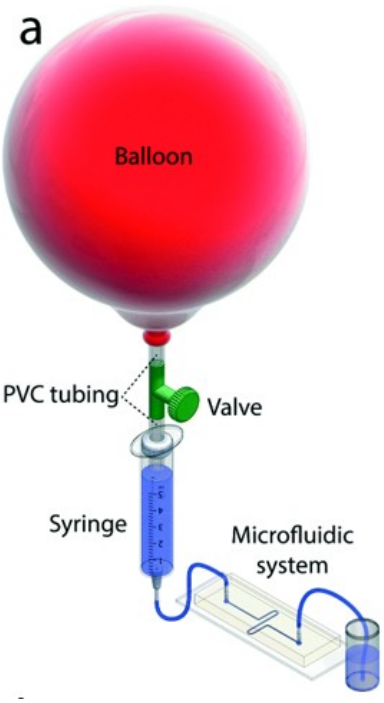

Figure 2.8 Schematic representing the working principle of the balloon pump (adapted from: [126]).

where a one metre column roughly generates 0.1 bar [129–134]. The hydrostatic pressure is directly proportional to the height of the water; thus, increasing the pressure will significantly affect the compactness of the device. A solution was proposed by utilizing a thinner water column, but this will influence the capillary forces and must be taken into account [135].

Another gravity-powered approach utilizing a syringe piston instead of hydrostatic pressure or manual actuation was proposed [136]. The system comprises a syringe, syringe holder, and loading masses. The loading masses are containers of the liquid to be delivered to the microfluidic chip. Although the system can achieve a stable high pressure of 7 bar for a long period (12 hours), it exhibits a slow response time when decreasing the pressure. Thus, this design may be applicable to passive microfluidic applications, but is restricted in active applications that require fast pressure control.

2.2.3 Microactuation

A brief discussion of microactuator pumps with small form factors is presented, including examples of both positive-displacement and pressure-driven microactuator pumps. For more in-depth information, the review articles [137, 138] offer a comprehensive overview of microactuation systems. The adoption of microactuator-based approaches in microfluidics remains limited due to the scarcity of both commercial and open-source projects. In addition, the complexity associated with integrating these technologies into applications further limits their adoption. Users with no background in microfluidics, such as biologists or chemists, face even more challenges when integrating microactuation systems into their applications. Nonetheless, microactuation approaches are highly advantageous for portable applications such as point-of-care. This review focuses only on off-the-shelf components and open-source microactuation systems, since implementing such systems described in research papers can be difficult for end users.

Microactuators produce significantly less power than macro-scale syringe and pressure-driven pumps. Nevertheless, their power meets the requirements of microfluidic systems. In fact, microfluidic devices generally demand high pressure and low flow rate. Despite the high pressure, the low flow rate results in a small hydraulic power (less than 0.1 mW), which can be supplied by microactuators. In addition, microactuator pumps can be better suited for active microfluidic devices, as they require less power compared to passive devices.

Bartels micropumps are commonly used commercial microactuators for microfluidic applications. These positive displacement pumps feature a double diaphragm pump

actuated by a piezoelectric element. They can drive both liquids and gases. Bartels offers the mp6 model, which can generate up to 5 mW of hydraulic power, and the BP7 model that produces up to 12 mW. The performance of these micropumps is influenced by inherent oscillation and noise.

Additionally, Bußmann et al. [139] developed a piezoelectric diaphragm micropump for transporting cells in microfluidic chips. The pump is capable of producing a backpressure of up to approximately 500 mbar and a flow rate of 12.5 ml/min (approximately 10 mW). After testing the effect of the actuation signals on cell transport, it was observed that utilizing hybrid actuation (which combines rectangular and sinusoidal waveform signals) improved transport efficiency and caused less damage to cells.

On the other hand, Wang et al. [140] developed a microactuator pump that adopts a pressure-driven approach rather than a positive displacement mechanism. The system consists of a piezoelectric microblower that generates high-pressure air flow. The air enters an in-situ liquid reservoir, pushing the liquid and precisely controlling its flow in microfluidic chips. Thus, these systems represent a promising solution for integrable microfluidic systems.

2.2.4 Positive-Displacement Actuation

The operating principle of positive displacement pumps generally involves holding a certain amount of fluid in a chamber and pushing it out using mechanical actuation [141]. Generating the mechanical force typically involves various mechanisms, including pistons, gears, motors, screws, or vanes. The type of mechanism used defines different types of positive displacement pumps. Such pumps are commonly employed in handling fluid

within microfluidic systems.

Referring to equation 2.3, the flow behavior in microfluidic systems driven by actuation methods depends on the pressure differential and flow rate. In positive displacement actuators, the flow rate is set as the independent variable, and the pressure differential is the dependent variable. Here, the two most commonly used positive-displacement pumps in microfluidics are reviewed: syringe pumps and peristaltic pumps.

Syringe Pumps

Syringe pumps are widely used in microfluidics, offering crucial advantages in diverse fields, such as chemical synthesis [107], drug delivery [106], and cell analysis [102]. Syringe pumps provide precise control over the flow rate. They are simple and user-friendly, even for non-experts in the field. Unlike pressure pumps, syringe pumps are cost-effective and more accessible for low-infrastructure laboratories, since they only require electric power to operate.

Figure 2.9 illustrates the working principle of syringe pumps. The electrically powered stepper motor rotates the lead screw, which in turn converts the rotational motion into linear motion. This motion is applied to the syringe plunger while the syringe body is fixed. The movement of the plunger produces a precise flow rate through the tube, driven into the microfluidic chip [142].

Despite their advantages, syringe pumps have limitations that restrict their adoption for certain microfluidic applications. The presence of persistent oscillations in their generated flow rate makes the use of syringe pumps undesirable for applications requiring high-precision flow control and monodisperse droplet generation. Korczyk et al. [143]

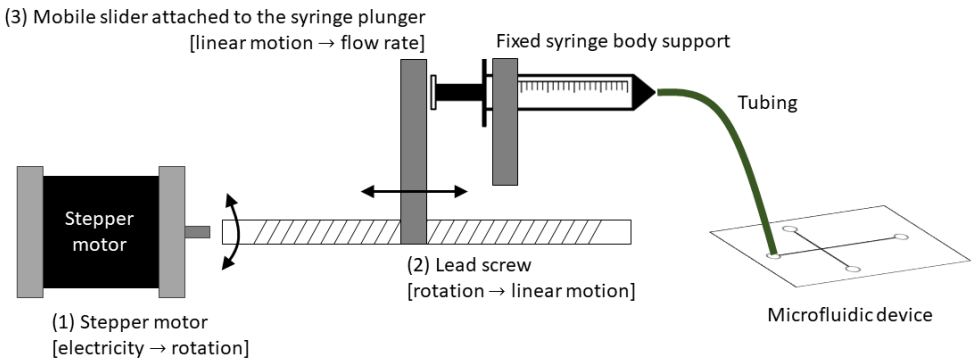

Figure 2.9 Schematic illustrating the operational mechanism of the syringe pump

demonstrated that syringe pumps generate more flow unsteadiness compared to pressure pumps. The study illustrated that the flow unsteadiness negatively affects the droplet volume consistency, which in turn affects the droplet dynamics and their manipulation in a microfluidic device. Additionally, Zeng et al. [144] compared the dynamic characteristics between the syringe pump and the pressure-driven system. The cause of the flow-rate fluctuation from the syringe pump was linked to the mechanical oscillations of the pump motor. Conversely, the stability of the flow from the pressure pump was greatly improved due to the absence of the periodic fluctuation caused by the syringe pump's motor.

The mechanical frequency induced by the mechanical operation of the syringe pump is described in Equation 3.1. The oscillation in the system can be reduced by adjusting the following parameters (flow rate, syringe diameter, Strouhal number), but they can not be fully eliminated.

$$f_{mech} = \frac{4 \cdot \overline{Q}_i}{\pi D^2 s} \tag{3.1}$$

where $f_{mech}[Hz]$ is the mechanical frequency of the syringe pump, $\overline{Q}_i[m^3/s]$ is the average inlet flow rate, $D[m]$ is the syringe inner diameter, and $s[m]$ is the pitch of the lead screw.

Another drawback of the syringe pumps is the limited volume of the syringe. Only the volume of a liquid enclosed in the syringe can be dispensed into the chip. In addition, the diameter of the syringe can directly impact the mechanical frequency. As indicated in Equation 3.1, larger diameters result in a lower frequency if the other parameters are held constant. Hence, selecting the syringe diameter can not be done randomly, as inappropriate selection can lead to an increase in the flow fluctuations and instability.

Zeng et al. [145] developed a mathematical model that explains how the frequency of the pump affects the amplitude of pressure fluctuations, introducing a dimensionless parameter known as the Strouhal Number. This parameter takes into account the pump frequency, channel geometry, and mechanical properties. It can be used to predict the performance of different microfluidic device setups. According to their findings, as the frequency of the pump increases and the elasticity of the channel decreases, the amplitude of pressure fluctuations decreases.

Syringe pumps are still widely used in various applications, such as calibrating highly repeatable flow rate sensors (e.g., using a micro-thermal sensing principle), regardless of their persistent oscillation. By averaging the measurement over long periods, the impact of the oscillations is minimized.

In Table 2-3, the key features of several syringe pumps available in the marketplace from different companies, as well as some open-source projects, are presented.

Lake et al. [146] presented a low-cost ($110) syringe pressure pump that uses

Table 2-3 Comparison of different types of syringe pumps

Model	**Company**	**Flow Rate**	**Accuracy (%)**	**Linear Force**	**Additional details**	**Price (USD)**
Pump 11 Elite	Harvard Apparatus	1.26 pl/min - 88.4 ml/min	±0.5	35 lbs	—	2500
Pump 11 PicoPlus	Harvard Apparatus	0.54 pl/min - 11.70 ml/min	0.35	35 lbs	—	2000
NE-300 Infusion	Darwin	12.2 nL/min - 20.95 ml/min	±1	18 - 35 lbs	Reproducibility: ± 0.1 %	400
Masterflex MFLX 74905-06	Avantor	0.54 pl/min - 88.8 ml/min	±0.5	30 lbs	Reproducibility: ±0.05	2500
Lake et al. [146]	Open-source	—	—	—	Feedback with pressure sensor	100
Czech et al. [147]	Open-source	0.01 - 10 ml/h	4	—	4 channels	700

feedback control to regulate the pressure into microfluidic chips. A widely accessible microcontroller (Arduino) and a pressure sensor were employed to implement a closed-loop control system, overcoming the limitations of commercial pumps (which generally operate in an open-loop manner). Two control algorithms, Bang-Bang and Proportional-Integral-Derivative (PID) controllers, were developed and tested. The Bang-Bang method maintained stable pressure within ±5% of the desired pressure, while PID provided ±1% pressure stability with a response time of less than 1 second. This performance rivals that of commercially available syringe pumps, which are relatively expensive and lack pressure feedback capabilities.

In addition, a portable and easy-to-use syringe pump capable of delivering a steady flow of fluids in microfluidic systems was presented by Zhang et al. [127]. The pump operates by using a compression spring (human-actuated) to generate the necessary pressure. The flow rate is regulated by passive valves located in the microfluidic chip. To demonstrate the pump efficiency and adaptability, tests with a microfluidic T-junction mixer and an inertial microfluidic chip for particle separation were conducted. Stable separation and accurate fluid mixing were accomplished. Thus, this design enables precise control over the flow, which is necessary for many microfluidic applications. In addition, relying on the spring enabled the systems to depend on external power applied by humans and to achieve full independence from electricity. Human-actuated systems are further discussed in Section 2.2.1.

Peristaltic Pumps

Another primary type of positive-displacement pump is the peristaltic pump. The operating principle of standard peristaltic pumps is illustrated in Figure2.10. The fluid

is confined in a flexible tube or hose. A rotating roller compresses the tube and pushes the fluid forward in a sequential manner: one roller traps the fluid, while the other passes over the tube, ejecting the fluid. The expansion of the tube behind the roller passively draws more fluid into the tube. The rotational motion is generated by a motor. By changing the rotational direction of the motor, bidirectional flow can be achieved.

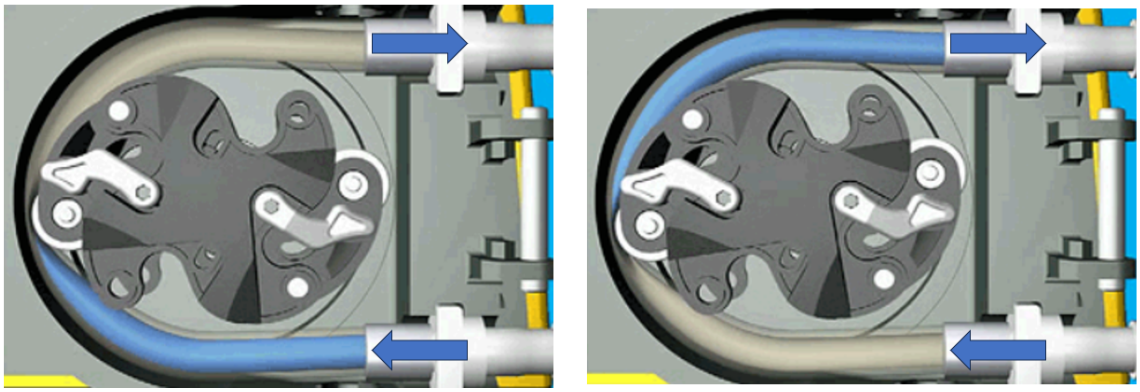

Figure 2.10 Schematic illustrating the operational mechanism of the peristaltic pump (adapted from “Peristaltic pump in motion" by Njmcca under CC BY-SA 3.0 via WikiMedia Commons)

The main advantage of the peristaltic pumps is their low risk of contamination, as only the inner surface of the tube comes into contact with the fluid. High sterility and cleanliness are required for certain microfluidic applications, particularly in the medical and food areas.

However, similar to the syringe pumps, peristaltic pumps exhibit continuous flow oscillation caused by the motor [148]. Equation 3.2 describes the relationship between the shaft rotational velocity and the number of rollers. The equation determines the period of main peaks in peristaltic pumps [149]. Secondary peaks are also observed due to mechanical interactions in the pump [149], but they are not included in this work.

$$T_i = \frac{2\pi}{n \cdot \omega} \tag{3.2}$$

where $T[s]$ is the period of the main peaks, $n[\ ]$ is the number of rollers per rotation, and $\omega[rad/s]$ is the rotation speed of the motor shaft.

Multiple peristaltic pumps are available on the market from different companies, offering various types, specifications, and price ranges. In addition, several open-source projects have been developed specifically for microfluidic applications. Behrens et al. [150] proposed a low-cost peristaltic pump that can handle small volumes of liquids in microfluidic chips for point-of-care diagnostics. The pump is easy to build because it is constructed using 3D printed components. The device was programmed using a widely accessible microcontroller (Arduino), providing precise control over a small amount of fluid up to 1.6 ml/min. This pump is suitable for a variety of applications involving precise measurement and fluid distribution in microchannels. It can also be used to apply forces mimicking physiological conditions for cellular studies.

Furthermore, Forouzandeh et al. [138] conducted a review summarizing numerous studies on the development and advancement of peristaltic micropumps. The study categorized different types of micropumps and analyzed critical performance parameters, such as operating frequency, stroke volume, and various actuation sequences. In addition, the actuation methods employed in micropumps, including piezoelectric, motor-driven, pneumatic, electrostatic, and thermal, along with their benefits and limitations in microfluidic applications, were discussed. However, one of the main disadvantages of micropumps is their challenging integration into systems due to the complex fabrication process.

2.3 Pneumatic Actuation for Microfluidics

Pneumatic systems provide numerous features that are desirable for many microfluidic applications, particularly for active microfluidic applications. These systems deliver highly stable and pulseless flow with fast response times. The development of pneumatic pumps and valves has advanced the field and contributed to many microfluidic tasks, such as droplet generation and trapping, particle sorting, etc. [151–155].

In contrast to the positive displacement systems (Equation 2.3), the pressure-driven system sets the pressure differential as the independent variable, while the flow rate is the dependent variable. Figure 2.11 illustrates the operating principles and additional components needed between the pressure pump output and the microfluidic chip. Pneumatic systems consist of pressure regulators to maintain control over the pressure of compressed air pushing liquid from the reservoir to the microfluidic chip. Compressed air is often considered external, as most commercial pumps require users to provide compressed air. The air-liquid interface in the vial avoids cross-contamination issues that can occur between liquid samples and pumps. Pressure pumps offer greater control over the pressure by relying on a microcontroller to generate a pressure signal that can be continuously adjusted to achieve the desired pressure defined by users. Thus, variations in physical parameters of the liquid samples (e.g., density, viscosity) do not have an impact on the system and do not require manual adjustment. Furthermore, pneumatic pumps provide versatility in managing various volumes, enabling control over multiple flows using only one pump.

Several studies have demonstrated the benefits of the pressure pump compared to other actuation methods. Pressure pumps outperform syringe pumps by generating droplets with less polydispersity at a standard T-junction, as demonstrated by the study done by Zeng

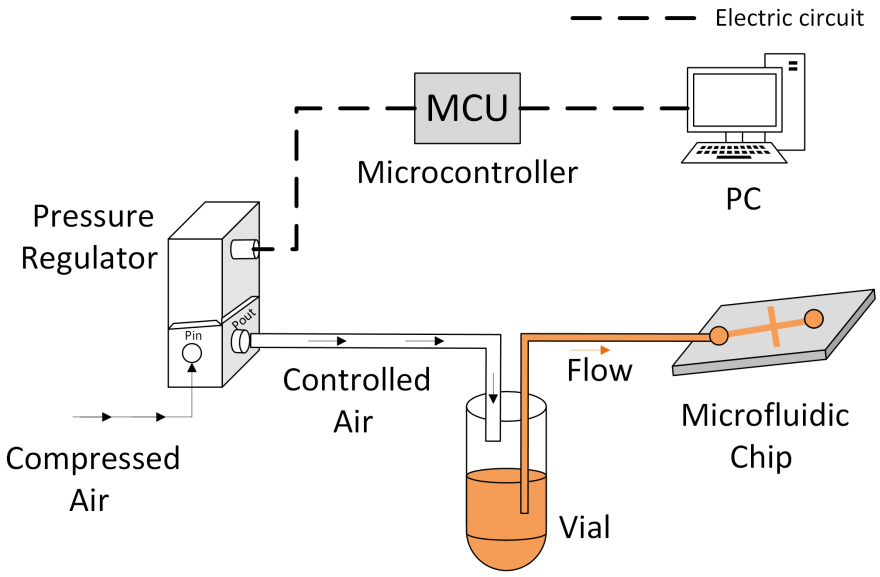

Figure 2.11 Schematic showing the pressure pump components

et al. [156]. Additionally, Sullender et al. [17] proved that pressure pumps should replace syringe pumps in studies assessing flow measurement accuracy, as pressure pumps provide a more stable and reliable flow compared to syringe pumps.

In this section, compression methods that provide compressed air for pneumatic-driven systems are first presented. Next, the available pressure regulation options for microfluidic devices are outlined, including commercial and open-source pressure pumps and regulators. Dual-valve pressure regulation methods and control strategies employed in these systems are also discussed. Finally, integrated pneumatic actuation systems that combine the compression unit and the regulator are presented and discussed.

2.3.1 Compression

The compressor is a device that supplies a mass flow rate at a pressure higher than

atmospheric pressure. Some laboratories are equipped with a centralized compressed air line, which reduces the emphasis on this component within the field. However, this component can have a significant impact and effect that needs to be considered on several factors such as accessibility, cost, efficiency, mass, and noise. For example, the portability and accessibility of compressed air are critical for point-of-care systems designed for use outside the laboratory. In addition, relying on bulky centralized compressed air systems diminishes the main advantages of microfluidic systems, which are their compact size and portability.

Accordingly, several air pumps and compressors available in the marketplace are compiled in Table 2-4. This table simplifies comparison and allows users to select compressors that best meet their application requirements, based on the compressors' performance specifications (Pressure and Flow Rate), portability (Dimensions and Weight), efficiency (Power Consumption), and affordability (Cost). Manufacturers provide compressors of the same type with different pressure and vacuum ranges. The table does not list every model by each manufacturer, but it provides a representative sample to illustrate the key differences in characteristics and costs. This table facilitated the selection of the air pump for our developed pressure pump in Chapter 4.

To facilitate a clear visual comparison, the compressors presented in Table 2-4 are grouped based on their maximum pressure, providing a visual comparison. A spider graph is used, presented in Figure 2.12, to compare the compressors that exceed 100 psi (only three). The remaining compressors, with maximum pressure below 50 psi, are compared using the bar graph shown in Figure 2.13.

For easier comparison, the axes in Figure 2.12 are normalized between 0 and 1. The graph indicates that the Puma DE07 and PACBRAKE HP10625 have comparable

Table 2-4 Comparison of different types of compressors

Model	Pressure Range (psi)	Flow Rate (CFM)	Dimensions (in) $L \times W \times H$	Weight (kg)	Power Requirements	Power Consumption (W)	Price (USD)
VIAIR 90 Series95	120	1.03	$5.4 \times 3.1 \times 4.6$	1.16	12 V,10 A	120	100
Puma DE07	135	1.36	$12.2 \times 7.5 \times 11$	8.6	12 V 46A	552	300
PACBRAKE HP10625	150	3.4	$11.5 \times 6 \times 9.5$	8	12V 45A	560	400
RK -07054-10	60	1.1	$7.6 \times 5.1 \times 7.6$	6.6	115V 0.8A	92	450
PondPro CA-65	50	5.5 @ 0 psi	$9.5 \times 6.8 \times 7.8$	6.8	115V 3.11A	350	600
Thomas 910CDC22/12	25	2 @ 0 psi	$7.9 \times 4.8 \times 5.9$	3.7	12 V 12.8A	153.6	650
Thomas 7006-0050	11.6	0.26 @ 0 psi	$4.8 \times 1.9 \times 3.1$	0.66	12 V	28	500
Thomas 107CDC20	35	1.4 @ 0 psi	$7.3 \times 4.0 \times 5.0$	2	12 V 8.5A	102	400
Elveflow Pressure Source	36	-	$6.3 \times 7.6 \times 7.7$	2	24 V 1.5A	36	1600
Schwarzer SP 625 EC-LC-DUs-DV	43	0.18 @ 0 psi	$1.2 \times 2.3 \times 3.5$	0.25	12V/24V ,1.7A/0.8 A	20	150
Schwarzer SSP 625 EC-LC-DV	26	0.21 @ 0 psi	$1.2 \times 2.1 \times 3.2$	0.22	12V/24V ,0.9A/0.5A	11	120
Thomas 2907CDC22 /12	15	3.2 @ 0 psi	$11.5 \times 4.3 \times 5.9$	5	12V 20A	240	900
Smart Product AP-3P04	11	0.03 @0psi	$2.6L \times \oslash 1.2$	0.06	12V 0.27A	3.24	50
PreciGenome PG-MP	-5.8 to 11.6	≤ 0.0388	$3.9 \times 1.9 \times 1.5$	2	110V 0.6A	66	400
Boxer 22K series	-6.5 to 8	0.05cfm @ 0 psi	$1.5 \times 0.9 \times 1.1$	0.032	3V to 4.5V	0.5 to 1.6	50
Jun-Air LVF-PVS -P-02-110	0 to 115	0.6 @ 0 psi	$15.2 \times 13.1 \times 13.5$	18	120 V, 0.9A	108	2500

characteristics. The VIAIR 90 Series 98 stands out with a smaller footprint (lower volume and weight), but at the cost of reduced maximum pressure. Therefore, PACBRAKE HP10625 is the recommended selection for applications where maximum pressure is critical, whereas VIAIR 90 Series 98 is preferable for applications requiring high pressure and a more compact design.

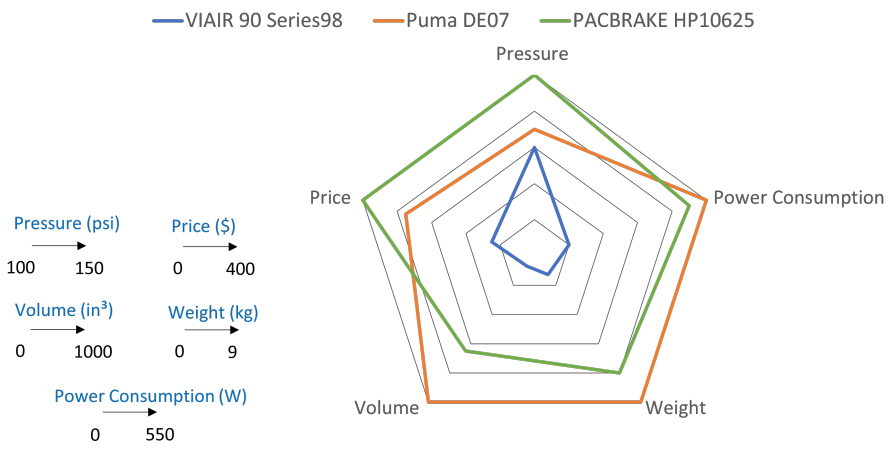

Figure 2.12 A spider chart comparing compressors with output above 100 psi. The axes are normalized between 0 and 1.

The models compared in Figure 2.13 do not include the full range of available compressors. For example, Thomas and Schwarzer provide different pressure and vacuum ranges for the same models. The models compared are representative, highlighting the significant differences in their characteristics. A key difference can be observed between piston compressors and diaphragm pumps. Diaphragm pumps (e.g., Thomas 7006-0050, Schwarzer SSP 625 EC-LC) are more compact and lighter, offering better portability. However, the lifespan of the diaphragm is shorter. In contrast, piston compressors (e.g., PondPro CA-65, Jun-Air LVF-PVS-P-02-110) are bulkier and offer higher pressure ranges.

2.3.2 Pressure Regulation

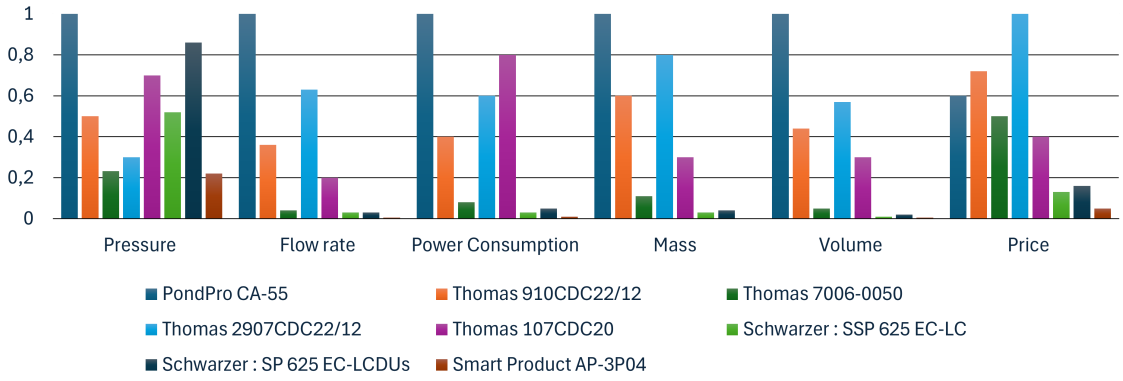

Figure 2.13 A spider chart comparing compressors with output above 100 psi. The axes are normalized between 0 and 1.

Precisely regulating compressed air is critical for the proper functioning of microfluidic devices and for accomplishing their intended tasks. For many microfluidic systems, the compressed air is regulated into multiple independent pressure outputs applied to the different inlets of a chip.

Microfluidic Pressure Pumps

The primary options for providing controlled air are commercial pressure pumps. An example is shown in Figure 2.14, illustrating the mechanism of the Elveflow OB1 pressure pump. The system regulates the compressed air provided externally to the desired pressure required by the user. The pump output is connected to a vial containing the fluid to be delivered to the microfluidic chip.

Table 2-5 presents a comparison of complete pressure pump systems, including both commercial and open-source systems suitable for microfluidic applications. Commercial pressure pumps exhibit high performance, offering precise and rapid flow control. However, the main disadvantages are their high cost, lack of customization, and the need for an external pressure source, which limits their accessibility to laboratories with limited

Figure 2.14 Elveflow OB1 commercial pressure pump (adapted from Elveflow website: Elveflow)

resources.

To improve the accessibility of pressure pumps, several studies have proposed open-source pressure pumps that offer flexibility, affordability, and adaptability across different microfluidic application fields. These systems often involve assembling multiple commercial pressure regulators (transducers) within a single enclosure and developing a control system to regulate them independently. For example, Gao et al. [20] developed µPump, shown in Figure 2.15, using a Control Air T900-CIM transducer. The system incorporates pressure transducers, electronic components, and a control system to achieve accurate regulation of the desired pressure. After performing tests, the pump exhibits the following characteristics: pressure accuracy of 0.09%, stability of 0.02%, and resolution of 0.02% of the full span. The system stabilizes and reaches 2 bar from 0 in less than 2 seconds. Documentations enabling users to duplicate the system are also provided. The system demonstrates rival characteristics to the commercial ones at a lower cost.

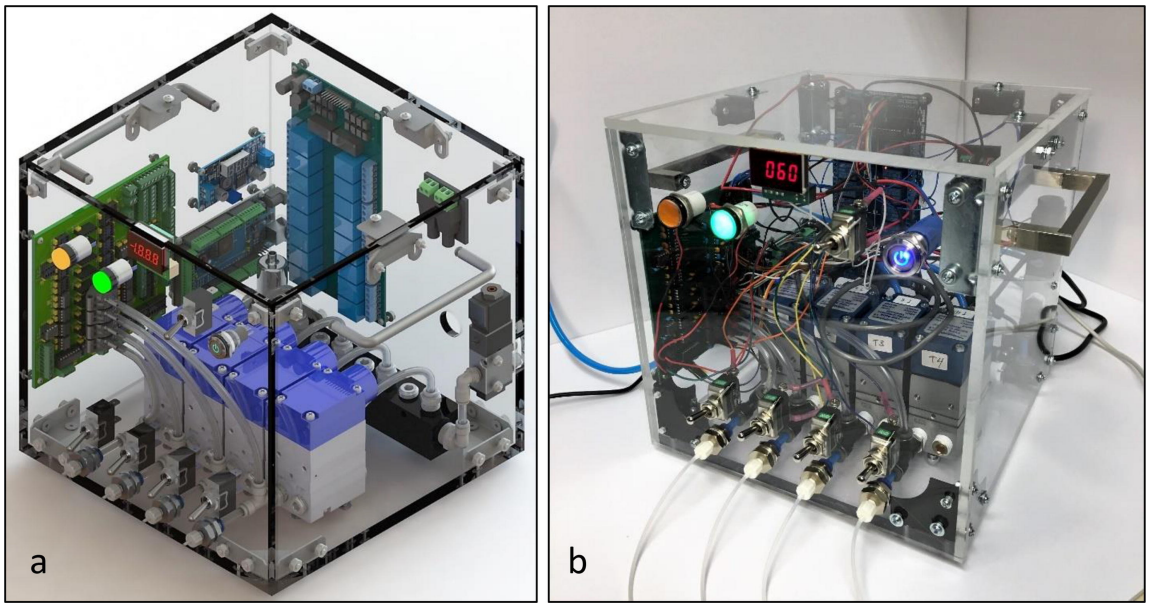

Figure 2.15 µPump Open-source pressure pump developed by GAO et al.; (a) 3D model of the system ; (b) Photograph of the real setup [20].

Similarly, Filatov et al. [22] utilized an electro-pneumatic regulator (SMC ITV0090-2L) to build their open-source pressure pump. The pump is designed specifically for droplet generation applications. Rather than providing detailed performance characteristics, the pump's performance was validated through droplet generation experiments, in which the ability to maintain a stable droplet generation regime for at least four hours was demonstrated.

Additionally, Ernits et al. [157] employed a piezoelectric regulator. After testing the experimental evaluation, the system was compared with the alternative commercial ones. Their pump is more affordable, but the commercial ones provide at least twice better accuracy. Moreover, the pump exhibits a slow settling time of 2100 ms, which makes it less suitable for applications requiring rapid pressure change, particularly for active microfluidic applications.

In contrast, an alternative open-source approach was followed by Sanchez et al. [21]. The authors developed an open-source pressure pump that utilizes two proportional solenoid valves instead of relying on the commercial regulators. However, the price of the developed regulator ($\simeq$ 700 $) and the settling time required to achieve the desired pressure ($\simeq$ 1300 ms) remain comparable to those of commercial regulators, such as Control Air T900-CIM used by Gao et al. [20]

Table 2-5 Comparison of different types of pressure pumps

Model (# of output)	**Flow rate**	**Pressure (psi)**	**Stability % FS / mbar**	**Response Time**	**Price (USD)**
Elveflow OB1 (2)	0.1 µL/min to 500 mL/min	-13 to 87	0.005 % / 0.1	50 ms	6,000
Fluigent Flow EZ (4)	$\sim$ 5 ml/min	11.6 to 100	0.1 % of measured value	30 ms	13,000
Precigenome PG-MFC (2)	10 ml/min	60	0.05 % / 0.5	0.5 s	4,000
Open-source E/P regulator [20] (4)	—	14.5	0.02 % / 2	$<$ 2 s	3,000
Open-source Solenoid Valves [21] (4)	—	1 to 10	— / 1	1.3 s	2,500

Pneumatic Pressure Regulators

Based on the reviewed literature, many open-source pressure pumps depend on (E/P or I/P) transducers to regulate the compressed air. Such systems typically feature one common compressed air inlet connected to a manifold, which houses multiple transducers. Each transducer can be controlled individually, providing multiple regulated air outlets from a single pump. Designing customized pressure transducers requires specialized knowledge and advanced equipment [158].

In this section, the commercially available pressure regulators (transducers) and proportional solenoid valves were reviewed and compiled in Table 2-6 and Table 2-7, respectively. These tables provide a comparison of performance, cost, and operating characteristics, and illustrate alternative approaches for regulating air in microfluidic systems.

Many transducers are mainly engineered for industrial applications requiring high flow rates and high pressure. However, in microfluidics, the requirements depend on the type of chip. Passive applications demand low flow rate, high pressure, and high stability, whereas active applications demand lower pressure with a fast response time. Additionally, most transducers are oversized and heavy. For example, the T900 from Control Air's "miniature" series provides a pressure range from 0 to 15 psig (101×10^3 Pa) with an air consumption of 1.5 scfh ($\approx 10^{-5}$ m^3/s). The power provided is more than 1 W, which exceeds the milliwatt power typically required by microfluidic applications. Using such large internal components in the pump results in excessive mass and bulk, leading to an overdesigned system.

Solenoid valves provide a lighter, lower-cost, and more compact option compared to the pressure transducers. However, they operate using a different mechanism. Pressure transducers operate by translating the electric signal (voltage or current) to a proportional output pressure, directly regulating the compressed air to the desired pressure. In contrast, solenoid valves regulate the flow by adjusting the valve opening according to a current signal, affecting flow rather than pressure directly. Thus, in order to achieve precise pressure regulation, two valves, a pressure sensor, and a control system are required.

Table 2-6 Comparison of different types of regulators

Actuator Model	**Accuracy (%)**	**Dimensions (in)** $L \times W \times H$	**Weight (kg)**	**Flow capacity**	**Pressure Output (psi)**	**Pressure Supply (psi)**	**Price (USD)**
CONTROLAIR 900 :CLM, CIM, CJM	±0.10 (1 mbar) (2 mbar) (4 mbar)	$1.5 \times 3.0 \times 3.7$	0.4	4.5 SFHM @ 25psi 12 SCFH @ 100 psi	0-15, 0-30, 0-60	25-65, 40-70, 70-80	650
CONTROLAIR 550 :CIM, CJM, CkM	<1 (estimated)	$1.5 \times 3.0 \times 5.1$	0.77	4.5 SCFH @ 25 psi 12 SCFH @ 100 psi	0-30, 0-60, 0-120	35-100, 65-145, 125-145	450
CONTROLAIR 1000P: IAEIE ,IAEGE, IAEKE (CL)	±0.1 (2 mbar) (4 mbar) (8 mbar)	$2.0 \times 2.1 \times 4.1$	0.42	8 SCFH @ 30 psi 17 SCFH @ 60 psi 34 SCFH @ 120 psi	0-30, 0-60, 0-120	45 , 75, 130,	900
EAA-550 :CIA, CJA, CKA	<1 (estimated)	$1.5 \times 2.2 \times 5.1$	0.77	12 SCFM @ 100 psi 20 SCFM @ 150psi	0-30, 0-60, 0-120	35-100, 65-150, 125-150	300
EAAT7800 :704, 705, 706	±0.25 (5 mbar) (10 mbar) (20 mbar)	$1.5 \times 2.2 \times 5.1$	1	11 SCFM @ 150 psi	0-30, 0-60, 0-120	35-150, 65-150, 125-150	400
Marsh Bellofram 1001: 966-210-000, 966-260-000, 966-218-000 966-280-000, 966-290-000	±0.25 (0.861 mbar) (2.5 mbar) (5 mbar) (10.34 mbar) (17.23 mbar)	$1.9 \times 2.9 \times 4.0$	1.5	—	0-5, 0-15, 0-30 0-60, 0-100	10-100 psi	800
ProportionAir QL3	±0.2	$2.0 \times 2.9 \times 5.3$	1	2 SCFM	0-110	15-165 (depends on desired pressure)	1200
Omega EP510-060	0.25Max (10.34mbar)	$1.9 \times 2.9 \times 4.0$	1.5	12 SCFM	0-60	100 psi	750
Omega IP610-030, IP610-060	±2.5 (51.7mbar) (103.4mbar)	$1.5 \times 2.9 \times 3.7$	0.77	12 SCFM	0-30, 0-60	35-100, 65-150	550
SMC ITV0010-2UBL ITV0030-2UBL ITV0050-2UBL	±1% F.S.	$1.9 \times 0.5 \times 3.2$	0.1	0.2 SCFM(max.)	0.14-14.5, 0.14-72, 0.01-130	0.01- 30, 0.01-145, 0.01-145	250
MCMaster-Carr 8083T1 , 8083T2	±1.3 (26mbar) , (130mbar)	$2.3 \times 1.6 \times 5.6$	—	35 SCFM @ 100 psi	0-29, 0-145	43 max, 152 max	600
Clippard CPC-CFF-BA, CPC-CFF-CA, CPC-CFF-DA, CPC-CFF-EA	±2.5F.s	$1.9 \times 0.5 \times 3.2$	0.1	2.7 to 65 l/min	0-5, 0-15, 0-30, 0-60	Vac.to 150	800

Table 2-7 Comparison of different types of solenoid valves

Model	**Response time (ms)**	**Hysteresis (%)**	**Control signal**	**Price (USD)**
Humphrey ProControl PV3PM1203250	5-8	8	0-200 mA	100
Clippard ET-P-05-0925	5-8	10	0-370mA (EVPD-2 driver available $\sim$ \$400)	100
Enfield Technologies PFV-W12E05-M075C-0100	<30	±5	Voltage control signal	250
McMaster 2555N12	5-8	±10	Voltage control signal (0-10 VDC)	100
Parker 935-300120-000	10 (typ.)	10 (typ.)	Suggested driving circuit in datasheet	100
iQ Tesla Proportional Valve	<20	<10	External driver available ($\sim$\$200)	100
BMT Fluid Control Solutions Miniature Proportional Valve	—	—	0-200 mA	150

Dual-Valve Pressure Regulation

Dual-valve regulation has been reported in various application domains, including pneumatic systems [23, 159], hydraulic servo systems [160], soft robotics [161], and electro-pneumatic actuators [162]. Pressure regulation is typically achieved in such systems using two independently controlled valves. An inlet valve, connected to the pressurized source, supplies pressure, while an outlet valve vents the excess pressure. By modulating the openings of these two valves, the net mass flow within the controlled volume can be adjusted, allowing the internal pressure to reach the desired pressure.

Dual-valve pressure regulation is well established in industrial pneumatic systems, where commercial pressure regulators offering high performance are available. However, these systems are typically closed-box solutions, with high costs and limited options for customization and integration into research applications. The pneumatic pressure control systems in the literature focus on bulky, high-pressure systems. For example, Li et al. [159] proposed a dual-valve pressure regulation for pneumatic brake systems in commercial vehicles.

Only a limited number of studies have investigated pressure control approaches tailored to the requirements of microfluidic applications. A recent study presented an open-source dual-valve pressure regulator for microfluidic applications [21]. Nevertheless, the proposed system does not focus on the rapid response required for active microfluidic applications, as an optimized closed-loop control strategy is not incorporated for this purpose. As a result, users requiring fast response and customizable solutions are left with limited options and must rely on commercial systems.

Control Concepts for Pressure Regulation

Regulating pressure using proportional valves exhibits inherent nonlinear behavior due to the compressibility of air, nonlinear valve flow dead zones, leakage effects, and time delays in the pneumatic systems. As a result, the application of model-based control approaches often requires linearizing the system and detailed mathematical equations [23].

A comprehensive investigation and comparison of all available control approaches for pressure regulation is beyond the scope of this thesis. Accordingly, the focus of this study is on the Proportional–Integral–Derivative (PID) control strategy due to its numerous advantages. This control method provides efficient control while being simple to implement, cost-effective, easy to replicate, and can be tuned experimentally without heavy reliance on an accurate system model or complex mathematical formulations [163]. These advantages align directly with the open-source objective of this project, which benefits from a common, straightforward approach.

Furthermore, the choice of the control strategy is closely linked to the selected hardware platform. Arduino is one of the most commonly used, widely accessible and affordable microcontrollers. However, this hardware limits the computational capabilities required for advanced control approaches. The selection of the Arduino for this project mirrors the PID selection by prioritizing accessibility and simplicity of the open-source equipment rather than absolute performance.

Proportional–Integral–Derivative (PID) control remains one of the most adopted control approaches for pressure regulation in the literature [160, 164, 165], and is also widely employed in commercial pressure regulators. The PID approach is primarily formulated for single-input, single-output systems, and additional design considerations need to be taken into account when a PID controller is applied to multi-input configurations, such as dual-valve control.

A variety of control approaches exist in the literature for pressure regulation. These approaches can be classified into two main families: model-based and data-driven, with some hybrid methods combining both. Model-based approaches rely on mathematical representations of the system dynamics. This category includes commonly used control methods such as PID, Linear Quadratic Regulator (LQR), Model Predictive Control (MPC), and nonlinear control methods such as sliding mode control. In contrast, data-driven approaches rely on experimental data or learning-based mechanisms and do not require a detailed physical model. Techniques belonging to this category include fuzzy or rule-based controllers, adaptive control with online system identification, and machine learning techniques.

Linear Quadratic Regulator (LQR) is an optimal state-feedback control technique that determines control inputs by optimizing a quadratic trade-off between system states and control effort. The LQR approach is also explored to a limited extent in this study. While LQR can naturally handle multi-input control configurations and can be implemented on the Arduino platform, this approach relies more heavily on the accuracy of the linearized system model, introducing additional complexity for users unfamiliar with control systems to retune the controller.

Szabo et al. [162] modeled and compared Proportional–Integral–Derivative (PID) and Linear Quadratic Regulator (LQR) controllers for an electro-pneumatic actuator that employs two solenoid valves. The study highlights that LQR can naturally enable separate control inputs for each valve, while the PID controller only provides one input signal, which requires additional logic to distribute a single control signal. However, LQR performed well in simulation but failed in certain experimental cases, whereas the PID controller achieved reliable performance.

2.3.3 Two-in-one System

Integrating both systems, compression and regulation, results in a standalone and more compact system. Few systems currently available in the marketplace are summarized in Table 2-8. Such systems are costly and generally restricted to only one output. However, at least two pressure outputs are needed for most microfluidic applications, and even more are required for complex systems.

Watson et al. [166] appear to be the only group that has developed a fully integrated system equipped with a pressure source and a pressure regulator using two proportional solenoid valves. Nonetheless, their system was designed for a different type of chip: pneumatic-driven microfluidic chips. Their design offers control over 32 solenoid valves rather than driving fluid into the chip.

Table 2-8 Comparison of two-in-one pumps (compression and regulation)

Model	**Flow Rate**	**Pressure (bar)**	**Stability**	**Response time**	**Price (USD)**
Elveflow Cobalt	5mL/min	2	0.1 mbar	75 ms	5 000
PneuWave Pump Corsolution	20nL/min-5.0mL/min	1 or 4	<0.1 CV % (1 mbar for 1 bar)	10 ms	10 000

2.4 Critical Analysis

Microfluidic systems are increasingly evolving from passive operation to actively controlled platforms [7, 37, 46, 167]. Reliable performance in pressure-driven active microfluidic applications strongly depends on the accuracy and responsiveness of the pressure or flow control [168, 169]. In addition, the recent emergence of digital twins in microfluidics further increases research interest in real-time and reliable actuation methods

to improve alignment between experimental systems and their numerical models [18,170].

A representative comparison of the different actuation approaches for microfluidic systems discussed in the previous Sections 2.2 and 2.3 is presented in Table2-9. Table 2-9 highlights the relative strengths and weaknesses of the main actuation methods as per key performance indicators introduced in Table 2.2.1 (power, response time, stability, efficiency, mass, volume, and cost). The table follows a qualitative and relative rating system, where each system's performance is rated as worse, average, or better relative to the others. This review aims to link features of actuation systems with their optimal selection for the diverse requirements of different microfluidic applications.

Table 2-9 Comparison of the actuation methods based on the key performance indicators (KPIs)

		KPI					
		Hydraulic power	Response time	Stability	Efficiency	Density	Cost
Pressure pump		●●●	●●●	●●●	●	●	●
Positive displacement actuation	Syringe pump	●●●	●	●	●●	●●	●●
	Peristaltic pump	●●●	●●	●	●●	●●	●●
External force	Gravity pump	●●	●	●●	●●●	●	●●●
	Human-powered	●●	●	●●	●●●	●●	●●●
Microactuation		●	●●	●●	●●	●●●	●●

Legend: ● = worse, ●● = average, ●●● = better

Human and gravity-actuated pumps generate limited hydraulic power. Their slow response time restricts their applicability mainly to passive microfluidic chips. Gravity-actuated pumps typically have a large volume to utilize the gravitational force. However, the extremely affordable cost, simplicity, and self-sufficiency of the external force actuation systems encourage widespread accessibility.

Microactuators provide the least hydraulic power, but it is sufficient for microfluidic

chips. Their lightweight and compact size make them ideal for portable systems. However, the scarcity of commercial systems and the complexity of system integration constrain their adoption.

Positive-displacement actuation methods (syringe and peristaltic pumps) are widely used in microfluidics and can offer high hydraulic power. These pumps are cost-effective and simple to operate. Syringe and peristaltic pumps are both standalone systems, as only electrical power is required for operation. However, both systems exhibit inherent oscillations and pulsed flow due to their working principle.

Compared to commonly used positive-displacement actuation methods (peristaltic and syringe pumps), pressure pumps demonstrate superior performance and provide high hydraulic power suitable for most microfluidic applications. Pressure pumps offer performance advantages such as stable, pulse-free flow with a fast dynamic response ($\sim$ 100 ms), which can be difficult to achieve using other actuation methods. As a result, pressure-based actuation is particularly well suited for active microfluidic applications, where reliable, precise control and fast response dynamics are required. These characteristics highlight the important role of pressure pumps in modern active microfluidic applications, as well as digital twin platforms.

For example, Zeng et al. [168] demonstrated that the pressure-driven pump reduced periodic flow rate fluctuations caused by the syringe pump stepper motor and led to improved response speed and control precision. Crawford et al. [171] demonstrated that actively regulating the droplet size in the microchannel by integrating a pressure-driven actuation within a feedback control loop led to a significant increase in droplet monodispersity. These representative examples highlight the suitability of pressure-driven pumping for actively controlled microfluidic systems.

However, the cost of commercial pressure-driven pumps is substantially higher ($\sim>$ 5000 $ for commercial pumps) compared to other actuation methods. Furthermore, these pumps often require an external pressure source to operate, which results in a large mass and volume that are undesirable for portable applications. Consequently, these factors limit accessibility for users and researchers with constrained budgets and restrict the use of pressure pumps to well-equipped laboratories. Moreover, commercial pressure pumps are often implemented as a closed system, which limits flexibility for hardware modification and control customization to meet specific application requirements. Thus, the integration of the commercial system into the closed-loop system used in modern active microfluidic applications may be constrained.

The open-source projects proposed to address the limitations of commercial pressure pumps, discussed in section 2.2.1, can achieve stability comparable to commercial systems. Nevertheless, these systems typically exhibit slower dynamic response, with a settling time of approximately ($\sim$ 1000 ms). Although these open-source solutions reduce the cost of pressure pumps, the price often remains relatively higher compared to other actuation methods ($\sim>$ 1000 $). Therefore, the open-source pressure pumps developed offer an alternative to the commercial pressure pump at a fraction of the cost. However, these systems are mainly tailored for passive microfluidic applications that only depend on a stable pressure source, not for active applications that require rapid pressure regulation. Assembling such systems may also require specialized skills that are not available to every user. In addition, to the best of the author's knowledge, none of the discussed studies offered a solution for the primary disadvantage of the pressure pumps: the need for a compressed air supply to operate.

The limitations of the available open-source solution can be primarily attributed to

their reliance on commercial regulators (electropneumatic or piezoelectric transducers) [20, 22, 157]. Commercial regulators are relatively affordable and widely available, but they are closed systems and designed primarily for large industrial projects rather than for direct use in microfluidic applications. Thus, most commercial regulators operate over pressure ranges higher than those required by active microfluidic applications. Also, these regulators require a relatively high minimum operating pressure range of which complicates the integration of a compact, built-in compression unit. In addition, these regulators exhibit a slower settling time than commercial pressure pumps designed specifically for microfluidic applications. Such properties might be sufficient for passive microfluidic applications but less suitable for active applications that require a fast settling time (< 100 ms) and low pressure (< 5 psi). For example, Frank et al. [172] used a commercial electro-pneumatic pressure regulator controlled through a programmable control system to achieve precise pressure regulation, while still relying on an external compressed air source. Such studies primarily focus on achieving stable and accurate pressure regulation with limited consideration of the dynamic response speed.

Therefore, expanding the accessibility of pressure pump technologies remains a crucial and active area of research. The limitations of both existing commercial and previously reported open-source systems highlight the need for open-source pressure pump solutions that eliminate the need for an external pressure source and reduce reliance on commercial pressure regulators. Given the rapid growth of active microfluidic systems and the application of digital twins in microfluidics, a clear gap exists in the availability of open-source pressure pumps suitable for these applications, often leaving users and researchers with limited options beyond commercial solutions.

In contrast to commercial regulators (e.g., electropneumatic or piezoelectric

transducers), proportional solenoid valves are used to achieve pressure regulation through flow control by implementing a specific configuration and closed-loop control strategies. Solenoid valves are more compact and less expensive than commercial regulators. Naz et al. [64] employ a single proportional solenoid valve in a closed-loop control system to regulate pressure for droplet microfluidic applications. This approach is tailored only for droplet generation applications and differs from a standalone pressure pump.

Pressure regulation using two proportional solenoid valves is widely used in industrial pneumatic, hydraulic, and robotic systems. Most existing implementations and studies target large-scale and high-pressure applications. On the other hand, commercial dual-valve pressure regulators are offered as closed-box solutions that limit their flexibility and ease of integration for specific microfluidic application requirements. To date, very few studies have investigated dual-valve pressure regulation in microfluidics. Sanchez et al. [21] have explored an open-source dual-valve pressure regulator. However, the system remains relatively slow and is not optimized for active microfluidic applications.

Nevertheless, a dual-valve pressure regulation that features fast response, low-pressure operation, and open-source accessibility has yet to be fully addressed for active microfluidic applications.

2.5 Summary

Microfluidics is a multidisciplinary field that has been applied across numerous scientific and engineering domains. An overview of its principles and representative applications is essential to highlight its broad potential and the advantages microfluidics offers to multiple fields. In addition, this may help provide readers from diverse academic backgrounds with a solid basis for understanding and interacting with the main

microfluidic concepts discussed in this thesis.

The selection of actuation methods has a significant impact on the application and integration of microfluidics, although their importance is sometimes underestimated. The appropriate actuation method depends on the specific microfluidic application, as each application imposes distinct requirements. Every method has its strengths and weaknesses, and none provides all the advantages simultaneously. Thus, the key performance indicators (KPIs) adopted in this study facilitate trade-offs in determining the optimal characteristics for different application requirements. In addition, the accessibility and simplicity of actuation systems promote the widespread adoption of microfluidics across various fields. While offering satisfactory results in research is essential for advancing the microfluidic field, this alone is not sufficient for users in other fields (such as biology and chemistry) who require less complex systems to benefit from this technology. Hence, open-source projects are crucial for improving accessibility to microfluidic technology and enabling its full potential to be realized across diverse application domains.

Pneumatic pumps deliver a more stable flow compared to commonly used actuation methods such as syringe and peristaltic pumps. Pressure pumps supply high power that is sufficient to cover a wider range of applications than other externally powered actuation (gravity and human-powered) and microactuators. Pressure pumps offer fast response times, versatility through multiple outputs (where only one pump can manage multiple outputs and flow rates), and a low risk of contamination (as only air comes into contact with the flow).

An open-source pressure pump that addresses the limitations of the available pressure pumps, including both commercial and open-source projects, is needed. Figure 2.16 summarizes these limitations and presents the proposed solution. Pressure pumps that

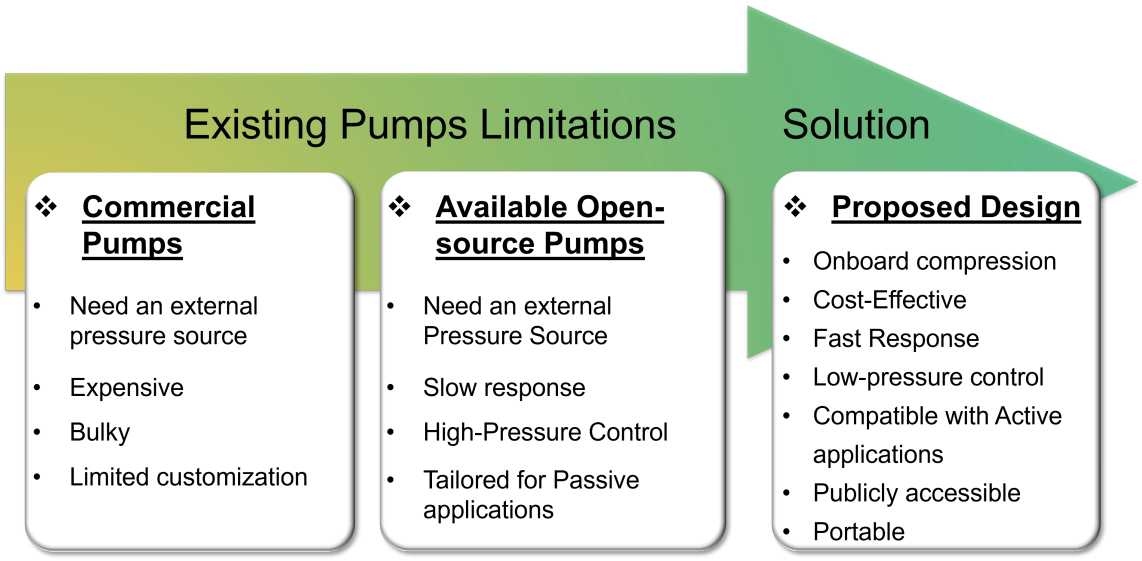

Figure 2.16 Diagram summarizing the limitations of existing pressure pumps and the implemented solution in this study

rely on bulky external compressors conflict with the main principle of microfluidics, which centers on miniaturization. Although commercial pumps offer high performance sufficient for both passive and active microfluidic applications, their accessibility is limited by their exorbitant costs. Available open-source projects offer solutions with lower prices, comparable stability, and customizable features. However, they typically exhibit slower response times and operate at higher pressure ranges, which are mainly suited for passive microfluidic applications.

Available open-source pressure pumps largely depend on commercial regulators, which are closed systems and primarily designed for industrial applications. With the increasing adoption of active microfluidic systems and digital twins in microfluidics, the development of an open-source pressure regulation system based on dual-valve control that is capable of providing fast dynamic response and precise pressure remains unexplored for microfluidic applications.

While many control strategies can be applied to dual-valve pressure regulation systems, the emphasis here is on a control approach that is reliable, easy to tune, and accessible to users from diverse technical backgrounds. Proportional–Integral–Derivative (PID) controller is commonly used for dual-valve pressure regulation and has demonstrated reliable performance in such systems.

Chapter 3 - Methodology

The work presented in this chapter corresponds to an article published in MDPI Actuators: Zein, M.; Moussahou, R.; Kelouwani, S.; Hébert, M. Precision Pressure Pump Featuring Dual-Valve Control and Onboard Compression for Microfluidic Systems. Actuators 2025.

This thesis proposes a pressure pump that is cost-efficient, publicly accessible, easy to replicate, and does not require an external pressure source to operate. It is capable of delivering precise low-pressure control with fast settling times, covering a wider range of applications, particularly active microfluidic systems.

To remove dependence on external compressed air sources supplied by bulky compressors, a compact built-in compression unit is integrated into the developed system. This unit provides the supply pressure required by the proposed regulator by delivering continuous compressed air up to 10 psi. This design enhances the portability of the pressure pump and improves accessibility for users and laboratories where compressed air infrastructure is unavailable.

The compressed air generated by a single integrated compression unit must be precisely regulated to provide one or multiple independent pressure outputs, which are then delivered to the inlets of a microfluidic chip. Instead of relying on commercial regulators, an open-source dual-valve pressure regulator is proposed and integrated into the developed pressure pump. The regulator operates using two proportional solenoid valves (for each independent pressure output) that interact to reach the desired pressure. To achieve the accuracy and fast response required for active microfluidic actuation, the regulator operation is controlled by a closed-loop Proportional–Integral–Derivative (PID) control strategy. The PID controller offers a practical balance between control

performance, robustness, and simplicity, while allowing straightforward experimental tuning and modification by other users. In addition, PID control can be implemented on an affordable and widely accessible microcontroller (Arduino). This controller selection supports the objective of the thesis to provide an open-source, affordable, and easily accessible system.

Experiments are conducted to evaluate the performance of the proposed regulator. The regulator is capable of handling precise pressure control with an accuracy of ±0.01 psi (±0.7 mbar) from the desired pressure, with a fast settling time of less than 100 ms. A comparative analysis is also performed to evaluate the performance of the proposed regulator against a Marsh Bellofram commercial pressure regulator. While both regulators achieve closely comparable accuracy, the herein proposed regulator exhibits a faster settling time ($\sim$ 100 ms vs. $\sim$ 200 ms), a more compact and lightweight design ($\sim$ 120 cm^3/0.3 kg vs. $\sim$ 400 cm^3/1.35 kg), and a lower cost ($\sim$ 250\$ vs. $\sim$ 1,000\$). The proposed regulator is a customizable alternative to the commercial regulators and is designed for easy replication. The publicly shared tuning methodology and system architecture facilitate adaptation of the proposed regulator to a wide range of experimental setups, including active microfluidic applications.

As illustrated in Figure 3.1, the developed pressure pump consists of three main modules: the compression unit, the regulator system, and the control circuit. The current project focuses only on one regulated pressure output, but the developed pump can be extended to provide multiple outputs by integrating additional regulator modules. The connections between the hardware components within each module are detailed to guide the assembly of the pump.

This chapter presents the methodology followed to develop the proposed open-source

pump that provides a precise and fast response suitable for active microfluidic applications. The compression unit, described in Section 3.1, provides the internal pressure source required for system operation. The power and signal circuits necessary to drive the compression unit, actuate the valves, and implement the control system are outlined in Section 3.2. Section 3.3 presents the development of the pressure regulator using two proportional solenoid valves, including the system modeling, controller design and tuning methodology, and the hardware implementation. Finally, the experimental procedure used to evaluate the regulator's performance and to validate it through comparison with a commercial pressure regulator is presented.

Additional building details to easily replicate the pump are provided in the supplementary material of the published article. The file includes a bill of materials, the PCB files, the software, and the mechanical assembly.

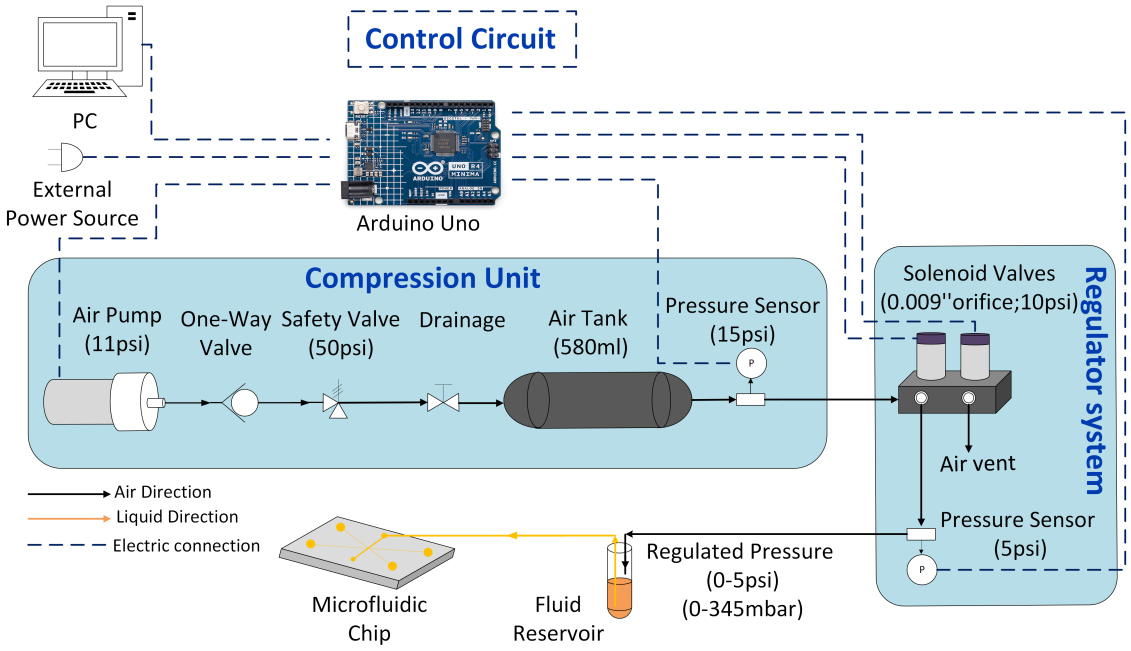

Figure 3.1 Schematic representation showing the three main modules of the system hardware: compression unit, regulator system, and control system.

3.1 Compression Unit

The compression unit consists of a SmartProducts air pump AP-3P04 that generates pressure up to 10 psi. The compressed air is stored in the Clippard reservoir AVT-PP-35 with a volume of 580 ml. Between the pump and the reservoir, a push-to-connect one-way valve and two tee connectors are installed through 1/4" OD × 0.16" polyurethane tubing. The one-way valve prevents backflow. One tee connector accommodates a safety valve to protect the system if pressure exceeds 50 psi, while the other hosts a drainage valve to release air from the system when required. To measure the pressure in the air tank, a tee connector that hosts a brass barbed straight fitting (1/16", # 10-32) is connected to the tank outlet. Silicone tubing (1/16" ID) is used to connect the barbed fitting to a Honeywell pressure sensor ABPDANV015PGAA5 (operating pressure 0 - 15 psi), mounted on the Arduino Shield printed circuit board (PCB).

The role of the air tank is to dampen the fluctuation caused by the air pump, provide a buffer to maintain steady airflow, and increase the lifespan of the air pump by reducing its operating time. The pressure in the tank reaches 9.5 psi in approximately 50 seconds. The system is programmed so that once this pressure is reached (9.5 psi), the pump turns off and restarts when the pressure drops below 5.5 psi. Minor disturbances caused by the pump's starting and stopping were noticed and are managed by the control system.

Users can choose other types of air pumps to customize the system to meet their application's requirements. The selected air pump's maximum pressure must be compatible with other components (safety valve, pressure sensor, pressure regulator etc.). The pump selection was guided by Table 2-4 from the review in Section 2.3.1 . However, a trade must be made between the pump's maximum pressure, expected lifespan, price, and footprint. The developed compression unit allows the pressure pump to be adapted

for a wider range of environments where the pressure source is a constraint. For better flexibility, our developed pressure pump can operate using an external pressure source if available.

If the input pressure supplied by the compression unit to the regulator system is higher than 10 psi, the control parameter must be validated. Higher input pressure can affect the system's ability to stabilize at a lower desired pressure. For example, when the input pressure to the regulator was 15 psi, the regulator could not stabilize at 1 psi. This issue may be related to the PID control parameters or the maximum operating pressure of the proportional solenoid valves. Further investigation is required to fully explain this phenomenon.

3.2 Control Circuit

The proportional solenoid valves are driven by current, with a 0-5 V input signal. Figure 3.2 presents the electronic circuit utilized that enables precise control over the current between 0-360 mA. The circuit was adapted from the VSO® LowPro GC Low Profile Proportional Valve datasheet. The circuit provides control over the electrical current within the required operating range to precisely actuate the proportional valve, enabling control over the flow. The electronic circuit comprises an operational amplifier (Texas Instruments LM358P), a transistor (STMicroelectronics TIP120), resistors, and capacitors. The operational amplifier compares the command signal from the Arduino (0-5 V provided using DACs) with the feedback signal across the 1 Ω resistor to determine the necessary voltage. The voltage divider, composed of resistors 3.3 KΩ and 422 Ω, scales the command signal to a level comparable with the feedback signal. The transistor supplies the high current required by the solenoid that the op-amp cannot provide. The capacitors minimize noise and stabilize the circuit. Two power supplies are required: 12 V is supplied

to the op-amp to ensure proper operation, and 6.5 V is applied to the solenoid valve through the transistor.

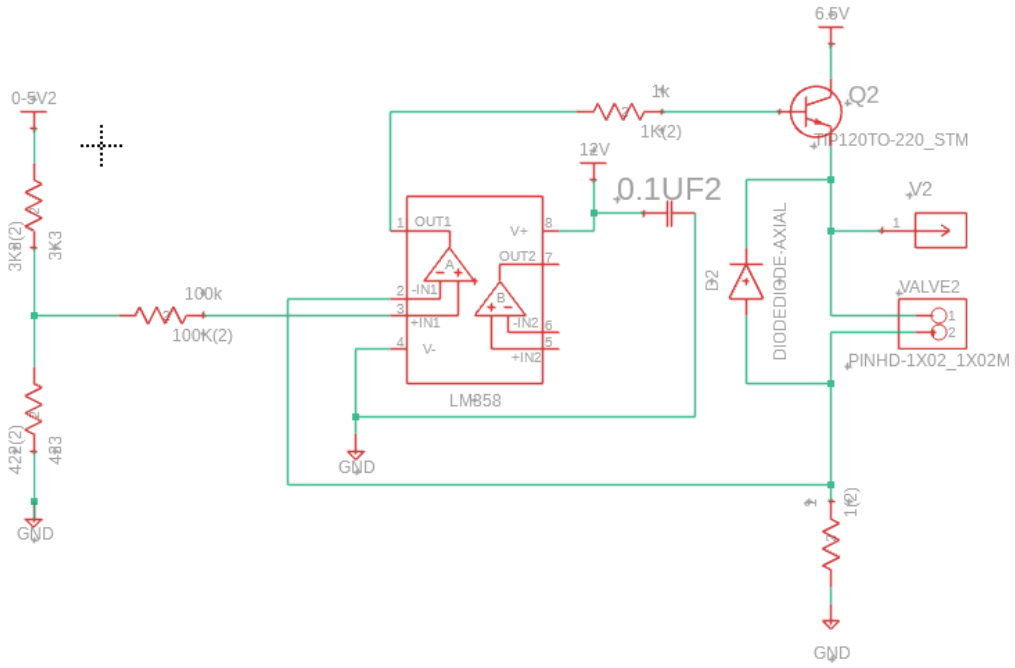

Figure 3.2 Schematic of the electronic circuit required for controlling current between 0 - 360 mA to drive the proportional solenoid valves.

The functionality of the circuit is tested by monitoring the response of the proportional solenoid valves to the supplied current. The valve begins to actuate at 100 mA and reaches full saturation at 300 mA. Subsequently, the circuit is implemented twice, once for each valve, on the designed "Solenoid Valves PCB" presented in Figure 3.3. The PCB also incorporates the feedback pressure sensor (ABPDANT005PGAA5, operating pressure 0 - 5 psi) that measures the regulated air exiting the manifold.

In addition, a second PCB is designed, "Arduino Shield PCB" (Figure 3.3) to deliver the necessary power and signal required by the "Solenoid Valves PCB". The Arduino Shield PCB is mounted directly onto the Arduino board via header pins. The PCB incorporates

two MCP4921-E/P 12-bit digital-to-analog converters (DAC) to convert the Arduino's digital values into a 0 - 5 V analog voltage supplied as the command signal for the valve circuit. Two voltage regulators (LD1085V) are included to step down the external 12 V power to the 6.5 V applied to the valves. To control the starting and stopping of the air pump via Arduino while providing the required power (12 V, 0.27 A), a MOSFET (RFP12N10L) is employed on the PCB. The PCB also incorporates a pressure sensor (ABPDANV015PGAA5, operating pressure 0 - 15 psi) to read the air tank pressure.

The design of each PCB has a ground plane, and the two are connected to form a common ground, which helps minimize noise in the circuit. The "Arduino Shield PCB" powers the "Solenoid Valves PCB" by four wires (12 V, 6.5 V, 5 V, ground) and three signal wires. The signal wires include (ps), which transmits the pressure sensor readings to the Arduino, and (V1, V2), which carry the command signal from the DACs.

The models and files for manufacturing both PCBs and the necessary electronic components are provided in the supplementary data. Users simply need to print the PCBs and solder the components in their designated locations.

3.3 Regulator system

An overview of the system operation for pressure regulation is shown in Figure 3.4. The pressure regulation comprises two proportional solenoid valves. The control system regulates both valves by adjusting their opening. One valve increases the pressure in the chamber by controlling the air entering, while the second valve decreases the pressure in the manifold by releasing air to the atmosphere. The control system adjusts the two valves based on the difference between the desired pressure set by the user and the real-time pressure measured by the sensor at the air exiting the chamber. This closed-loop system

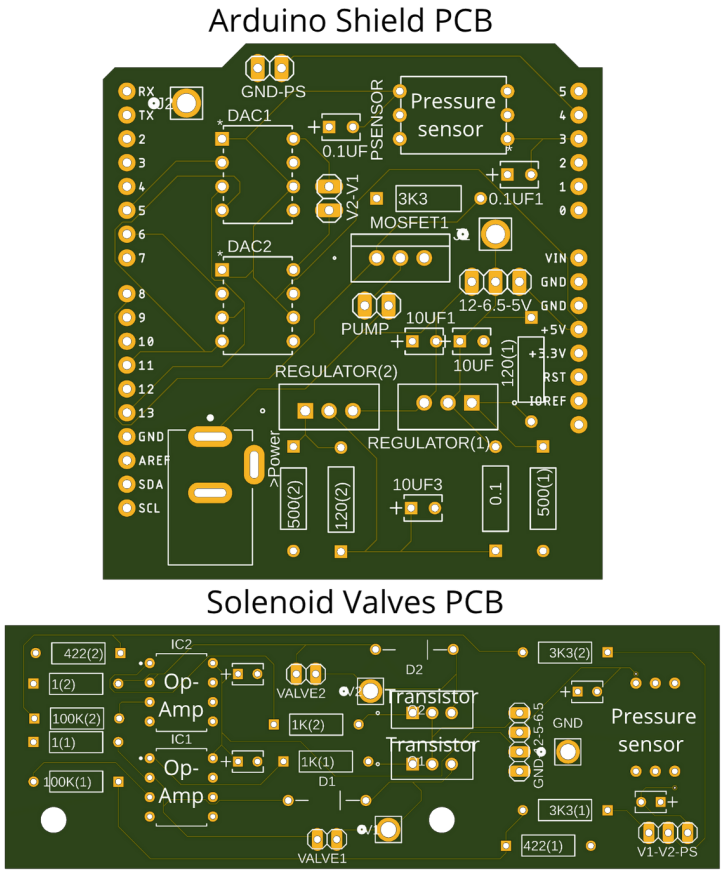

Figure 3.3 PCBs designed to integrate power and signal connections

continuously regulates the valves to maintain a stable and precise pressure.

The objective of this work is to provide a control approach that can be easily adopted and tuned by different users across diverse setups. These setups may be affected by factors such as air leakage, tubing length, sensor placement, and actuation delay, which can vary between prototypes. As a result, a control strategy that is easy to retune to accommodate these variations is required. Proportional–Integral–Derivative (PID) control is a commonly used control method, characterized by its simplicity, reliability, and ease of tuning, and has proven effective in pressure regulation. According to the advantages PID offers and the objective of this study, this control strategy is employed to regulate the mechanism of the proposed dual-valve pressure regulator.

The linear quadratic regulator (LQR) controller is also partially explored as a control strategy for the proposed pressure regulator. However, additional work is required to overcome the identified challenges and complete its implementation to reach the desired performance. For future developments, the LQR model and the methodology followed are explained in Appendix A of this thesis.

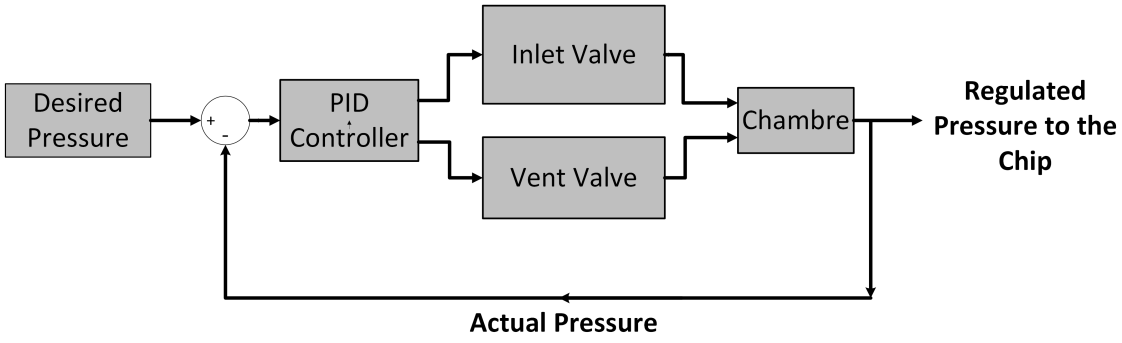

Figure 3.4 Block diagram of the closed-loop control system for pressure regulation.

3.3.1 Pressure Dynamic Modeling

The model of the dual-valve pressure regulation developed here supports controller design and simulation, rather than fully representing the detailed fluid dynamics of the system. Simplifications are adopted to reduce model complexity while retaining the dominant pressure dynamics required for controller design.

The system operates at low pressure($\leq$ 10 psi) and room temperature, which are far from the critical point of air; hence, air is modeled as an ideal gas. In addition, the compressed air generated by the compressor passes through an air tank, fittings, and pneumatic lines before reaching the regulator chamber. This provides sufficient time for any small temperature rise caused by compression to dissipate through thermal exchange with the surrounding environment; therefore, the regulator chamber is treated as an isothermal system, with the air temperature in the regulator chamber equal to the ambient room temperature. The volume of air in the chamber is constant and is estimated to be approximately $5.6 \times 10^{-6}\,\mathrm{m}^3$. Air leakage is neglected in the Simulink model.

According to the conservation of mass, the net mass flow rate into the chamber is defined as the difference between the inlet and outlet mass flow rates (Equation 3.1).

$$\dot{m_{net}} = (\dot{m}_{in} - \dot{m}_{out}) \tag{3.1}$$

The ideal gas law is expressed as :

$$PV = mR_xT \tag{3.2}$$

where P is the absolute pressure in the chamber (Pa), V is the chamber volume (m^3), m is the mass of air (kg), R_x is the specific gas constant for air (287 J/(kg·K)), and T is the air temperature inside the chamber (room temperature 295 K).

The pressure dynamics in the chamber are governed by the Equation 3.4 obtained by differentiating Equation 3.2 with respect to time,

$$\dot{P} = \frac{R_x T}{V}(\dot{m}_{net}) \tag{3.3}$$

$$\dot{P} = \frac{R_x T}{V}(\dot{m}_{in} - \dot{m}_{out}) \tag{3.4}$$

where $\dot{P}$ is the rate of change of pressure (Pa/s).

The mass flow rate $\dot{m}_{\text{in}}$ entering the chamber and the mass flow rate exiting the chamber $\dot{m}_{\text{out}}$ are regulated by control inputs applied to the corresponding proportional solenoid valves. The valve dynamics are approximated using first-order transfer functions relating the control input to the mass flow rate:

$$\dot{m}(s) = \frac{K}{\tau s + 1} u(s) \tag{3.5}$$

where u is the control input applied to the valve, K is the gain, defined as the ratio between the steady-state output and a constant input, and τ is the valve time constant.

The time constant (τ) is approximated using the response time specified in the manufacturer's datasheet (8 ms). The gain K is identified experimentally.

Using a flow rate sensor, the steady-state mass flow rate is measured as a function of the current applied to the proportional solenoid valve under a supply pressure of 7 psi, corresponding to the midpoint of the compression unit operating pressure range between 5.5 and 9.5 psi, as shown in Figure 3.5. The valve shows a dead zone where no flow occurs when the input current is below 0.1 A. Above 0.1 A, the relation between the current and the mass flow rate is observed to be approximately linear, and K is calculated as the slope of the line in Figure 3.5, $K = 1.8405\ \mathrm{LPM\,A^{-1}} (\approx 3.7 \times 10^{-5}\ \mathrm{kg\,s^{-1}\,A^{-1}})$.

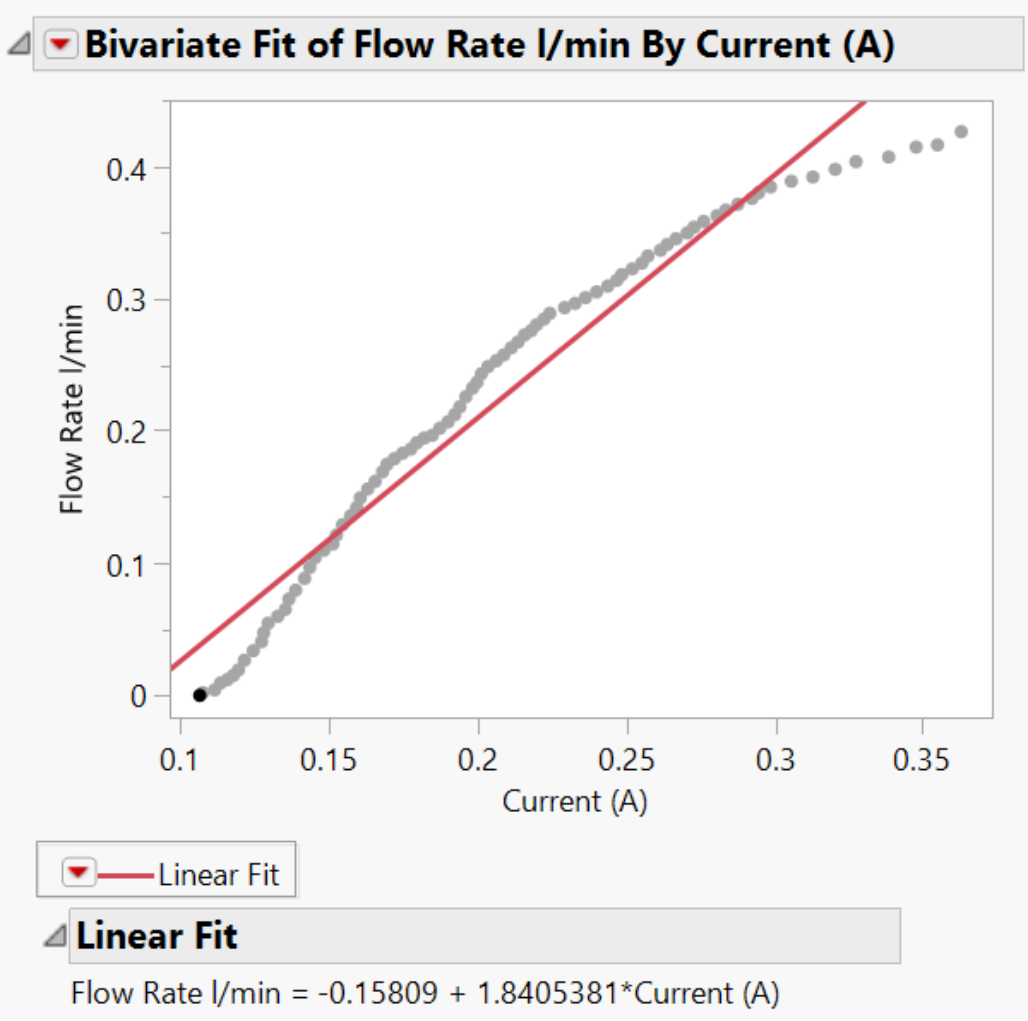

Figure 3.5 Experimental flow rate response to the applied current for the proportional solenoid valve.

Since the real system is implemented on an Arduino microcontroller, it operates in discrete time. The sampling time was determined experimentally by measuring the time between two consecutive executions of the control loop. The average sampling time was found to be approximately 7ms based on a sample of 500 measurements. This sampling time was adopted in the Simulink model to ensure consistency between simulation and experimental implementation.

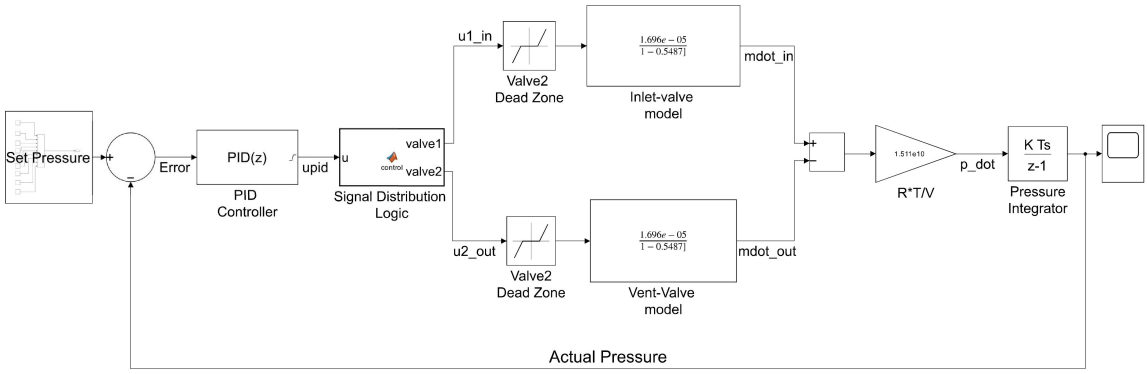

Figure 3.6 Simulink model of the pressure regulation system

To enable system simulation, controller design and tuning, the derived pressure dynamics Equation 3.4 and valve models Equation3.5 are implemented in Simulink. Figure 3.6 presents the complete pressure regulation system built by mapping the governing equations into interconnected functional blocks. The valve dynamics are represented using a discrete first-order transfer block. The net mass flow rate, obtained from the difference between the inlet and outlet mass flow rates from the valves, is multiplied by constant RT/V $(287 \times 295)/(5.6 \times 10^{-6})$ and integrated to obtain the actual pressure. The pressure integrator is initialized at atmospheric pressure, as the pressure dynamics are formulated in terms of absolute pressure.

The system operates in a closed loop, where measured pressure is subtracted from the set pressure. The resulting error is processed by the PID controller. The PID controller

generates a single control signal; hence, a MATLAB Function block is used to implement logic that allocates this signal between the inlet and outlet valves based on the sign of the controller output.

The initial control logic was designed such that when the PID controller output is negative, the inlet valve opens while the outlet valve closes, and vice versa. However, this method introduced fluctuations, hindering stabilization and causing a delay before reaching steady-state. To mitigate these fluctuations, a strategy was implemented to enable the valves to open simultaneously at inverse degrees rather than sequentially. This strategy is implemented in the Arduino code and is expressed by the following equation:

$$u_{1in} = \begin{cases} u_{pid}, & \text{if } u_{pid} > 0 \\ U_{\max} - |u_{pid}|, & \text{if } u_{pid} < 0 \\ u_{1f}, & \text{if } u_{pid} = 0 \end{cases} \tag{3.6}$$

$$u_{2out} = \begin{cases} U_{\max} - u_{pid}, & \text{if } u_{pid} > 0 \\ |u_{pid}|, & \text{if } u_{pid} < 0 \\ u_{2f}, & \text{if } u_{pid} = 0 \end{cases} \tag{3.7}$$

where u_{1in} and u_{2out} are the control signals applied to valve 1 and valve 2, respectively, u_{pid} is the PID controller output, $U_{\max}$ is the maximum DAC output value where the valves are fully open at 3000, and u_{1f} and u_{2f} represents the final values applied to the valve 1 and valve 2, respectively, when u reaches 0.

The Arduino code to run the pressure pump is made available to users in the

supplementary data.

Furthermore, an additional work is conducted to analyze the behavior of the controlled air supplied by the pressure pump in the liquid reservoir, where pressurized air acts on the air–liquid interface to drive fluid toward the microfluidic chip. The formulated mathematical model, the implementation in Simulink, and the simulation results are presented in the Appendix B. The design allows the prediction of the fluid flow rate based on the mass flow rate of the supplied air. Further experimental validation is required to explore the full potential of this design.

3.3.2 Controller Design and Tuning

While the published article does not include a detailed control model for controller gain selection, in order to avoid excessive complexity for users from different backgrounds, a numerical model is developed in this thesis to support a scientifically grounded selection of the control gains.

The proposed pressure regulation system is nonlinear due to saturation effects, valve dead zones, and the signal distribution logic. These characteristics complicate the tuning of the PID controller, which typically relies on linear models and a single-input, single-output system.

To enable controller tuning based on a mathematical model, the pressure dynamics are expressed in terms of the net mass flow rate entering the chamber as described by Equation 3.3. The dual-valve pressure regulation system can then be represented by a single control input acting on the net mass flow. Hence, a simplified control-oriented model is implemented on Simulink, in which the PID controller directly regulates the net mass flow rate using a single control signal.

The Proportional–Integral–Derivative (PID) controller generates the control signal based on the pressure tracking error obtained from the feedback loop. The controller applies proportional, integral, and derivative actions to drive the system pressure to the desired setpoint. This control law is expressed in the time domain as:

$$u(t) = K_p e(t) + K_i \int_0^t e(\tau)\, d\tau + K_d \frac{de(t)}{dt} \tag{3.8}$$

where the pressure error is defined as

$$e(t) = P_{\text{set}}(t) - P(t) \tag{3.9}$$

with P_{set} is the desired set pressure and $P(t)$ is the measured chamber pressure.

The Laplace-domain representation of the PID controller is given by:

$$C(s) = K_p + \frac{K_i}{s} + K_d s = \frac{K_d s^2 + K_p s + K_i}{s} \tag{3.10}$$

where C(s) is the PID controller

The main goal is to provide a stable pressure regulation while achieving a fast response to pressure changes. Thus, the controller gains are selected using a frequency-domain approach by selecting a desired gain crossover frequency ω_c. In control theory, the gain crossover frequency ω_c is defined as the frequency at which the magnitude of the open-loop transfer function is equal to one.

$$|L(j\omega_c)| = 1 \tag{3.11}$$

The open-loop transfer function of the system is described as :

$$L(s) = C(s)G(s) \tag{3.12}$$

where G(s) is the linearized pressure dynamic transfer function.

Although ω_c is defined in the open-loop systems, it highly affects the closed-loop dynamics, in particular, the speed of response.

The closed-loop transfer function can be written as :

$$T(s) = \frac{L(s)}{1+L(s)} = \frac{C(s)G(s)}{1+C(s)G(s)} \tag{3.13}$$

The closed-loop bandwidth ω_b is defined in the control theory as the frequency at which the magnitude of the closed-loop transfer function decreases by 3 dB :

$$|T(j\omega_b)| = \frac{1}{\sqrt{2}} \tag{3.14}$$

For well-stabilized closed-loop systems with sufficient phase margin, the closed-loop bandwidth ω_b directly influences the system settling time and is approximated as $t_s \approx 4/\omega_b$. Under these same conditions, the closed-loop bandwidth ω_b is approximately proportional to, and often of the same magnitude as, the gain crossover frequency ω_c

($\omega_b \approx \omega_c$).

Therefore, the relation between the settling time and gain crossover frequency ω_c can be approximated as:

$$t_s \approx \frac{4}{\omega_c} \tag{3.15}$$

This relation shows that increasing the magnitude of the gain crossover frequency ω_c results in a faster closed-loop response. However, the selected value of ω_c must be adequate to ensure stability margins.

To allow the use of MATLAB tuning tools, the MATLAB function `linearize(mdl, io)` is used to extract an equivalent linear time-invariant (LTI) model from the simplified control-oriented model implemented in Simulink. The MATLAB tuning algorithm `pidtune(sys,'PID',`ω_c`)` is then used to calculate the PID gains corresponding to a selected gain crossover frequency ω_c. The algorithm is based on frequency-domain loop-shaping methods, where the proportional (K_p), integral (K_i), and derivative (K_d) gains are computed such that the magnitude of the open-loop transfer function equals unity (Equation 3.11) while maintaining sufficient stability margins.

However, the simplified model does not fully capture all the system's dynamics. Therefore, multiple values of the gain crossover frequency ω_c are examined. The PID controller gains corresponding to each selected ω_c are implemented and analyzed in simulation and experimentally to select the gain values that lead to the fastest response time while maintaining stable operation.

3.3.3 Hardware Setup

The pressure regulator is assembled using two Clippard proportional solenoid valves (EV-PM-05-0905-V). The two valves are mounted on the EFB-2M Fill and Bleed Manifold. The Supply port (S) is attached to the pressure output from the compression unit via a straight fitting (1/4" OD - 1/8" NPT Male). The first valve controls the flow entering the manifold, while the second valve vents excess air to the atmosphere through the exit port (E). The regulated pressure (0-5 psi) exits the manifold through the outlet port (O) via a straight fitting. A 1/4" tee branch is then connected to direct air to the Honeywell pressure sensor ABPDANT005PGAA5 (operating pressure 0 - 5 psi) mounted on the Arduino Shield PCB and to the microfluidic chip. Arduino is used as the microcontroller for the system due to its wide accessibility and popularity among a broad range of users. The Arduino runs the PID controller, reads the sensors and manages the closed-loop pressure regulation system.

3.3.4 Experimental Evaluation of the Pressure Regulator

After assembling the system and implementing the final controller gain values, the performance of the developed pressure regulator is experimentally evaluated and validated. The regulator is tested by progressively raising the set pressure from 0 to 5 psi in increments of 0.5 psi. This test is repeated over 20 trials. The system performance is evaluated by assessing pressure regulation accuracy, quantified as the average error between the set pressure and the measured pressure obtained from the pressure sensor, and by determining the settling time (95% criterion) at each pressure level.

To validate the developed pressure regulator, a comparative experimental test is conducted with the commercial pressure regulator Marsh Bellofram

(T2000-2KSTNF05DF00500). Figure 3.7 presents the procedure followed to conduct this comparison test. The green blocks represent the developed pressure regulator, supplied by the onboard compression unit that delivers pressure up to 10 psi. The developed regulator operates in a closed-loop system to reach the desired pressure.

The gray blocks correspond to the commercial regulator Marsh Bellofram. Supplying the commercial regulator with compressed air using the built-in compression unit was insufficient to achieve stable operation, as the commercial regulator requires a higher inlet pressure (a minimum of 20 psi). Hence, the system is supplied by an external pressure source providing a pressure of 20 psi. Moreover, the commercial regulator operates in an open-loop mode with respect to the Arduino, which provides the set pressure signal, and the regulator internally adjusts its opening to reach the desired pressure.

The blue blocks indicate the common procedures for both regulators. Thus, apart from the differences in supply pressure and inherent control architecture, nearly the same experimental procedure is followed to evaluate and compare both systems.

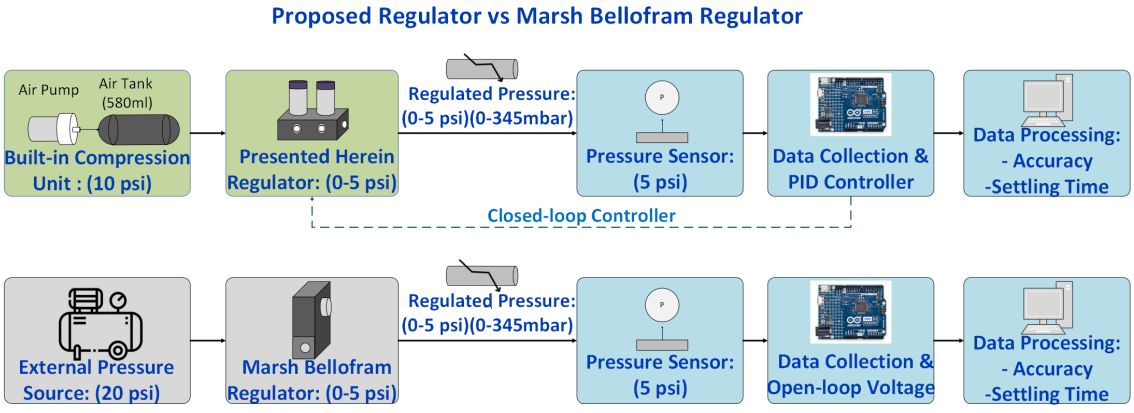

Figure 3.7 Test plan diagram presenting the experimental procedures followed to compare the developed pressure regulator with the commercial Marsh Bellofram regulator.

Chapter 4 - Results

First, the simulation and experimental results related to the tuning and selection of the pressure regulator controller gains are presented in Section 4.1. The system performance evaluation results are reported in Section 4.2. Section 4.3 shows a performance comparison between the developed regulator and the commercial regulator(Marsh Bellofram). Finally, the integrated pressure pump prototype and a comparison between existing pressure pump solutions are presented in Section 4.4.

4.1 Controller Gain Selection

Figure 4.1 presents the simulated and experimental dynamic pressure responses of the developed pressure regulator to a step change in the pressure setpoint. The setpoint is progressively increased to the set pressure from 0 to 5 psi in increments of 0.5 psi, and then dropped back to 0 psi in the same manner. Both the model-based and the experimental systems successfully achieve the desired pressure with close alignment. Despite the minor discrepancies remaining between the two systems, the model captures the dominant pressure dynamics of the real system and is sufficient for the controller design.

Table 4-1 shows the PID controller gains computed for different crossover frequencies ω_c using the linearized control-oriented model. As the crossover frequency ω_c increases, the corresponding PID controller gains also increase. The set of the crossover frequency values ω_c between 15 and 40 rad/s is selected as a trade-off between response speed and stability. This is because the experimental tests revealed that for ω_c below 15 rad/s, the system response is slow, while for crossover frequencies above 40 rad/s, the system exhibits unstable and oscillatory behavior. This behavior is not observed in the

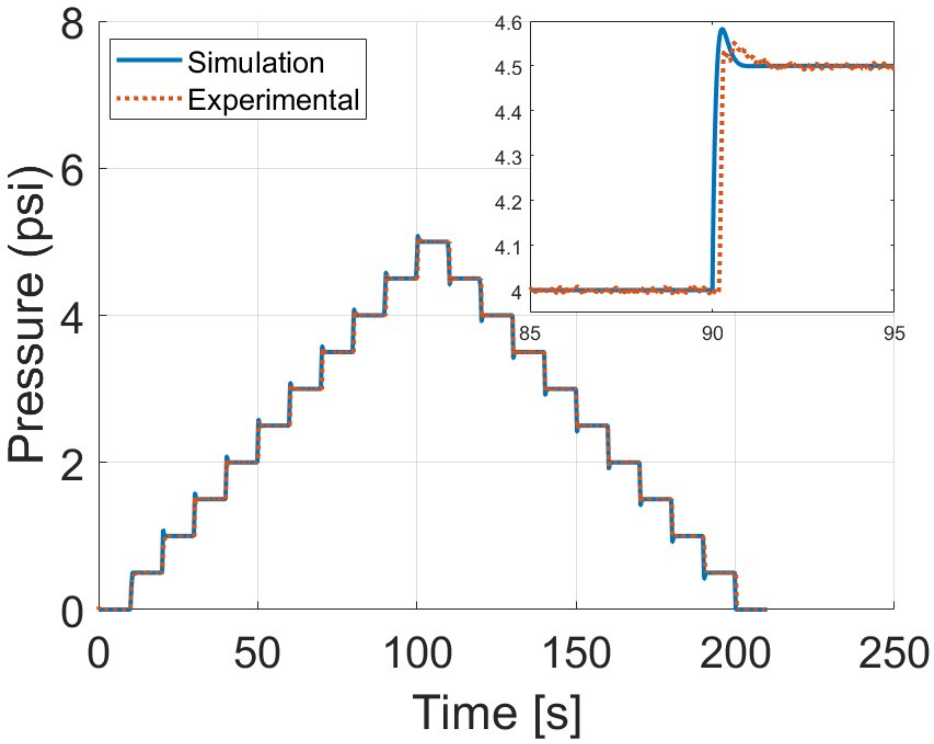

Figure 4.1 Simulated and Experimental pressure response of the developed pressure regulator at pressure levels from 0 to 5 psi, with a zoomed view of the step change between 4 and 4.5 psi.

simulation results since the simulation model does not reflect all the physical dynamics and limitations of the real system.

Table 4-1 PID controller gains computed at different crossover frequencies ω_c

ω_c (rad/s)	K_p	K_i	K_d
15	0.184	0.471	0.0016
20	0.2482	1.0187	0.0018
25	0.312	1.3771	0.0021
30	0.3764	1.6719	0.0023
40	0.5095	3.1441	0.0027

To identify the controller gains that yield the fastest pressure response, the settling time at each pressure level is calculated across the set of crossover frequencies ω_c. The corresponding controller gains listed in Table 4-1 are applied to both the simulated model and the experimental setup. The resulting settling times are summarized in Table 4-2. The simulation results (Table 4-2 (a)) show faster settling times as the crossover frequency ω_c increases.

In contrast, the experimental results (Table 4-2(b)) show slower settling times and a different trend as the crossover frequency ω_c increases. For crossover frequencies ω_c above 20 rad/s, the experimental settling times begin to increase. This behavior occurs because, at higher crossover frequencies ω_c (above 20 rad/s), the overshoot and the amplitude of oscillations increase, which results in longer settling times in the experimental response as shown in Figure 4.2. For ω_c below 20 rad/s, the system response is slower, but no overshoot is observed. As a result, the controller gains leading to the fastest settling time are obtained at ω_c =20 rad/s, with an overshoot of approximately 12%.

Both the simulated and experimental results show a slower response and different dynamic behavior at a pressure level of 0.5 psi compared to the other pressure levels.

Table 4-2 Settling time T_s at pressure levels between 0 to 5 psi across the range of crossover frequencies ω_c.

(a) Simulation results

ω_c (rad/s)	0.5	1.0	1.5	2.0	2.5	3.0	3.5	4.0	4.5	5.0
15	1.108	0.066	0.058	0.0521	0.0467	0.041	0.037	0.034	0.030	0.027
20	0.687	0.149	0.044	0.040	0.036	0.033	0.030	0.027	0.025	0.022
25	0.604	0.126	0.038	0.035	0.032	0.030	0.028	0.026	0.023	0.021
30	0.568	0.106	0.034	0.032	0.030	0.028	0.026	0.024	0.023	0.021
40	0.348	0.103	0.029	0.027	0.02	0.024	0.022	0.021	0.019	0.018

(b) Experimental results

ω_c (rad/s)	0.5	1.0	1.5	2.0	2.5	3.0	3.5	4.0	4.5	5.0
15	2.826	0.630	0.324	0.200	0.187	0.202	0.161	0.139	0.130	0.118
20	2.877	0.170	0.194	0.152	0.141	0.132	0.116	0.096	0.107	0.113
25	2.99	0.277	0.250	0.280	0.301	0.299	0.274	0.081	0.102	0.08
30	2.705	0.266	0.260	0.249	0.263	0.266	0.254	0.261	0.254	0.247
40	2.946	0.509	0.668	0.529	0.538	0.544	0.377	0.259	0.284	0.296

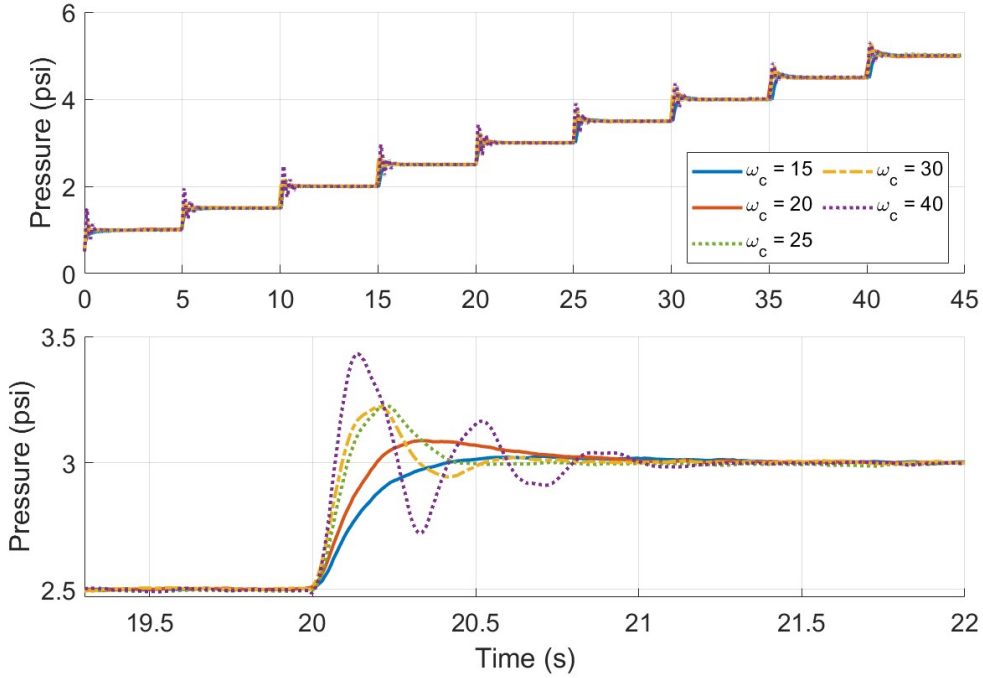

Figure 4.2 Simulated and Experimental pressure response of the developed pressure regulator at pressure levels from 0 to 5 psi, with a zoomed view of the step change between 2.5 and 3 psi.

4.1.1 Experimental Validation and Gain Refinement

Additional experimental validation is conducted to analyze and refine the controller gains, ensuring system stability and identifying the gains that lead to the fastest settling time. A series of tests is performed to monitor the regulator system's performance while adjusting the controller gain parameters (K_p, K_i, and K_d). Two gains are held constant while the third gain is varied in increments of approximately 5% until instability or a degradation in the system's performance is observed. Two main measures are considered to evaluate the system's performance: accuracy in maintaining the desired pressure (mean error between the actual and desired pressures), and settling time (95%), which quantifies the time required for the system to stabilize at the set pressure.

The gain values that resulted in effective and stable performance are presented in Figure 4.3. This range of values can also be a starting point for users to tune their controllers based on the specific requirements of their applications. However, these values were obtained with a supply pressure of 10 psi from the compression unit. Supplying the regulator with pressure higher than 10 psi may affect the system's behavior and require adjustment of these values.

To select the optimal gain values for the developed pressure regulator, a trade-off between settling time and accuracy is performed, as shown by the Pareto front in Figure 4.4. Each marker represents a different set of gain values (K_p, K_i, K_d). The red-marked point indicates the best trade-off, corresponding to the gain values: $K_p = 0.225$, $K_i = 1$, $K_d = 0.011$.

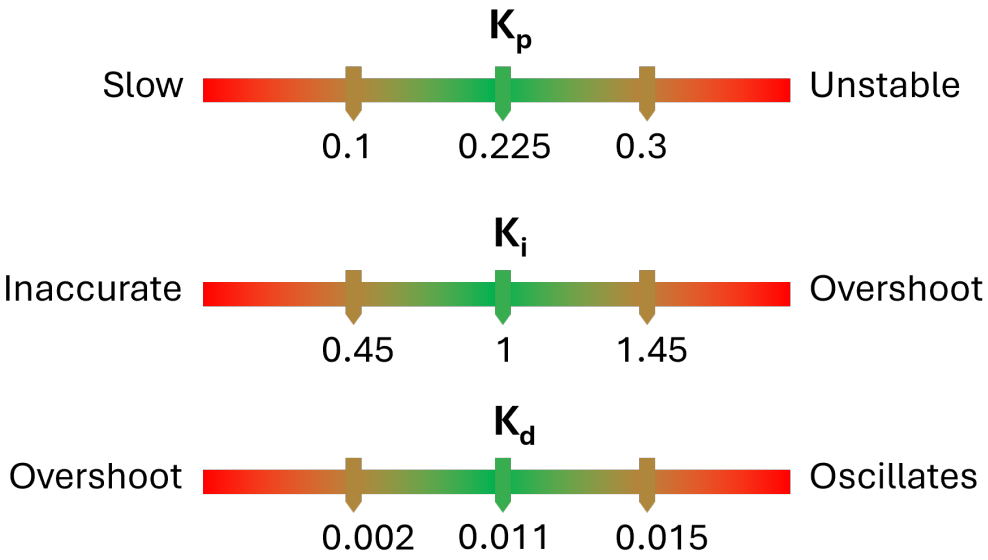

Figure 4.3 PID controller gains ranges that may achieve stable performance.

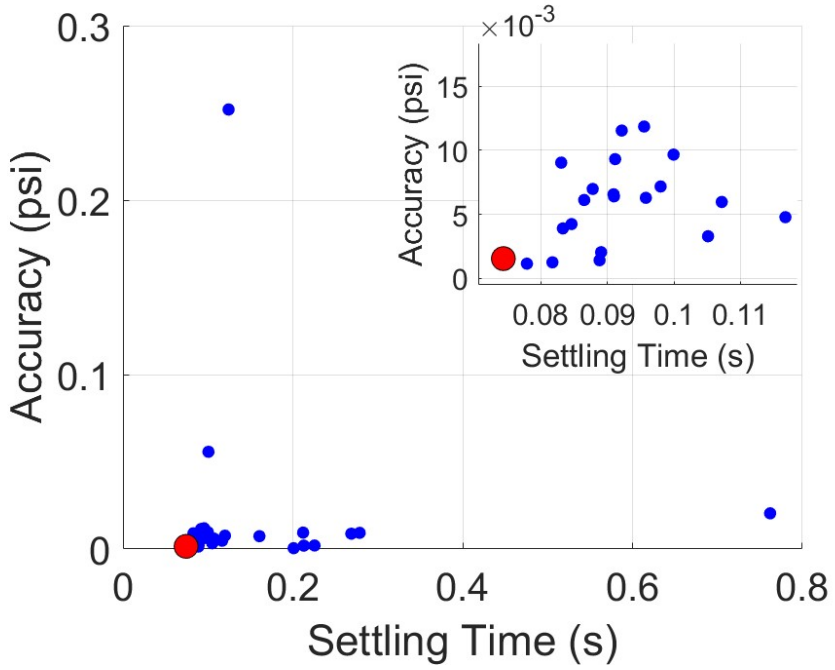

Figure 4.4 Pareto font showing the trade-off between accuracy and settling time across different PID gain sets (K_p, K_i, K_d).

4.2 Pressure Regulator Performance Evaluation

Since some instability and deterioration are observed only at the low pressure of 0.5 psi. This may be addressed by adjusting the PID gain values accordingly, but such tuning may affect the resulting performance at higher pressure levels. Therefore, the performance at the low pressure of 0.5 psi is excluded later from the quantitative evaluation.

To evaluate the settling time of the regulator, the system's response is recorded 20 times, and the settling times at each pressure level for each trial are calculated, as summarized in Table 4-3. For each trial, the average settling time is computed and recorded in the last column of the table. Color coding is used to visually identify the difference in settling times. The fastest settling times are indicated by the green colors, while the slowest settling times are marked by the red colors. Minor inconsistencies in the settling times are observed only at the low pressure of 1 psi, which are considered outside the pump's quantified settling time (the pump can reach this level, but not as fast as at higher pressures). At higher pressure, the system achieves high consistency and fast settling times. The developed regulator's overall average settling time for the 20 trials is 80 ms, with a variation (2*standard deviation (σ)) of ±12 ms.

To assess system accuracy, the average errors are calculated between the desired pressure and the actual pressure measured by the pressure sensor. At each pressure level (0 - 5 psi), the average error is evaluated from a dataset of 500 sample points over 20 trials. Figure 4.5 shows the results with 20 dots at each pressure level, corresponding to the 20 trials. The graph demonstrates that the accuracy of the system is highly stable, where the maximum mean error plus twice the standard deviation (σ) is about ±0.01 psi at 2.5 psi. All other mean errors at each pressure level fall within this range. Therefore, the developed pressure pump achieves high accuracy, with an error margin of ± 0.01 psi(± 0.2 %F.S)

Table 4-3 Measured settling times for the herein developed regulator.

	Pressure (psi)									
Trial	1	1.5	2	2.5	3	3.5	4	4.5	5	Mean settling time (s)
1	0.962	0.105	0.091	0.086	0.089	0.074	0.066	0.072	0.070	0.086
2	0.753	0.115	0.093	0.086	0.082	0.077	0.072	0.067	0.068	0.082
3	0.731	0.111	0.093	0.095	0.132	0.069	0.069	0.076	0.065	0.093
4	0.382	0.102	0.096	0.082	0.077	0.073	0.077	0.071	0.075	0.077
5	0.561	0.092	0.087	0.079	0.076	0.073	0.070	0.068	0.068	0.076
6	0.545	0.158	0.164	0.081	0.080	0.074	0.071	0.066	0.066	0.080
7	0.927	0.134	0.090	0.096	0.091	0.085	0.080	0.077	0.072	0.090
8	0.225	0.134	0.096	0.096	0.091	0.085	0.080	0.077	0.072	0.091
9	1.022	0.125	0.094	0.085	0.086	0.086	0.073	0.076	0.065	0.086
10	0.095	0.112	0.089	0.085	0.081	0.076	0.066	0.071	0.068	0.081
11	0.757	0.116	0.093	0.084	0.076	0.074	0.068	0.064	0.061	0.076
12	0.193	0.109	0.157	0.082	0.081	0.075	0.072	0.068	0.065	0.081
13	0.651	0.100	0.098	0.092	0.078	0.075	0.070	0.067	0.065	0.078
14	0.562	0.177	0.090	0.079	0.075	0.070	0.062	0.092	0.071	0.079
15	0.608	0.163	0.096	0.082	0.075	0.075	0.070	0.066	0.066	0.075
16	0.576	0.169	0.144	0.088	0.079	0.076	0.064	0.067	0.064	0.079
17	0.565	0.084	0.083	0.149	0.072	0.062	0.066	0.063	0.062	0.072
18	0.571	0.164	0.077	0.078	0.073	0.071	0.068	0.057	0.061	0.073
19	0.611	0.167	0.077	0.146	0.074	0.069	0.060	0.063	0.061	0.074
20	0.535	0.162	0.087	0.153	0.072	0.063	0.060	0.063	0.060	0.072
Overall Mean Settling time ± 2σ : 0.08 ± 0.012 s (80 ± 12 ms)										

Although the regulator is capable of providing control at higher operating pressures than 0 - 5 psi, this study primarily targets low-pressure applications where precise pressure control is critical, as commonly required in active microfluidic applications. Users seeking much higher operating pressure should ensure that all system components are compatible with the increased pressure range (pressure sensors, compressors, etc.).

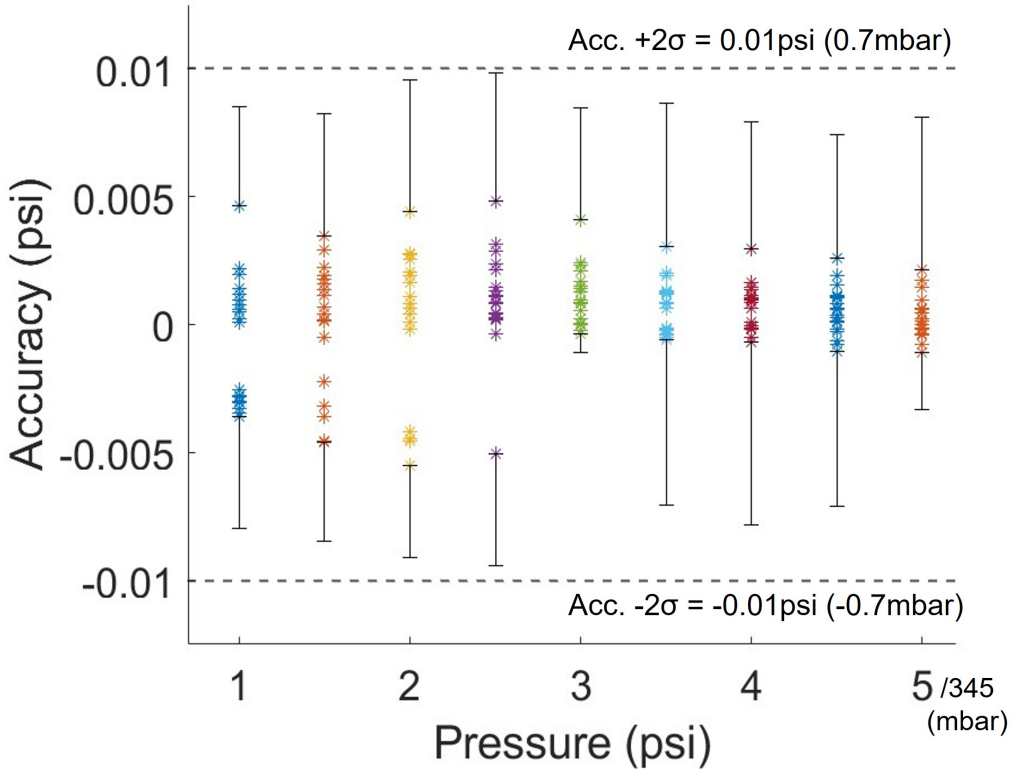

Figure 4.5 Mean errors at each pressure level (1 - 5 psi) from 500 sample points across 20 trials. All data points within ±2σ fall within ± 0.01 psi (0.7 mbar) of the setpoint.

4.3 Regulators Comparative Analysis

The effectiveness of the developed regulator is validated by a benchmarking study comparing its performance with that of a commercial pressure regulator. Referring to Table 2-6, the Marsh Bellofram (T2000 2KSTNF05DF00500) regulator was selected because it provides an operating pressure range (0 - 5 psi) that matches the range of the herein

proposed regulator. There are comparatively fewer commercial regulators available for low-pressure operating ranges than for high-pressure ranges .This further highlights the importance of developing a pressure regulator that operates within this low-pressure range.

The dynamic responses of the commercial regulator compared with the proposed regulator are shown in Figure 4.6 at the same pressure levels (from 0 - 5 psi) previously described in Section 4.2. Both regulators exhibit similar responses, but a slightly higher overshoot is observed in the behavior of the proposed regulator, as seen in Figure 4.6.

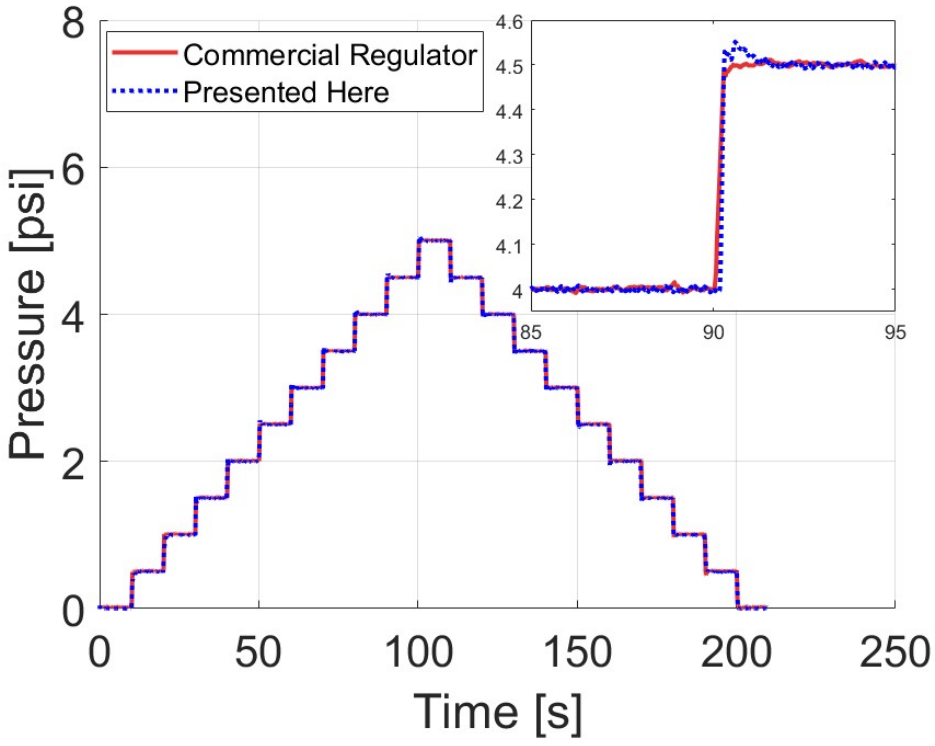

Figure 4.6 Comparison of the dynamic responses of the herein proposed regulator and the Marsh Bellofram regulator, with an inset showing the 4 - 4.5 psi step change.

To evaluate the performance of the commercial regulator, its accuracy was similarly assessed by computing the average standard deviation across the tested pressure levels. The overall standard deviation across 10 trials is approximately 0.005 psi. The accuracy

range is then ± 0.01 psi, determined as twice the standard deviation (± 2σ). This value is similar to the accuracy of the herein proposed regulator. Thus, the developed regulator is capable of providing performance comparable to that of commercial regulators. The only exception is at a low pressure level of 0.5 psi, where the commercial regulator maintains more consistent performance. For reference, when higher pressure was supplied to the commercial regulator (above 20 psi), a deterioration in performance at low pressure (0.5 psi) was detected.

Table 4-4 presents the settling times for the commercial regulator, evaluated using the same process as Table 4-3. Only 10 trials were performed rather than 20. The commercial regulator shows superior repeatability only at the low pressure of 1 psi, whereas the herein developed regulator achieves faster settling times at all other pressure levels.

Table 4-4 Settling times of the commercial regulator (March BelloFram T2000 2KSTNF05DF00500).

	Pressure (psi)									
Trial	1	1.5	2	2.5	3	3.5	4	4.5	5	Mean settling time (s)
1	0.244	0.223	0.210	0.278	0.187	0.177	0.167	0.155	0.147	0.199
2	0.241	0.225	0.267	0.199	0.187	0.178	0.216	0.156	0.144	0.201
3	0.235	0.222	0.209	0.195	0.192	0.181	0.166	0.206	0.145	0.195
4	0.236	0.221	0.215	0.202	0.189	0.178	0.163	0.157	0.139	0.189
5	0.233	0.226	0.210	0.195	0.192	0.175	0.163	0.161	0.148	0.189
6	0.232	0.225	0.208	0.201	0.216	0.176	0.161	0.160	0.143	0.191
7	0.224	0.214	0.205	0.216	0.180	0.168	0.162	0.100	0.144	0.179
8	0.230	0.217	0.207	0.196	0.181	0.169	0.155	0.103	0.138	0.177
9	0.226	0.217	0.199	0.192	0.182	0.170	0.155	0.147	0.140	0.181
10	0.255	0.238	0.228	0.213	0.207	0.191	0.183	0.175	0.165	0.206
Overall Mean Settling time ± 2σ : 0.191 ± 0.019 s (191± 19 ms)										

The characteristics of both regulators are compared in Table 4-5. The two regulators demonstrate nearly identical accuracy. The developed regulator achieves 100 ms faster settling times, is smaller and lighter, and, importantly, less expensive. On the other hand, the commercial regulator offers higher stability at low pressure (0.5 psi). Nevertheless, a fast settling time is more critical than high accuracy and stability for active microfluidic

applications. To summarize, the commercial regulator is primarily designed for industrial applications. The proposed regulator is tailored for active microfluidics, offering high performance and affordability to increase accessibility.

Table 4-5 Comparison of the pressure regulators characteristics (Herein Presented vs Marsh Bellofram regulator)

	Accuracy (psi / F.S%)	**Settling Time (ms)**	**Weight & Volume (kg/cm³)**	**Cost ($ USD)**
Presented Here	0.01 / 0.2	80 ± 12	0.3 / 120	250
Marsh Bellofram	0.01 / 0.2	191 ± 19	1.35 / 403	1000

4.4 Integrated Pressure pump Final Design

The compression unit reaches 10 psi in the air tank in under 1 minute and supplies it to the regulator system. The pressure regulator controls the compressed air pressure between 0-5 psi with a fast response time (≈92ms) and high accuracy ±0.01 psi (±0.7 mbar), making it suitable for active microfluidic applications. The proposed pressure pump integrates the compression unit and the pressure regulator, as presented in Figure 4.7. This prototype setup (Figure 4.7) is essential for testing the pump's performance before housing it in a portable enclosure that is shown in the final design (Figure 4.8). This setup may also be preferable for users seeking easier assembly or who intend to create their own custom enclosure.

The pump enclosure in the final version, shown in Figure 4.8, was developed by Ruddy Moussahou, who documents comprehensive instructions guiding users to replicate it in the supplementary data. The design promotes portability and compactness of the system, but it requires additional efforts and time to assemble. It is space-efficient $\sim$ 330 in³ (0.0054 m³) and lightweight $\sim$ 3 lbs. The pump only requires a USB connection to a computer to run the Arduino code and a 12 V external power supply from a wall adapter.

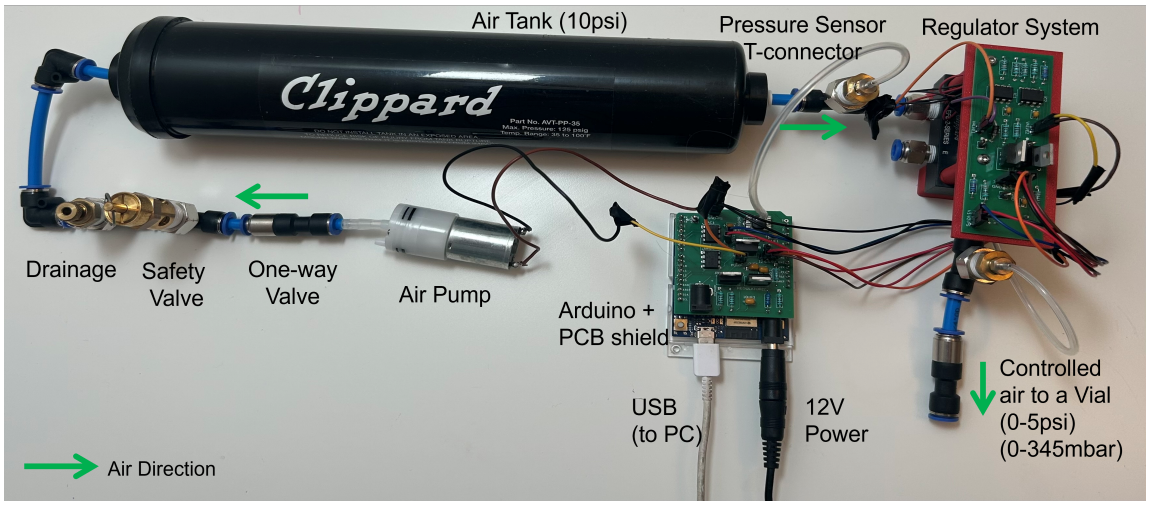

Figure 4.7 Assembled Pressure pump prototype for testing and functional use without enclosure.

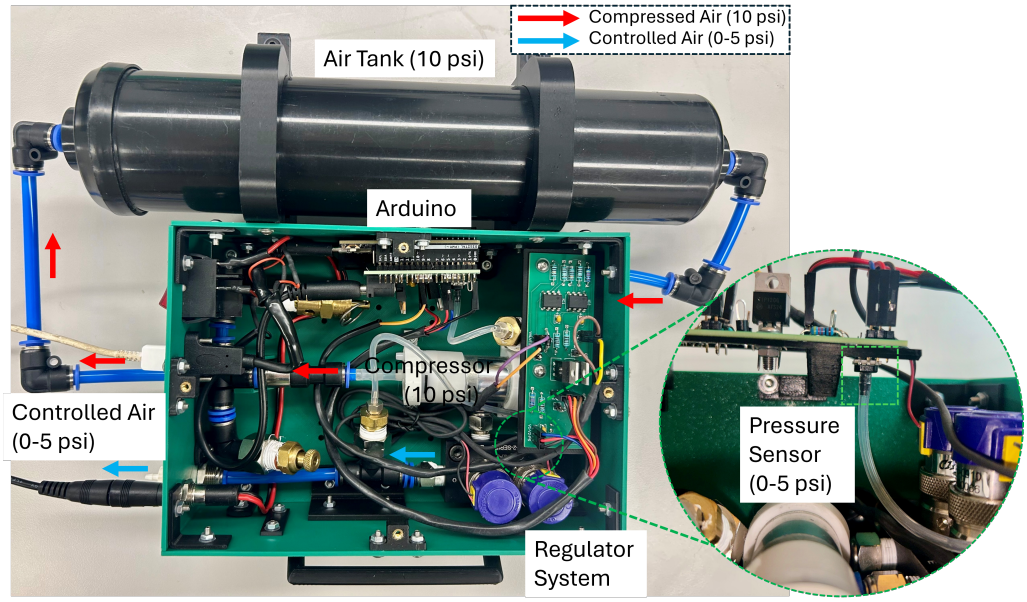

Figure 4.8 Final assembly of the pressure pump enclosed in a portable box, with a zoomed view showing the feedback pressure sensor in the regulator system. (The pump enclosure was designed and implemented by Ruddy Moussahou)

The characteristics of the herein presented pump are summarized in Table 4-6 and compared with those of commercial pumps (Fluigent MFCTMS, Elveflow OB1TM) and open-pressure pumps. The presented pump is highly cost-effective and delivers a close performance compared to the commercial pumps. In contrast to the open-source pressure pumps, the presented pump offers much faster settling times at a lower cost, which makes it more compatible for active microfluidic applications. Most importantly, the presented pressure pump functions without depending on an external pressure source.

Table 4-6 Characteristics of the herein presented pressure pump vs. existing pumps.

Pump	**Pressure Range (psi)**	**Accuracy (psi / % F.S.)**	**Settling Time (ms)**	**Number of Channels**	**Cost ($ USD)**
Presented Here	1 – 5	0.01 / 0.2	92	1	650
Fluigent MFCS	0 – 15	0.03 / 0.25	100	4	10,000
Elveflow OB1	0 – 3	0.00045 / 0.015	50	2	6000
Open-source µpump [20]	0 – 30	0.027 / 0.09	2000	4	3000
Open-source Sanchez et al. [21]	1 – 10	0.016 / 0.16	1600	4	2400

In this study, only one output channel is implemented so far, whereas other pumps offer multiple channels. However, the presented pump is adaptive and can be modified to support additional channels according to users' requirements. This can be achieved by duplicating the regulator and either employing a more powerful compressor or using an external pressure source.

Chapter 5 - Conclusion

This thesis addressed the limitations of existing pressure pumps for microfluidic applications, particularly their reliance on external pressure sources, limited accessibility, and lack of openness for customization and integration into active microfluidic systems.

Microfluidics is a rapidly developing technology that offers significant benefits across a wide range of applications. Microfluidics enables innovations that are hard or impossible to achieve using conventional methods. However, the adoption of this multidisciplinary technology is often constrained by a knowledge barrier faced by users, as well as the high cost and limited accessibility of essential components, particularly pressure pumps. As microfluidics increasingly shifts toward active systems, the need for precise, fast, and reliable pressure actuation has grown. In this context, pressure pumps outperform other commonly used actuation methods, syringe and peristaltic pumps, in meeting these requirements.

The development of open-source pressure pumps has gained increasing attention in microfluidic research to improve the accessibility of this essential tool. However, existing open-source pressure pump solutions continue to rely on external pressure sources, requiring bulky compressors that conflict with the miniaturization objectives of microfluidic systems. More importantly, these systems often overlook dynamic response speed, which is a critical requirement for active microfluidic applications. These open-source pumps often remain dependent on commercial regulators that are implemented as closed systems, which limits their accessibility, restricts control-system customization, and complicates integration into active microfluidic applications and emerging digital-twin-based methodologies that require flexible and fast closed-loop pressure control.

Overall, analysis of the existing literature points to a clear gap: the lack of a standalone, portable, customizable open-source pressure pump that operates independently of commercial regulators and is capable of providing the precise and fast settling time required for active microfluidic applications. In addition, there is a need to further investigate dual-valve pressure regulation as an alternative to commercial regulator platforms to achieve better control flexibility, improved dynamic performance suited to active microfluidic applications, and reduced cost.

An open-source pressure pump that overcomes the limitations of the current commercial and open-source models is proposed in this thesis. This pump enhances portability by incorporating an internal pressure source, which eliminates the need for bulky external compressors and supports the miniaturization of microfluidics. The proposed system is also equipped with a dual-valve pressure regulation method instead of relying on the closed-system and industrial-oriented commercial pressure regulators. A simplified dynamic model of the pressure regulation system is established to support controller design and tuning. Based on this model, PID controller gains are selected and experimentally refined to achieve stable and responsive pressure control.

Experimental validation demonstrated that the proposed pressure pump accurately regulates pressure within the desired pressure range, achieves fast settling times, and stable closed-loop behavior across multiple pressure setpoints. Comparative results with a commercial Marsh Bellofram regulator showed that the proposed regulator offers faster settling time ($\sim$ 100 ms vs. $\sim$ 200 ms), a smaller footprint ($\sim$ 120 cm^3/0.3 kg vs. $\sim$ 400 cm^3/1.35 kg), and a more affordable price ($\sim$ \$250 vs. $\sim$ \$1000), while maintaining comparable pressure regulation accuracy (±0.01 psi). These results confirm the effectiveness of the dual-valve architecture and its suitability for active microfluidic

applications requirements.

The proposed pump integrates the built-in compression unit and the dual-valve regulation system while providing a lower cost than existing pressure pumps. Compared to available open-source solutions, the proposed system achieves faster settling times, making this pump compatible with both active and passive microfluidic applications. In contrast to commercial alternatives, this pump remains open-source, customizable to meet specific users' requirements, more accessible, and affordable. This balanced combination of performance, accessibility, and affordability directly addresses the gap identified in the literature.

Future work will focus on upgrading the pump to support multiple outputs. This will be accomplished by integrating more of the pressure regulators presented herein and modifying the control system code. However, the air pump's capacity to handle multiple outputs needs to be verified to assess whether a more powerful air pump is required. Furthermore, additional improvements can be made by reducing the heat and noise generated by the onboard compression. The system's portability could also be improved by replacing the external electric power source with a battery.

Future work will further investigate alternative modeling and linearization approaches to enable LQR implementation. Moreover, more advanced control strategies will be explored for dual-valve pressure regulation, allowing for potential improvement and a direct performance comparison with the PID approach implemented in this work.

References

[1] E. K. Sackmann, A. L. Fulton, and D. J. Beebe, "The present and future role of microfluidics in biomedical research," *Nature*, vol. 507, no. 7491, pp. 181–189, 2014.

[2] L. Amirifar, M. Besanjideh, R. Nasiri, A. Shamloo, F. Nasrollahi, N. R. de Barros, E. Davoodi, A. Erdem, M. Mahmoodi, V. Hosseini *et al.*, "Droplet-based microfluidics in biomedical applications," *Biofabrication*, vol. 14, no. 2, p. 022001, 2022.

[3] K. S. Elvira, X. C. i Solvas, R. C. Wootton, and A. J. Demello, "The past, present and potential for microfluidic reactor technology in chemical synthesis," *Nature chemistry*, vol. 5, no. 11, pp. 905–915, 2013.

[4] J. Xu, T. Wu, and Y. Zhang, "Soft microrobots in microfluidic applications," *Biomedical Materials & Devices*, vol. 1, no. 2, pp. 1028–1034, 2023.

[5] T. Wang, C. Yu, and X. Xie, "Microfluidics for environmental applications," *Microfluidics in Biotechnology*, pp. 267–290, 2020.

[6] H.-T. Nguyen, H. Thach, E. Roy, K. Huynh, and C. M.-T. Perrault, "Low-cost, accessible fabrication methods for microfluidics research in low-resource settings," *Micromachines*, vol. 9, no. 9, p. 461, 2018.

[7] M. Hébert, J. Huissoon, and C. L. Ren, "A perspective of active microfluidic platforms as an enabling tool for applications in other fields," *Journal of Micromechanics and Microengineering*, vol. 32, no. 4, p. 043001, 2022.

[8] T. Wenzel, "Open hardware: From diy trend to global transformation in access to laboratory equipment," *PLoS Biology*, vol. 21, no. 1, p. e3001931, 2023.

[9] J. P. Hausberg and S. Spaeth, "Why makers make what they make: motivations to contribute to open source hardware development," *R&D Management*, vol. 50, no. 1, pp. 75–95, 2020.

[10] M. Oellermann, J. W. Jolles, D. Ortiz, R. Seabra, T. Wenzel, H. Wilson, and R. L. Tanner, "Open hardware in science: The benefits of open electronics," *Integrative and comparative biology*, vol. 62, no. 4, pp. 1061–1075, 2022.

[11] J. H. Shin and S. Choi, "Open-source and do-it-yourself microfluidics," *Sensors and Actuators B: Chemical*, vol. 347, p. 130624, 2021.

[12] C.-A. Kieffer, S. Ritty, T. Boudot, N. Petit, J. Weber, and A. Le Nel, "A high precision fluid handling system based on pressure actuation: multi-inlets flow-rate control," in *3rd European Conference on Microfluidics*, 2012.

[13] P. Zhu and L. Wang, "Passive and active droplet generation with microfluidics: a review," *Lab on a Chip*, vol. 17, no. 1, pp. 34–75, 2017.

[14] M. Hébert, M. Courtney, and C. L. Ren, "Semi-automated on-demand control of individual droplets with a sample application to a drug screening assay," *Lab on a Chip*, vol. 19, no. 8, pp. 1490–1501, 2019.

[15] M. Hébert, J. P. Huissoon, and C. L. Ren, "A novel approach to determining the hydrodynamic resistance of droplets in microchannels using active control and grey-box system identification," *Journal of Micromechanics and Microengineering*, vol. 33, no. 8, p. 085005, 2023.

[16] V. Narayanamurthy, Z. Jeroish, K. Bhuvaneshwari, P. Bayat, R. Premkumar, F. Samsuri, and M. M. Yusoff, "Advances in passively driven microfluidics and lab-on-chip devices: A comprehensive literature review and patent analysis," *RSC advances*, vol. 10, no. 20, pp. 11 652–11 680, 2020.

[17] C. T. Sullender, A. Santorelli, L. M. Richards, P. K. Mannava, C. Smith, and A. K. Dunn, "Using pressure-driven flow systems to evaluate laser speckle contrast imaging," *Journal of Biomedical Optics*, vol. 28, no. 3, pp. 036 003–036 003, 2023.

[18] N. Gyimah, O. Scheler, T. Rang, and T. Pardy, "Deep reinforcement learning-based digital twin for droplet microfluidics control," *Physics of Fluids*, vol. 35, no. 8, 2023.

[19] W. Zeng, B. Wang, H. Chang, and P. Neužil, "Quantitative study of droplet generation by pressure-driven microfluidic flows in a flow-focusing microdroplet generator," *Physics of Fluids*, vol. 36, no. 3, 2024.

[20] R. Z. Gao, M. Hébert, J. Huissoon, and C. L. Ren, "μpump: An open-source pressure pump for precision fluid handling in microfluidics," *HardwareX*, vol. 7, p. e00096, 2020.

[21] H. S. Sanchez and C. B. Chang, "Open-source pneumatic pressure pump for drop-based microfluidic flow controls," *Engineering research express*, vol. 5, no. 3, p. 035014, 2023.

[22] N. A. Filatov, I. A. Denisov, A. A. Evstrapov, and A. S. Bukatin, "Open-source pressure controller based on compact electro-pneumatic regulators for droplet microfluidics applications," *IEEE Transactions on Instrumentation and Measurement*, vol. 71, pp. 1–10, 2022.

[23] E. Richer and Y. Hurmuzlu, "A high performance pneumatic force actuator system: Part i—nonlinear mathematical model," *Journal of dynamic systems, measurement, and control*, vol. 122, no. 3, pp. 416–425, 2000.

[24] H. Zhang, J. Fang, H. Yu, H. Guo, and H. Zhang, "Second-order adaptive robust control of proportional pressure-reducing valves using phenomenological model," *Transactions of the Institute of Measurement and Control*, vol. 46, no. 12, pp. 2367–2377, 2024.

[25] H. Wang, X. Wang, J. Huang, and L. Quan, "Flow control for a two-stage proportional valve with hydraulic position feedback," *Chinese Journal of Mechanical Engineering*, vol. 33, no. 1, p. 93, 2020.

[26] G. M. Whitesides, "The origins and the future of microfluidics," *nature*, vol. 442, no. 7101, pp. 368–373, 2006.

[27] S. C. Jacobson, A. W. Moore, and J. M. Ramsey, "Fused quartz substrates for microchip electrophoresis," *Analytical Chemistry*, vol. 67, no. 13, pp. 2059–2063, 1995.

[28] C. M. Matzke, R. J. Kottenstette, S. A. Casalnuovo, G. C. Frye-Mason, M. L. Hudson, D. Y. Sasaki, R. P. Manginell, and C. C. Wong, "Microfabricated silicon gas chromatographic microchannels: fabrication and performance," in *Micromachining and Microfabrication Process Technology IV*, vol. 3511. SPIE, 1998, pp. 262–268.

[29] H. Becker and C. Gärtner, "Polymer microfabrication methods for microfluidic analytical applications," *ELECTROPHORESIS: An International Journal*, vol. 21, no. 1, pp. 12–26, 2000.

[30] Y. Xia and G. M. Whitesides, "Soft lithography," *Angewandte Chemie International Edition*, vol. 37, no. 5, pp. 550–575, 1998.

[31] D. Qin, Y. Xia, and G. M. Whitesides, "Soft lithography for micro-and nanoscale patterning," *Nature protocols*, vol. 5, no. 3, p. 491, 2010.

[32] S. M. Scott and Z. Ali, "Fabrication methods for microfluidic devices: An overview," *Micromachines*, vol. 12, no. 3, p. 319, 2021.

[33] H. Bruus, *Theoretical microfluidics*. Oxford university press, 2007, vol. 18.

[34] K. W. Oh, K. Lee, B. Ahn, and E. P. Furlani, "Design of pressure-driven microfluidic networks using electric circuit analogy," *Lab on a Chip*, vol. 12, no. 3, pp. 515–545, 2012.

[35] T. M. Squires and S. R. Quake, "Microfluidics: Fluid physics at the nanoliter scale," *Reviews of modern physics*, vol. 77, no. 3, pp. 977–1026, 2005.

[36] C. N. Baroud, F. Gallaire, and R. Dangla, "Dynamics of microfluidic droplets," *Lab on a Chip*, vol. 10, no. 16, pp. 2032–2045, 2010.

[37] Y. Zhang, T. Zheng, L. Wang, L. Feng, M. Wang, Z. Zhang, and H. Feng, "From passive to active sorting in microfluidics: A review," *Reviews on Advanced Materials Science*, vol. 60, no. 1, pp. 313–324, 2021.

[38] S. Yan, J. Zhang, D. Yuan, and W. Li, "Hybrid microfluidics combined with active and passive approaches for continuous cell separation," *Electrophoresis*, vol. 38, no. 2, pp. 238–249, 2017.

[39] H. E. Meijer, M. K. Singh, T. G. Kang, J. M. Den Toonder, and P. D. Anderson, "Passive and active mixing in microfluidic devices," in *Macromolecular symposia*, vol. 279, no. 1. Wiley Online Library, 2009, pp. 201–209.

[40] J. Green, A. Holdø, and A. Khan, "A review of passive and active mixing systems in microfluidic devices," *The International Journal of Multiphysics*, vol. 1, no. 1, pp. 1–32, 2007.

[41] Y. Chen, P. Li, P.-H. Huang, Y. Xie, J. D. Mai, L. Wang, N.-T. Nguyen, and T. J. Huang, "Rare cell isolation and analysis in microfluidics," *Lab on a Chip*, vol. 14, no. 4, pp. 626–645, 2014.

[42] A. Fergola, A. Ballesio, F. Frascella, L. Napione, M. Cocuzza, and S. L. Marasso, "Droplet generation and manipulation in microfluidics: A comprehensive overview of passive and active strategies," *Biosensors*, vol. 15, no. 6, p. 345, 2025.

[43] Z. Z. Chong, S. H. Tan, A. M. Gañán-Calvo, S. B. Tor, N. H. Loh, and N.-T. Nguyen, "Active droplet generation in microfluidics," *Lab on a Chip*, vol. 16, no. 1, pp. 35–58, 2016.

[44] S.-Y. Teh, R. Lin, L.-H. Hung, and A. P. Lee, "Droplet microfluidics," *Lab on a Chip*, vol. 8, no. 2, pp. 198–220, 2008.

[45] M. Wu, Y. Gao, A. Ghaznavi, W. Zhao, and J. Xu, "Ac electroosmosis micromixing on a lab-on-a-foil electric microfluidic device," *Sensors and Actuators B: Chemical*, vol. 359, p. 131611, 2022.

[46] J. Sun, Z. Shi, M. Li, J. Sha, M. Zhong, S. Chen, X. Liu, and S. Jia, "Numerical and experimental investigation of a magnetic micromixer under microwires and uniform magnetic field," *Journal of Magnetism and Magnetic Materials*, vol. 551, p. 169141, 2022.

[47] M. Hébert, W. Baxter, J. P. Huissoon, and C. L. Ren, "A quantitative study of the dynamic response of soft tubing for pressure-driven flow in a microfluidics context," *Microfluidics and Nanofluidics*, vol. 24, pp. 1–13, 2020.

[48] M. Hébert, J. P. Huissoon, and C. L. Ren, "A silicone-based soft matrix nanocomposite strain-like sensor fabricated using graphene and silly putty®," *Sensors and Actuators A: Physical*, vol. 305, p. 111917, 2020.

[49] M. Hébert, J. Huissoon, and C. L. Ren, "A quantitative study of the dynamic response of compliant microfluidic chips in a microfluidics context," *Journal of Micromechanics and Microengineering*, vol. 32, no. 8, p. 085004, 2022.

[50] P. Umbanhowar, V. Prasad, and D. A. Weitz, "Monodisperse emulsion generation via drop break off in a coflowing stream," *Langmuir*, vol. 16, no. 2, pp. 347–351, 2000.

[51] A. S. Utada, E. Lorenceau, D. R. Link, P. D. Kaplan, H. A. Stone, and D. Weitz, "Monodisperse double emulsions generated from a microcapillary device," *Science*, vol. 308, no. 5721, pp. 537–541, 2005.

[52] C. N. Baroud, M. R. de Saint Vincent, and J.-P. Delville, "An optical toolbox for total control of droplet microfluidics," *Lab on a Chip*, vol. 7, no. 8, pp. 1029–1033, 2007.

[53] J.-P. Raven and P. Marmottant, "Periodic microfluidic bubbling oscillator: Insight into the stability of two-phase microflows," *Physical review letters*, vol. 97, no. 15, p. 154501, 2006.

[54] S. Sugiura, M. Nakajima, and M. Seki, "Effect of channel structure on microchannel emulsification," *Langmuir*, vol. 18, no. 15, pp. 5708–5712, 2002.

[55] G. Gharib, İ. Bütün, Z. Muganlı, G. Kozalak, İ. Namlı, S. S. Sarraf, V. E. Ahmadi, E. Toyran, A. J. Van Wijnen, and A. Koşar, "Biomedical applications of microfluidic devices: a review," *Biosensors*, vol. 12, no. 11, p. 1023, 2022.

[56] T. Thorsen, R. W. Roberts, F. H. Arnold, and S. R. Quake, "Dynamic pattern formation in a vesicle-generating microfluidic device," *Physical review letters*, vol. 86, no. 18, p. 4163, 2001.

[57] P. Garstecki, M. J. Fuerstman, H. A. Stone, and G. M. Whitesides, "Formation of droplets and bubbles in a microfluidic t-junction—scaling and mechanism of break-up," *Lab on a Chip*, vol. 6, no. 3, pp. 437–446, 2006.

[58] C. Shen, F. Liu, L. Wu, C. Yu, and W. Yu, "Dripping, jetting and regime transition of droplet formation in a buoyancy-assisted microfluidic device," *Micromachines*, vol. 11, no. 11, p. 962, 2020.

[59] S. L. Anna, N. Bontoux, and H. A. Stone, "Formation of dispersions using "flow focusing" in microchannels," *Applied physics letters*, vol. 82, no. 3, pp. 364–366, 2003.

[60] R. Dreyfus, P. Tabeling, and H. Willaime, "Ordered and disordered patterns in two-phase flows in microchannels," *Physical review letters*, vol. 90, no. 14, p. 144505, 2003.

[61] A. Sattari, P. Hanafizadeh, and M. Hoorfar, "Multiphase flow in microfluidics: From droplets and bubbles to the encapsulated structures," *Advances in Colloid and Interface Science*, vol. 282, p. 102208, 2020.

[62] C. Cramer, P. Fischer, and E. J. Windhab, "Drop formation in a co-flowing ambient fluid," *Chemical engineering science*, vol. 59, no. 15, pp. 3045–3058, 2004.

[63] N. Shi, M. Mohibullah, and C. J. Easley, "Active flow control and dynamic analysis in droplet microfluidics," *Annual Review of Analytical Chemistry*, vol. 14, pp. 133–153, 2021.

[64] S. A. Naz, E. H. Doeven, S. Adams, A. Z. Kouzani, R. M. Guijt *et al.*, "Development of a robust closed loop pressure control system for droplet generation," *Sensors and Actuators A: Physical*, p. 116596, 2025.

[65] S.-H. Tan, N.-T. Nguyen, L. Yobas, and T. G. Kang, "Formation and manipulation of ferrofluid droplets at a microfluidic t-junction," *Journal of Micromechanics and Microengineering*, vol. 20, no. 4, p. 045004, 2010.

[66] Y. Wu, T. Fu, Y. Ma, and H. Z. Li, "Active control of ferrofluid droplet breakup dynamics in a microfluidic t-junction," *Microfluidics and Nanofluidics*, vol. 18, no. 1, pp. 19–27, 2015.

[67] F. Wen, Z. Ying *et al.*, "Application of an ultrasound-assisted polymer surfactant-enhanced emulsification microextraction for determination of aromatic amines in water sample," *Chinese Journal of Analytical Chemistry*, vol. 43, no. 7, pp. 957–963, 2015.

[68] C.-Y. Lee, C.-L. Chang, Y.-N. Wang, and L.-M. Fu, "Microfluidic mixing: a review," *International journal of molecular sciences*, vol. 12, no. 5, pp. 3263–3287, 2011.

[69] G. Yesiloz, M. S. Boybay, and C. L. Ren, "Effective thermo-capillary mixing in droplet microfluidics integrated with a microwave heater," *Analytical chemistry*, vol. 89, no. 3, pp. 1978–1984, 2017.

[70] R. H. Lam and W. J. Li, "A digitally controllable polymer-based microfluidic mixing module array," *Micromachines*, vol. 3, no. 2, pp. 279–294, 2012.

[71] N. Nitta, T. Sugimura, A. Isozaki, H. Mikami, K. Hiraki, S. Sakuma, T. Iino, F. Arai, T. Endo, Y. Fujiwaki *et al.*, "Intelligent image-activated cell sorting," *Cell*, vol. 175, no. 1, pp. 266–276, 2018.

[72] A. Isozaki, Y. Nakagawa, M. Loo, Y. Shibata, N. Tanaka, D. Setyaningrum, J.-W. Park, Y. Shirasaki, H. Mikami, D. Huang *et al.*, "Sequentially addressable dielectrophoretic array for high-throughput sorting of large-volume biological compartments," *Science advances*, vol. 6, no. 22, p. eaba6712, 2020.

[73] N. Godino, F. Pfisterer, T. Gerling, C. Guernth-Marschner, C. Duschl, and M. Kirschbaum, "Combining dielectrophoresis and computer vision for precise and fully automated single-cell handling and analysis," *Lab on a Chip*, vol. 19, no. 24, pp. 4016–4020, 2019.

[74] E. A. Phillips, T. J. Moehling, K. F. Ejendal, O. S. Hoilett, K. M. Byers, L. A. Basing, L. A. Jankowski, J. B. Bennett, L.-K. Lin, L. A. Stanciu *et al.*, "Microfluidic rapid and autonomous analytical device (microraad) to detect hiv from whole blood samples," *Lab on a Chip*, vol. 19, no. 20, pp. 3375–3386, 2019.

[75] B. K. Yap, S. N. M. Soair, N. A. Talik, W. F. Lim, and L. Mei I, "Potential point-of-care microfluidic devices to diagnose iron deficiency anemia," *Sensors*, vol. 18, no. 8, p. 2625, 2018.

[76] C.-J. Kim, D. Y. Ki, J. Park, V. Sunkara, T.-H. Kim, Y. Min, and Y.-K. Cho, "Fully automated platelet isolation on a centrifugal microfluidic device for molecular diagnostics," *Lab on a Chip*, vol. 20, no. 5, pp. 949–957, 2020.

[77] W. C. Nelson and C.-J. im, "Droplet actuation by electrowetting-on-dielectric (ewod): A review," *Journal of Adhesion Science and Technology*, vol. 26, no. 12-17, pp. 1747–1771, 2012.

[78] X. Ding, P. Li, S.-C. S. Lin, Z. S. Stratton, N. Nama, F. Guo, D. Slotcavage, X. Mao, J. Shi, F. Costanzo *et al.*, "Surface acoustic wave microfluidics," *Lab on a Chip*, vol. 13, no. 18, pp. 3626–3649, 2013.

[79] Y. Zhang and N.-T. Nguyen, "Magnetic digital microfluidics–a review," *Lab on a Chip*, vol. 17, no. 6, pp. 994–1008, 2017.

[80] D. Baigl, "Photo-actuation of liquids for light-driven microfluidics: state of the art and perspectives," *Lab on a Chip*, vol. 12, no. 19, pp. 3637–3653, 2012.

[81] M. A. Unger, H.-P. Chou, T. Thorsen, A. Scherer, and S. R. Quake, "Monolithic microfabricated valves and pumps by multilayer soft lithography," *science*, vol. 288, no. 5463, pp. 113–116, 2000.

[82] Y. Wang, Z. Li, X. Huang, W. Ji, X. Ning, K. Liu, J. Tan, J. Yang, H.-p. Ho, and G. Wang, "On-board control of wax valve on active centrifugal microfluidic chip and its application for plasmid dna extraction," *Microfluidics and Nanofluidics*, vol. 23, no. 10, p. 112, 2019.

[83] O. Cybulski, S. Jakiela, and P. Garstecki, "Whole teflon valves for handling droplets," *Lab on a Chip*, vol. 16, no. 12, pp. 2198–2210, 2016.

[84] D. Wong and C. L. Ren, "Microfluidic droplet trapping, splitting and merging with feedback controls and state space modelling," *Lab on a Chip*, vol. 16, no. 17, pp. 3317–3329, 2016.

[85] D. Wong, K. Erkorkmaz, and C. L. Ren, "Robodrop: a multi-input multi-output control system for on-demand manipulation of microfluidic droplets based on computer vision feedback," *IEEE/ASME Transactions on Mechatronics*, vol. 25, no. 2, pp. 1129–1137, 2020.

[86] K. Ward and Z. H. Fan, "Mixing in microfluidic devices and enhancement methods," *Journal of Micromechanics and Microengineering*, vol. 25, no. 9, p. 094001, 2015.

[87] C. Chen, Y. Zhao, J. Wang, P. Zhu, Y. Tian, M. Xu, L. Wang, and X. Huang, "Passive mixing inside microdroplets," *Micromachines*, vol. 9, no. 4, p. 160, 2018.

[88] S. N. Agnihotri, M. R. Raveshi, R. Nosrati, R. Bhardwaj, and A. Neild, "Droplet splitting in microfluidics: A review," *Physics of Fluids*, vol. 37, no. 5, 2025.

[89] A. Ebrahimi, K. Icoz, R. Didarian, C.-H. Shih, E. A. Tarim, B. Nasseri, A. Akpek, B. Cecen, A. Bal-Ozturk, K. Güleç *et al.*, "Molecular separation by using active and passive microfluidic chip designs: a comprehensive review," *Advanced Materials Interfaces*, vol. 11, no. 2, p. 2300492, 2024.

[90] V. Lecault, A. K. White, A. Singhal, and C. L. Hansen, "Microfluidic single cell analysis: from promise to practice," *Current opinion in chemical biology*, vol. 16, no. 3-4, pp. 381–390, 2012.

[91] K. S. Elvira, "Microfluidic technologies for drug discovery and development: friend or foe?" *Trends in Pharmacological Sciences*, vol. 42, no. 7, pp. 518–526, 2021.

[92] S. E. Alavi, S. Alharthi, S. F. Alavi, S. Z. Alavi, G. E. Zahra, A. Raza, and H. E. Shahmabadi, "Microfluidics for personalized drug delivery," *Drug Discovery Today*, vol. 29, no. 4, p. 103936, 2024.

[93] R. Maia, V. Carvalho, R. Lima, G. Minas, and R. O. Rodrigues, "Microneedles in advanced microfluidic systems: A systematic review throughout lab and organ-on-a-chip applications," *Pharmaceutics*, vol. 15, no. 3, p. 792, 2023.

[94] A. Enders, A. Grünberger, and J. Bahnemann, "Towards small scale: overview and applications of microfluidics in biotechnology," *Molecular biotechnology*, vol. 66, no. 3, pp. 365–377, 2024.

[95] S. Mehraji and D. L. DeVoe, "Microfluidic synthesis of lipid-based nanoparticles for drug delivery: recent advances and opportunities," *Lab on a Chip*, vol. 24, no. 5, pp. 1154–1174, 2024.

[96] M. Safarkhani, B. Farasati Far, E. C. Lima, S. Jafarzadeh, P. Makvandi, R. S. Varma, Y. Huh, M. Ebrahimi Warkiani, and N. Rabiee, "Integration of mxene and microfluidics: a perspective," *ACS biomaterials science & engineering*, vol. 10, no. 2, pp. 657–676, 2024.

[97] X. Wu, A. Chen, X. Yu, Z. Tian, H. Li, Y. Jiang, and J. Xu, "Microfluidic synthesis of multifunctional micro-/nanomaterials from process intensification: structural engineering to high electrochemical energy storage," *ACS nano*, vol. 18, no. 32, pp. 20 957–20 979, 2024.

[98] B. A. AlMashrea, A. M. Almehdi, and S. Damiati, "Simple microfluidic devices for in situ detection of water contamination: a state-of-art review," *Frontiers in Bioengineering and Biotechnology*, vol. 12, p. 1355768, 2024.

[99] P. Aryal, C. Hefner, B. Martinez, and C. S. Henry, "Microfluidics in environmental analysis: advancements, challenges, and future prospects for rapid and efficient monitoring," *Lab on a Chip*, vol. 24, no. 5, pp. 1175–1206, 2024.

[100] W. Suqi, C. L. J. Rong, H. A. Abdulbari, and W. K. Mahmood, "Microfluidic approaches in water quality monitoring: An insight and a comprehensive review," *ChemBioEng Reviews*, vol. 11, no. 2, pp. 215–230, 2024.

[101] N. Ota, Y. Yonamine, T. Asai, Y. Yalikun, T. Ito, Y. Ozeki, Y. Hoshino, and Y. Tanaka, "Isolating single euglena gracilis cells by glass microfluidics for raman analysis of paramylon biogenesis," *Analytical Chemistry*, vol. 91, no. 15, pp. 9631–9639, 2019.

[102] J. Ma, G. Tran, A. M. Wan, E. W. Young, E. Kumacheva, N. N. Iscove, and P. W. Zandstra, "Microdroplet-based one-step rt-pcr for ultrahigh throughput single-cell multiplex gene expression analysis and rare cell detection," *Scientific Reports*, vol. 11, no. 1, p. 6777, 2021.

[103] X. Guo, Q. Shen, Z. Chen, Z. He, and X. Yan, "Harnessing microfluidic technology for bacterial single-cell analysis in mammals," *TrAC Trends in Analytical Chemistry*, vol. 166, p. 117168, 2023.

[104] E. M. Vedula, J. L. Alonso, M. A. Arnaout, and J. L. Charest, "A microfluidic renal proximal tubule with active reabsorptive function," *PLoS One*, vol. 12, no. 10, p. e0184330, 2017.

[105] B. Kwak, A. Ozcelikkale, C. S. Shin, K. Park, and B. Han, "Simulation of complex transport of nanoparticles around a tumor using tumor-microenvironment-on-chip," *Journal of Controlled Release*, vol. 194, pp. 157–167, 2014.

[106] A. Y. Shourabi, N. Kashaninejad, and M. S. Saidi, "An integrated microfluidic concentration gradient generator for mechanical stimulation and drug delivery," *Journal of Science: Advanced Materials and Devices*, vol. 6, no. 2, pp. 280–290, 2021.

[107] B.-H. Kwon, K. G. Lee, T. J. Park, H. Kim, T. J. Lee, S. J. Lee, and D. Y. Jeon, "Continuous in situ synthesis of znse/zns core/shell quantum dots in a microfluidic reaction system and its application for light-emitting diodes," *Small*, vol. 8, no. 21, pp. 3257–3262, 2012.

[108] W. Liang, F. Jin, Y. Zhao, L. Shi, Q. Liu, Z. Wang, Y. Wang, M. Zhang, J. Zhu, and S. Yuan, "Synthesis of single-crystal lini0. 8co0. 1mn0. 1o2 materials for li-ion

batteries by microfluidic technology," *Chemical Engineering Journal*, vol. 464, p. 142656, 2023.

[109] L. Xu, A. Wang, X. Li, and K. W. Oh, "Passive micropumping in microfluidics for point-of-care testing," *Biomicrofluidics*, vol. 14, no. 3, 2020.

[110] A. P. Iakovlev, A. S. Erofeev, and P. V. Gorelkin, "Novel pumping methods for microfluidic devices: a comprehensive review," *Biosensors*, vol. 12, no. 11, p. 956, 2022.

[111] R. Burger, D. Kirby, M. Glynn, C. Nwankire, M. O'Sullivan, J. Siegrist, D. Kinahan, G. Aguirre, G. Kijanka, R. A. Gorkin III *et al.*, "Centrifugal microfluidics for cell analysis," *Current opinion in chemical biology*, vol. 16, no. 3-4, pp. 409–414, 2012.

[112] M. Tang, G. Wang, S.-K. Kong, and H.-P. Ho, "A review of biomedical centrifugal microfluidic platforms," *Micromachines*, vol. 7, no. 2, p. 26, 2016.

[113] I. Maguire, R. O'kennedy, J. Ducrée, and F. Regan, "A review of centrifugal microfluidics in environmental monitoring," *Analytical Methods*, vol. 10, no. 13, pp. 1497–1515, 2018.

[114] L. Clime, J. Daoud, D. Brassard, L. Malic, M. Geissler, and T. Veres, "Active pumping and control of flows in centrifugal microfluidics," *Microfluidics and Nanofluidics*, vol. 23, pp. 1–22, 2019.

[115] J. Hess, S. Zehnle, P. Juelg, T. Hutzenlaub, R. Zengerle, and N. Paust, "Review on pneumatic operations in centrifugal microfluidics," *Lab on a Chip*, vol. 19, no. 22, pp. 3745–3770, 2019.

[116] J. Park, D. H. Han, and J.-K. Park, "Towards practical sample preparation in point-of-care testing: user-friendly microfluidic devices," *Lab on a Chip*, vol. 20, no. 7, pp. 1191–1203, 2020.

[117] Z. Du, L. Chen, and S. Yang, "Advancements in the research of finger-actuated poct chips," *Microchimica Acta*, vol. 191, no. 1, p. 65, 2024.

[118] J. Park and J.-K. Park, "Integrated microfluidic pumps and valves operated by finger actuation," *Lab on a Chip*, vol. 19, no. 18, pp. 2973–2977, 2019.

[119] K. Iwai, K. C. Shih, X. Lin, T. A. Brubaker, R. D. Sochol, and L. Lin, "Finger-powered microfluidic systems using multilayer soft lithography and injection molding processes," *Lab on a Chip*, vol. 14, no. 19, pp. 3790–3799, 2014.

[120] X. Qiu, J. A. Thompson, Z. Chen, C. Liu, D. Chen, S. Ramprasad, M. G. Mauk, S. Ongagna, C. Barber, W. R. Abrams *et al.*, "Finger-actuated, self-contained immunoassay cassettes," *Biomedical microdevices*, vol. 11, pp. 1175–1186, 2009.

[121] J. Park and J.-K. Park, "Finger-actuated microfluidic device for the blood cross-matching test," *Lab on a Chip*, vol. 18, no. 8, pp. 1215–1222, 2018.

[122] J. Park, H. Roh, and J.-K. Park, "Finger-actuated microfluidic concentration gradient generator compatible with a microplate," *Micromachines*, vol. 10, no. 3, p. 174, 2019.

[123] J. Park and J.-K. Park, "Finger-actuated microfluidic display for smart blood typing," *Analytical Chemistry*, vol. 91, no. 18, pp. 11 636–11 642, 2019.

[124] M. E. Haque, A. J. Conde, W. N. MacPherson, S. R. Knight, R. M. Carter, and M. Kersaudy-Kerhoas, "A microfluidic finger-actuated blood lysate preparation device enabled by rapid acoustofluidic mixing," *Lab on a Chip*, vol. 23, no. 1, pp. 62–71, 2023.

[125] S. Yan, S. H. Tan, Y. Li, S. Tang, A. J. Teo, J. Zhang, Q. Zhao, D. Yuan, R. Sluyter, N.-T. Nguyen *et al.*, "A portable, hand-powered microfluidic device for sorting of biological particles," *Microfluidics and Nanofluidics*, vol. 22, pp. 1–10, 2018.

[126] P. Thurgood, J. Y. Zhu, N. Nguyen, S. Nahavandi, A. R. Jex, E. Pirogova, S. Baratchi, and K. Khoshmanesh, "A self-sufficient pressure pump using latex balloons for microfluidic applications," *Lab on a Chip*, vol. 18, no. 18, pp. 2730–2740, 2018.

[127] X. Zhang, K. Xia, and A. Ji, "A portable plug-and-play syringe pump using passive valves for microfluidic applications," *Sensors and Actuators B: Chemical*, vol. 304, p. 127331, 2020.

[128] S. B. Park and J. H. Shin, "Fully 3d-printed, nonelectric, spring-powered syringe pump for operating microfluidic devices," *Sensors and Actuators B: Chemical*, vol. 405, p. 135289, 2024.

[129] K. Zhang, Q. Liang, S. Ma, T. He, X. Ai, P. Hu, Y. Wang, and G. Luo, "A gravity-actuated technique for flexible and portable microfluidic droplet manipulation," *Microfluidics and nanofluidics*, vol. 9, pp. 995–1001, 2010.

[130] C. Kim, D. H. Hwang, S. Lee, and S.-J. Kim, "Water-head pumps provide precise and fast microfluidic pumping and switching versus syringe pumps," *Microfluidics and Nanofluidics*, vol. 20, pp. 1–8, 2016.

[131] W. Gao, M. Liu, S. Chen, C. Zhang, and Y. Zhao, "Droplet microfluidics with gravity-driven overflow system," *Chemical Engineering Journal*, vol. 362, pp. 169–175, 2019.

[132] D. W. Lee, N. Choi, and J. H. Sung, "A microfluidic chip with gravity-induced unidirectional flow for perfusion cell culture," *Biotechnology progress*, vol. 35, no. 1, p. e2701, 2019.

[133] K. R. Bajgiran, A. S. Cordova, R. Elkhanoufi, J. A. Dorman, and A. T. Melvin, "Simultaneous droplet generation with in-series droplet t-junctions induced by gravity-induced flow," *Micromachines*, vol. 12, no. 10, p. 1211, 2021.

[134] Y. Zai, Z. Wang, Y. Ding, C. Min, Y. Liu, H. Zhao, E. Su, and N. He, "Gravity-driven flow control in a fully integrated microfluidic cartridge for molecular point-of-care testing," *Electrophoresis*, 2023.

[135] A.-J. Mäki, S. Hemmilä, J. Hirvonen, N. N. Girish, J. Kreutzer, J. Hyttinen, and P. Kallio, "Modeling and experimental characterization of pressure drop in gravity-driven microfluidic systems," *Journal of Fluids Engineering*, vol. 137, no. 2, p. 021105, 2015.

[136] A. K. Fajrial, A. Vega, G. Shakya, and X. Ding, "A frugal microfluidic pump," *Lab on a Chip*, vol. 21, no. 24, pp. 4772–4778, 2021.

[137] S. Mohith, P. N. Karanth, and S. Kulkarni, "Recent trends in mechanical micropumps and their applications: A review," *Mechatronics*, vol. 60, pp. 34–55, 2019.

[138] F. Forouzandeh, A. Arevalo, A. Alfadhel, and D. A. Borkholder, "A review of peristaltic micropumps," *Sensors and Actuators A: Physical*, vol. 326, p. 112602, 2021.

[139] A. Bußmann, T. Thalhofer, S. Hoffmann, L. Daum, N. Surendran, O. Hayden, J. Hubbuch, and M. Richter, "Microfluidic cell transport with piezoelectric micro diaphragm pumps," *Micromachines*, vol. 12, no. 12, p. 1459, 2021.

[140] X. Wang, H. Jiang, Y. Chen, X. Qiao, and L. Dong, "Microblower-based microfluidic pump," *Sensors and Actuators A: Physical*, vol. 253, pp. 27–34, 2017.

[141] D. B. Parker *et al.*, "Positive displacement pumps-performance and application," in *Proceedings of the 11th International Pump Users Symposium*. Turbomachinery Laboratories, Department of Mechanical Engineering, Texas A&M . . ., 1994.

[142] B. Wijnen, E. J. Hunt, G. C. Anzalone, and J. M. Pearce, "Open-source syringe pump library," *PloS one*, vol. 9, no. 9, p. e107216, 2014.

[143] P. M. Korczyk, O. Cybulski, S. Makulska, and P. Garstecki, "Effects of unsteadiness of the rates of flow on the dynamics of formation of droplets in microfluidic systems," *Lab on a Chip*, vol. 11, no. 1, pp. 173–175, 2011.

[144] W. Zeng, S. Li, and Z. Wang, "Characterization of syringe-pump-driven versus pressure-driven microfluidic flows," in *2015 International Conference on Fluid Power and Mechatronics (FPM)*. IEEE, 2015, pp. 711–715.

[145] W. Zeng, I. Jacobi, D. J. Beck, S. Li, and H. A. Stone, "Characterization of syringe-pump-driven induced pressure fluctuations in elastic microchannels," *Lab on a Chip*, vol. 15, no. 4, pp. 1110–1115, 2015.

[146] J. R. Lake, K. C. Heyde, and W. C. Ruder, "Low-cost feedback-controlled syringe pressure pumps for microfluidics applications," *PLoS One*, vol. 12, no. 4, p. e0175089, 2017.

[147] T. L. Czech, P. P. Nelson, C. Thölken, P. Meyer, T. Hess, H.-R. Chung, and T. Adhikary, "Pi-seq—a customizable multichannel syringe pump for microfluidics," *HardwareX*, vol. 18, p. e00517, 2024.

[148] M. D. Biviano, M. V. Paludan, A. H. Christensen, E. V. Østergaard, and K. H. Jensen, "Smoothing oscillatory peristaltic pump flow with bioinspired passive components," *Physical Review Applied*, vol. 18, no. 6, p. 064013, 2022.

[149] M. P. McIntyre, G. van Schoor, K. R. Uren, and C. P. Kloppers, "Modelling the pulsatile flow rate and pressure response of a roller-type peristaltic pump," *Sensors and Actuators A: Physical*, vol. 325, p. 112708, 2021.

[150] M. R. Behrens, H. C. Fuller, E. R. Swist, J. Wu, M. M. Islam, Z. Long, W. C. Ruder, and R. Steward Jr, "Open-source, 3d-printed peristaltic pumps for small volume point-of-care liquid handling," *Scientific reports*, vol. 10, no. 1, p. 1543, 2020.

[151] O. C. Jeong and S. Konishi, "Experimental study on a single particle trap with a pneumatic vibrator matrix," *Microfluidics and nanofluidics*, vol. 6, no. 1, pp. 139–144, 2009.

[152] R. Gorkin III, L. Clime, M. Madou, and H. Kido, "Pneumatic pumping in centrifugal microfluidic platforms," *Microfluidics and nanofluidics*, vol. 9, no. 2, pp. 541–549, 2010.

[153] P. E. Guevara-Pantoja, R. J. Jiménez-Valdés, J. L. García-Cordero, and G. A. Caballero-Robledo, "Pressure-actuated monolithic acrylic microfluidic valves and pumps," *Lab on a Chip*, vol. 18, no. 4, pp. 662–669, 2018.

[154] S. H. Jin, B. Lee, J. S. Kim, and C.-S. Lee, "Improvement strategy of a microfluidic sorter using a pneumatic bilayer valve," *Chemical Engineering Science*, vol. 245, p. 116834, 2021.

[155] Y. Zhou, Z. Yu, M. Wu, Y. Lan, C. Jia, and J. Zhao, "Single-cell sorting using integrated pneumatic valve droplet microfluidic chip," *Talanta*, vol. 253, p. 124044, 2023.

[156] W. Zeng, I. Jacobi, S. Li, and H. A. Stone, "Variation in polydispersity in pump-and pressure-driven micro-droplet generators," *Journal of Micromechanics and Microengineering*, vol. 25, no. 11, p. 115015, 2015.

[157] M. Ernits, O. Reinsalu, A. Kyritsakis, V. Linko, and V. Zadin, "Low-cost, open-source, high-precision pressure controller for multi-channel microfluidics," *Biosensors*, vol. 15, no. 3, p. 154, 2025.

[158] W. H. Ko, J. Hynecek, and S. F. Boettcher, "Development of a miniature pressure transducer for biomedical applications," *IEEE Transactions on Electron Devices*, vol. 26, no. 12, pp. 1896–1905, 1979.

[159] G. Li, X. Wei, Z. Wang, and H. Bao, "Study on the pressure regulation method of new automatic pressure regulating valve in the electronically controlled pneumatic brake systems in commercial vehicles," *Sensors*, vol. 22, no. 12, p. 4599, 2022.

[160] S.-j. Su, Y.-y. Zhu, C.-j. Li, W.-x. Tang, and H.-r. Wang, "Dual-valve parallel prediction control for an electro-hydraulic servo system," *Science Progress*, vol. 103, no. 1, p. 0036850419875662, 2020.

[161] M. S. Xavier, A. J. Fleming, and Y. K. Yong, "Design and control of pneumatic systems for soft robotics: A simulation approach," *IEEE Robotics and Automation Letters*, vol. 6, no. 3, pp. 5800–5807, 2021.

[162] A. Szabo, T. Becsi, and P. Gaspar, "Control design and validation for floating piston electro-pneumatic gearbox actuator," *Applied Sciences*, vol. 10, no. 10, p. 3514, 2020.

[163] M. Hamdan and Z. Gao, "A novel pid controller for pneumatic proportional valves with hysteresis," in *Conference record of the 2000 IEEE industry applications conference. Thirty-fifth IAS annual meeting and world conference on industrial applications of electrical energy (Cat. No. 00CH37129)*, vol. 2. IEEE, 2000, pp. 1198–1201.

[164] M. Shiee, A. Sharifi K, M. Fathi, and F. Najafi, "An experimental comparison of pwm schemes to improve positioning of servo pneumatic systems," *The International Journal of Advanced Manufacturing Technology*, vol. 82, no. 9, pp. 1765–1779, 2016.

[165] X. B. Tran, "Pid control for a pneumatic servo system," *Old Journal*, no. 138B, pp. 12–17, 2019.

[166] C. Watson and S. Senyo, "All-in-one automated microfluidics control system," *HardwareX*, vol. 5, p. e00063, 2019.

[167] E. A. Galan, H. Zhao, X. Wang, Q. Dai, W. T. Huck, and S. Ma, "Intelligent microfluidics: The convergence of machine learning and microfluidics in materials science and biomedicine," *Matter*, vol. 3, no. 6, pp. 1893–1922, 2020.

[168] W. Zeng and H. Fu, "Precise measurement and control of the pressure-driven flows for microfluidic systems," *Electrophoresis*, vol. 41, no. 10-11, pp. 852–859, 2020.

[169] E. Miller, M. Rotea, and J. P. Rothstein, "Microfluidic device incorporating closed loop feedback control for uniform and tunable production of micro-droplets," *Lab on a Chip*, vol. 10, no. 10, pp. 1293–1301, 2010.

[170] S. T. Mahmud, W. Ma, T. Thomsen, C. Chen, R. Rex, A. Lai, L. L. Sohn, and A. Randles, "Microfluidic digital twin for enhanced single-cell analysis," in *International Conference on Computational Science*. Springer, 2025, pp. 283–297.

[171] D. Crawford, C. Smith, and G. Whyte, "Image-based closed-loop feedback for highly mono-dispersed microdroplet production," *Scientific reports*, vol. 7, no. 1, p. 10545, 2017.

[172] P. Frank, S. Haefner, M. Elstner, and A. Richter, "Fully-programmable, low-cost,"do-it-yourself" pressure source for general purpose use in the microfluidic laboratory," *Inventions*, vol. 1, no. 2, p. 13, 2016.

[173] M. Hébert and M. Zein, "Short-and long-term dynamic modelling of pressure-driven flow for droplet microfluidic applications," in *APS Division of Fluid Dynamics Meeting Abstracts*, 2024, pp. T18–007.

Appendix A - Linear Quadratic Regulator (LQR)

LQR is particularly effective for systems with multiple control inputs. This control approach was also investigated considering the need to control two valves to maintain pressure. Although this control approach was not fully completed and implemented in the final design, the partial work and the challenges are documented here for future studies.

The inherent dynamics of the pressure regulator system imply several challenges. Thus, the simplified linearized model adopted for controller design did not adequately capture the nonlinear behavior of the system observed during experimental implementation. This can be attributed to several factors, including the indirect relationship between valve current and chamber pressure, valve dead zones and saturation effects, the nonlinear relation between flow rate and pressure variations, and the compressibility of air within the chamber.

This appendix presents the methodology followed to derive a simplified state-space model of the pressure regulator system for LQR controller design. The adopted assumptions aim to reduce model complexity while retaining the dominant system dynamics.

The volume of the chamber is constant, and the air temperature is assumed to be at room temperature. By differentiating the ideal gas law (Equation 3.2) with respect to time, the rate of change of pressure can be related to the net mass flow rate in the chamber Equation 3.4.

According to Figure 3.5, the relation between the current and the mass flow rate is assumed to be approximately linear. Thus, the mass flow rates through the inlet and vent valves can be expressed as linear functions of their respective currents:

$$\dot{P} = \frac{R_x T}{V}(\alpha * i_{in} - \beta * i_{out}) \tag{A.1}$$

where α and β are the slopes obtained from the graph of Figure 3.5. Both have the same value ($\approx$ 1.8405 LPM/A), since identical valves are used, with one corresponding to the inlet valve and the other to the vent valve.

Therefore, Equation A.1 relates the pressure dynamics in the chamber to the current applied to the inlet and vent valve. This relation was then used to derive the state-space model required for implementing the LQR control system. In this model, the system output y corresponds to the chamber pressure, which is directly measured by the pressure sensor.

$$\dot{P} = 0 \cdot P + \begin{bmatrix} \frac{R_x T}{V}\alpha & -\frac{R_x T}{V}\beta \end{bmatrix} \begin{bmatrix} i_{in} \\ i_{out} \end{bmatrix} \tag{A.2}$$

$$y = 1 \cdot P \tag{A.3}$$

where i_{in} is the current applied to the inlet valve and i_{out} is the current applied to the vent valve.

Linear Quadratic Regulator (LQR) computes an optimal state-feedback control law by minimizing a quadratic cost function that balances regulation accuracy and control effort:

$$J = \int_0^\infty \left(X_e^\top Q X_e + u^\top R u \right) dt \tag{A.4}$$

where Q and R are tuning parameters that reflect the desired trade-off between regulation performance and control effort. Q assigns weight to system state accuracy relative to the desired operating point, while the matrix R controls the level of actuation effort.

After obtaining the state-space model of the system, appropriate matrices Q and R were selected. The algebraic Riccati equation was then solved numerically using MATLAB `lqr(A,B,Q,R)` function to obtain the state-feedback gain matrix K

The resulting LQR control law was subsequently implemented in the Arduino code to drive the inlet and vent valves and is given by:

$$u_{\mathrm{LQR}}(t) = -KX_e(t) \tag{A.5}$$

$u_{LQR}(t)$ is the control output of the LQR(control current) applied to both the inlet and outlet valves. This control output is then converted to the 12-bit DAC command using a linear scaling ratio. $X_e(t)$ is the difference between the set pressure and the actual pressure measured by the sensor (to allow the controller to drive the system to the desired pressure). After testing the pump, the designed system did not achieve stable regulation at the desired pressure. The observed response was oscillatory and unstable: one valve would fully open while the other closed, alternating repeatedly based on the sign value of the pressure error in a repeated alternation. Minor stabilization occurred by slightly opening one valve continuously, but precise regulation was not sufficient. Since the state vector is limited to the pressure in the reservoir, the resulting LQR controller behaves similarly to a PID controller with only a proportional term acting on the pressure error. Consequently, to achieve stable pressure regulation, the state vector must be augmented to introduce integral action. Although the LQR system could still be feasible to control this

system with additional work on linearization and finding alternative solutions, the main objective in this thesis is to provide a simple and user-friendly pressure pump that can be constructed by a non-expert in this field. Therefore, a PID controller was designed to include both proportional and integral actions required to precisely regulate the pressure.

Appendix B - Extended Study: Liquid Reservoir Analysis

As explained in the working principle of the pressure pump in Section 2.3, the air pump delivers controlled air to a reservoir containing a specified volume of fluid. The controlled air then pushes the fluid into a microfluidic chip. During the study of the pneumatic actuation system, additional work was conducted to understand the dynamic behavior of the air-liquid interface in the reservoir before it is supplied to the microfluidic chip. This appendix presents the derived equations, the developed Simulink models, and the obtained results.

To model the system, the reservoir is considered as a piston-cylinder analogy, where air acts as the massless piston that compresses and pushes the fluid outside the system without mixing with it. The system is assumed to be adiabatic, as the time scale of the pressure changes is much faster than that of heat transfer; hence, heat transfer is neglected. Since the system operates at room temperature and low pressure, which are far from the critical point of air, air is modeled as a dry ideal gas and humidity is neglected. The temperature of the air entering the reservoir is assumed to be equal to the temperature of the air inside the reservoir. These modeling assumptions are also adopted in a related pneumatic system reported by Richer et al. [23]. In addition, air enters the reservoir while the liquid exits it; thus, the design is treated as an open system.

The rate form of the energy balance equation (Equation B.1) is used according to the first law of thermodynamics:

$$\dot{E}_{\text{in}} - \dot{E}_{\text{out}} = \frac{dE_{\text{sys}}}{dt} \tag{B.1}$$

where the rate of change of the energy in the system ($\frac{dE_{\text{sys}}}{dt}$) is equal to the difference

between the energy entering the system ($\dot{E}_{\text{in}}$) the energy leaving the system $\dot{E}_{\text{out}}$.

The energy entering the system ($\dot{E}_{\text{in}}$) is equal to the mass flow rate of air entering the reservoir multiplied by its enthalpy (h) (Equation B.2). Since ideal gas is assumed, the enthalpy is expressed in terms of the inlet air temperature (T_{in}) and specific heat at constant pressure (c_p) :

$$\dot{E}_{\text{in}} = \dot{m}_a h = \dot{m}_a c_p T_{in} \tag{B.2}$$

The power done by the system ($\dot{W}_{\text{boundary}}$) is the work exerted by the air on the fluid inside the reservoir. This work is the instantaneous pressure (P) multiplied by the volumetric flow rate. The volumetric flow rate is the product of the reservoir cross-sectional area (A) and the fluid displacement rate ($\dot{X}$).

$$\dot{E}_{\text{out}} = \dot{W}_{\text{boundary}} = PA\dot{X} \tag{B.3}$$

For an ideal gas, the total internal energy (U) is expressed as the mass of the gas (m) multiplied by the temperature and the specific heat at constant volume (c_v)

$$U = m c_v T \tag{B.4}$$

Using the ideal gas equation, the product of the air mass and temperature is represented in terms of the pressure of air (P) and the volume of the air in the reservoir (V) as:

$$mT = \frac{PV}{R_x} \tag{B.5}$$

Since the air pushes the fluid out of the reservoir, both the volume of air (V) and the pressure of air (P) in the reservoir are variables. Thus, by neglecting kinetic and gravitational energy effects, the rate of change of the total internal energy is written as follows:

$$\frac{dE_{\text{sys}}}{dt} = c_v \frac{d}{dt}\left(\frac{PV}{R_x}\right) = \frac{c_v}{R_x}\left(P\dot{V} + \dot{P}V\right) \tag{B.6}$$

The volume of air in the reservoir is equal to the initial volume (V_0) added to the additional volume added as the air pushes the fluid:

$$V = V_0 + AX \tag{B.7}$$

By substituting the Equation B.2, Equation B.3, and Equation B.6 into the rate form of the energy balance equation (Equation B.1), the first equation used in the Simulink model (Equation B.8) is obtained. The equation has five variables: mass flow rate of air $\dot{m}_{\text{air}}$, pressure (P), the fluid displacement (X), rate of change of pressure $\dot{P}$, and the rate of change of the fluid displacement $\dot{X}$.

$$\dot{P} = \frac{R_{\text{x}}\, T_{in}}{V_0 + AX}\left(\gamma \dot{m}_{\text{air}}\right) - \frac{\gamma P A}{V_0 + Ax}\dot{X} \tag{B.8}$$

By using the Hagen-Poiseuille Law :

$$\Delta P = R_{\text{chip}} Q = R_{\text{chip}} A \dot{X} \tag{B.9}$$

where ΔP is the pressure drop across the microfluidic chip, R_{chip} is the hydraulic resistance of the microlfuidic chip.

The second equation implemented in the Simulink model is written as:

$$\dot{x} = \frac{1}{R_{\text{chip}} A} \left(P + \rho g (h - X) - P_{\text{atm}}\right) \tag{B.10}$$

where ρ is the density of air, g is the gravity, h is the initial volume of the fluid, and P_{atm} is the atmospheric pressure.

According to the continuity equation, the volume flow rate of the fluid in the system pushed by the air is equal to the volume flow rate of the fluid exiting the system. Thus, the mass flow rate of the fluid sample exiting the system to the microfluidic chip ($\dot{m}_w$) is written in terms of the rate of change of the fluid displacement ($\dot{X}$) as:

$$A\dot{X} = \frac{\dot{m}_w}{\rho} \tag{B.11}$$

$$\dot{m}_w = A\dot{X}\rho \tag{B.12}$$

After formulating the differential equations, the Simulink model was built by implementing Equations B.8, B.10, and B.12. The model receives the mass flow rate of air supplied by the air pump as input and provides the fluid sample mass flow rate exiting the liquid reservoir

as output. Since the Simulink model is too detailed to present clearly, a schematic in Figure B.1 is provided to better illustrate the model's functionality. Equation B.8 calculates the rate of change of air pressure($\dot{P}$) as a function of the air mass flow rate ($\dot{m}_a$) (input), the pressure (P), and the rate of change of fluid displacement($\dot{X}$). In Simulink, integrator blocks are used to solve the differential equations, overcoming the interdependence barrier between variables (P, $\dot{P}$, $\dot{X}$, and X). By determining $\dot{P}$, P is obtained, which is then used in Equation B.10 to calculate $\dot{X}$. The sample fluid mass flow rate $\dot{m}_w$ is then determined by multiplying the $\dot{X}$ by the gain, as defined in EquationB.12.

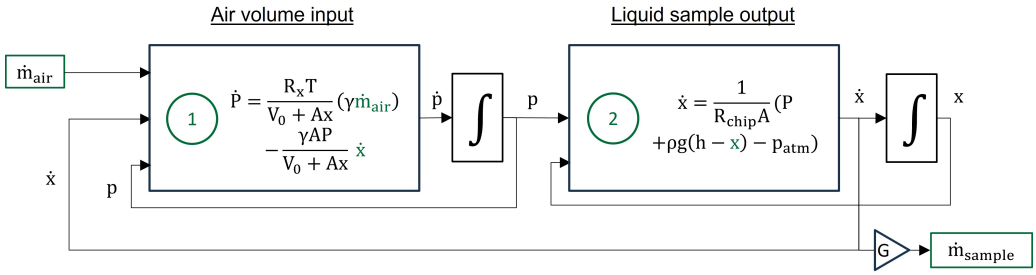

FIGURE B.1 – Schematic representing the Simulink model [173].

Figure B.2 presents a selection of the simulation results from the Simulink model. The microscale structure of the microfluidic channels imposes very high resistance on the fluid entering the chip. This leads the fluid in the reservoir to take hours to empty. To better present the simulation, the results are divided into short-term and long-term behavior, as the intermediate period shows relatively little change.

The simulation demonstrated satisfactory results. The designed model captures the short-term and long-term dynamics of the liquid reservoir. The system is capable of predicting the pressure and flow changes in the reservoir. Moreover, the mass flow rate of the fluid exiting the reservoir is determined based on the mass flow rate of air input to the system. Further experiments will be conducted in the future to validate the performance of the model. Experimental results will be compared to the results obtained from the simulation.

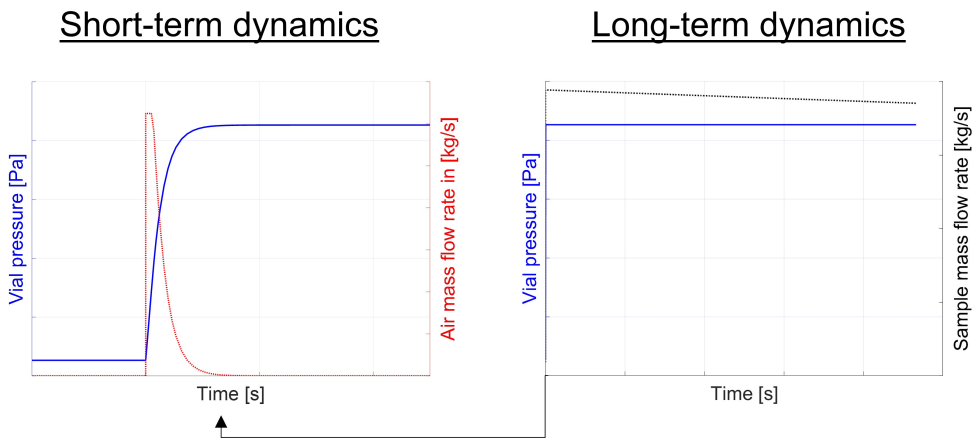

FIGURE B.2 – Simulation results of the designed Simulink model [173].

To conclude, the designed model can provide a valuable tool for microfluidic systems, including estimating uncertainties, guiding design decisions, as well as enabling control and optimization.